学位論文

Beliaev Theory of Spinor Bose-Einstein Condensates and Its Applications

（スピノルボース・アインシュタイン凝縮体における
ベリアエフ理論とその応用）

平成 25 年 12 月　博士（理学）申請

東京大学大学院理学系研究科

物理学専攻

グェン　タン　フク

Abstract

Due to the coexistence of phase coherence and magnetic order, Bose-Einstein condensates with internal degrees of freedom, i.e., spinor BECs, are considered to serve as an ideal table-top playground for the studies of various phenomena in different fields of physics. They have been widely used in studying spin textures and topological defects, coherent spin dynamics, quantum symmetry breaking, quantum phase transitions, etc. However, the theoretical framework used in these works is based on the mean-field theory in which the effects of quantum fluctuations are ignored. Despite the success of the mean-field theory in the description of spinor BECs, there are particular features whose account must rely on a beyond-mean-field theory as the effects of quantum fluctuations become significant. In this thesis, we develop the Beliaev theory, which is a Green's function approach beyond the Bogoliubov theory, for spinor BECs to study the effects of quantum fluctuations on the condensates' phase structures, elementary excitations, stabilities, and phase transitions.

First, we point out that the Bogoliubov theory fails to capture the metastable states associated with first-order quantum phase transitions in spin-2 BECs. In fact, we show that these metastable states are induced by quantum fluctuations, and only by going to the next-order approximation, i.e., the Beliaev theory, can we show that they indeed appear around the phase boundaries. Besides the fluctuation-induced metastability, we find another important class of first-order quantum phase transitions in both spin-1 and spin-2 BECs. In this class, there is no metastable state to all orders of approximation since it is prohibited by a high symmetry of the Hamiltonian at the phase boundary, resulting in a characteristic flat energy landscape. Despite being first-order phase transitions, the flat energy landscape leads to the criticality in the dynamics of the condensate through these transitions in a manner similar to second-order phase transitions.

Second, we succeed in deriving the analytic expression for the energy gap of the so-called quasi-Nambu-Goldstone (quasi-NG) modes, which are excitations not generated by spontaneous symmetry breaking, in the nematic phase of spin-2 BECs. Although quasi-NG modes are gapless at the mean-field level, we prove that with quantum corrections they acquire a nonzero energy gap. From the obtained magnitude of the energy gap, we can evaluate the critical temperature above which a topological defect such as a vortex of spin nematicity would decay by emitting thermally excited quasi-NG modes. We also study how the propagation of quasi-NG modes in space is affected by the particle-number density fluctuations of the condensate.

Third, we calculate the damping rates of various types of quasiparticles in a spin-2 BEC including phonons, magnons, and quasi-NG modes. They actually have finite lifetime and decay via numerous channels of collision with the condensate atoms. Using either the Fermi's golden rule or the spinor Beliaev theory, we obtain the analytic expressions for the damping rates of phonons and magnons, from which the power-law dependence of the damping rates on the momentum is deduced. In contrast, the damping of quasi-NG modes is suppressed due to the energy conservation.

List of Publications

The following five articles are the publications on which this thesis is based:

(i) N. T. Phuc, Y. Kawaguchi, and M. Ueda, *Beliaev theory of spinor Bose-Einstein condensates*, Ann. Phys. **328**, 158 (2013).

(ii) N. T. Phuc, Y. Kawaguchi, and M. Ueda, *Fluctuation-induced and symmetry-prohibited metastabilities in spinor Bose-Einstein condensates*, Phys. Rev. A **88**, 043629 (2013).

(iii) N. T. Phuc, Y. Kawaguchi, and M. Ueda, *Critical dynamics of a first-order quantum phase transition without metastability*, in preparation.

(iv) N. T. Phuc, Y. Kawaguchi, and M. Ueda, *Emergent energy gap of quasi-Nambu-Goldstone modes and their propagations in spinor Bose-Einstein condensates*, in preparation.

(v) N. T. Phuc, Y. Kawaguchi, and M. Ueda, *Beliaev dampings of magnons and phonons in spinor Bose-Einstein condensates*, in preparation.

The following two publications are not directly related to this thesis.

(vi) N. T. Phuc, Y. Kawaguchi, and M. Ueda, *Effects of thermal and quantum fluctuations on the phase diagram of a spin-1* ^{87}Rb *Bose-Einstein condensate*, Phys. Rev. A **84**, 043645 (2011).

(vii) Y. Kawaguchi, N. T. Phuc, and P. B. Blakie, *Finite-temperature phase diagram of a spin-1 Bose gas*, Phys. Rev. A **85**, 053611 (2012).

Contents

Chapter 1

Introduction

In quantum fluids, the phase coherence between the constituent particles can amplify the effects of a microscopic interaction so that they are observable in macroscopic properties [1]. Superfluid ^{4}He, the first such system in Nature, was found by Kapitza [2], Allen, and Misener [3] in 1938, followed by the discoveries of a wide range of systems from the various superfluids and superconductors in condensed-matter physics to neutron stars and color superconductors in cosmology and high-energy physics. Among them, materials such as superfluid ^{3}He and p-, d-wave superconductors display a number of remarkable features due to the interplay between their internal degrees of freedom and the coherent motion of the center-of-mass degree of freedom [4].

However, the parameters of the above systems, e.g., the magnitude of the interparticle interaction, are predetermined by Nature and cannot be manipulated at will. Furthermore, in such complex systems the primary physical principles governing the system's properties are sometimes masked by side effects, making it difficult for them to be unveiled. On the other hand, since the first experimental realizations of Bose-Einstein condensates (BECs) in 1995 [5, 6, 7], ultracold atoms have attracted attention of scientists not only in atomic physics but also in many other fields of physics. The study of ultracold atoms, for example, in an optical lattice is expected to help us understand further about high-$T_{\rm c}$ superconductors in condensed-matter physics. Compared to other systems, the interaction between ultracold atoms can be described to a good approximation in terms of a small number of well-defined parameters. This is because the atomic gases are so dilute that the average distance between atoms is much larger than the effective range of interaction, making the details of the interaction irrelevant. At ultralow temperatures, the collision of two atoms is dominated by the s-wave channel, and the result of the collision can be described by a single parameter: the s-wave scattering length a. As long as a is not too large, physical properties of the system are functions of the dimensionless parameter na^3, where n is the particle-number density. Furthermore, the magnitude of the interaction, which is proportional to the scattering length, can be varied under control by using the so-called Feshbach resonance [8, 9]. Since the properties of ultracold atoms can be readily manipulated and measured in experiments, they are considered to be an ideal table-top quantum simulator to study universal properties of other physical systems.

For alkali-metallic atoms with a single electron in the s-orbital of the outermost shell, due to the hyperfine interaction the eigenvalues of $\hat{\mathbf{F}}^2$ and $\hat{F}_z$ are the good quantum numbers with $\hat{\mathbf{F}} = \hat{\mathbf{I}} + \hat{\mathbf{J}}$ being the total spin of the atom. Here $\hat{\mathbf{I}}$ and $\hat{\mathbf{J}}$ are the nuclear and electronic spins, respectively. For these atoms, the hyperfine states $|F, m_F\rangle$ $(m_F = -F, \ldots, F)$ play the role of internal degrees of freedom in a way similar to the spin degrees of freedom of a single electron. In the beginning after the realization of the first BECs, atoms are confined in a magnetic trap and only atoms in the low-field-seeking hyperfine states can be trapped by the magnetic field; therefore, the internal degrees of freedom of the atoms become irrelevant. After that, thanks to

the introduction of the optical trap [10], atoms in all hyperfine states can now be confined in the trap as they feel almost the same trapping potential. This is due to the electric dipole moment that is induced on the polarizable atoms by the optical electric field, leading to the "spinor" behavior of the atoms. Similar to other quantum fluids with internal degrees of freedom, spinor gases, in particular spinor BECs, have exhibited a number of fascinating features due to the interplay between the phase coherence and the magnetic order [11, 12]. Noticeable examples are the coherent spin-mixing dynamics [13], formation of spin domains and topological defects due to spontaneous symmetry breaking [14], periodic magnetic patterns arising from dynamical instabilities [15], collapsing dynamics of a condensate triggered by the magnetic dipole-dipole interaction [16], etc. Remarkably, these phenomena can be well described at least qualitatively based on the mean-field theory.

However, this is not always true. I, in collaboration with Prof. Masahito Ueda and Prof. Yuki Kawaguchi, find that there are particular features of spinor BECs that the mean-field theory cannot give an accurate description even qualitatively. This is because the essence of these features is based on the effects of quantum fluctuations that are ignored in the mean-field theory. As an illustration, let us consider a condensate of atoms in the $F = 2$ hyperfine spin manifold. The order parameter of the system has five components corresponding to the five magnetic sublevels $m_F = -2, \cdots, 2$. Depending on the relative strengths of spin-dependent interactions, the ground state can be one of a number of phases, whose order parameters are not transformed continuously between each other at the phase boundaries (see Fig. 1.1). The distinct symmetries of these phases in spin space also imply that the phase transitions are first order. From the conventional wisdom, it is expected that these first-order transitions are accompanied by metastable states. However, the excitation spectrum obtained by the Bogoliubov analysis indicates that there is no metastable state associated with any of these phase transitions. Moreover, spin-dynamics measurements of the spin-2 ^{87}Rb BEC [17] seem to have observed a metastability as the dynamics of the condensate was found to be extremely slow if the system had been prepared in either one of two initial states: the ground state and a metastable state. We point out that this inconsistency in fact originates from the fact that the Bogoliubov spectrum [18] is obtained by considering a small amplitude expansion of the order parameter around the mean field with the linearized Gross-Pitaevskii energy functional which consists of only terms up to the fourth order in the order parameter [19]. This energy functional is equivalent to the Landau's $\phi^2 + \phi^4$ model of second-order phase transitions. In contrast, the description of first-order phase transitions requires higher-order terms beyond ϕ^4, and in gaseous BECs these higher-order terms only arise from quantum fluctuations. In other words, in the system under consideration the metastability, if it exists, is induced by fluctuations.

Consequently, it is necessary to develop a theoretical framework for spinor BECs in which the effects of quantum fluctuations are taken into account. In fermionic systems, we often use a formalism such as the Hartree-Fock approximation in which the motion of a particle and the influence it receives from the interaction with the other particles are treated self-consistently. In the language of Feynman diagrams, the Green's function appearing in each diagrammatic contribution to the self-energy is taken to be the interacting Green's function, which is to be updated by the newly obtained self-energy [20]. However, the situation becomes much more complicated for the case of bosons. A similar approach applied to a BEC leads to an artifact of the excitation spectrum of phonons having a nonzero energy gap [21, 22]. This contradicts the Nambu-Goldstone theorem which states that the phonon excitations arising from spontaneous symmetry breaking should be gapless [23, 24]. The origin of this discrepancy is that unlike the case of fermions, the Green's function and self-energy of a BEC contain the so-called anomalous component besides the normal one. This anomalous component represents the creation of a pair of noncondensed particles out of the condensate. The replacement of a noninteracting Green's

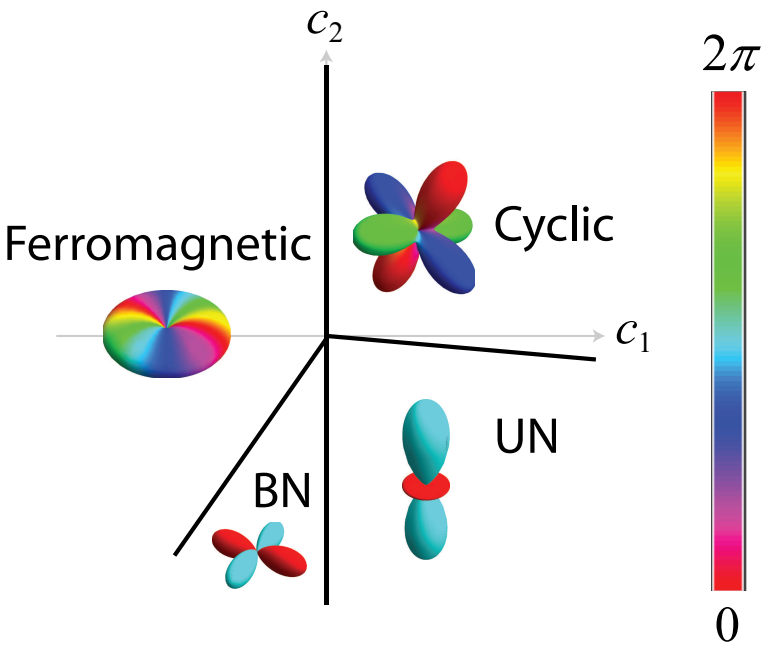

Figure 1.1: Ground-state phase diagram of $F = 2$ Bose-Einstein condensates. Depending on the relative strengths of the spin-dependent interactions c_1 and c_2, the ground state can be one of the four phases: ferromagnetic, cyclic, uniaxial-nematic (UN), and biaxial-nematic (BN) phases. The spinor order parameter $\boldsymbol{\xi} = (\xi_2, \ldots, \xi_{-2})^{\mathrm{T}}$ for each phase is given in Sec. 4.1. The insets show the surface plots of $|\psi(\theta, \phi)|^2 \equiv |\sum_{m=-2}^{2} \xi_m Y_2^m(\theta, \phi)|^2$, where Y_2^m's are the spherical harmonic functions of rank 2 and the hue indicates the phase of $\psi(\theta, \phi)$ according to the color gauge on the right.

function by an interacting one in the Feynman diagrams of the anomalous self-energy leads to double counting of contributions from different diagrams [25]. Therefore, to avoid double counting and the ensuing artifact of a gapful phonon mode, we apply a perturbation theory in which for a given order of approximation the contribution from each Feynman diagrams can be calculated in a fully controlled manner. Such a perturbation theory is valid as long as the interaction in the atomic gas is not too strong, which is the case of typical experiments. The Green's function approach that takes into account the next-order approximation beyond the Bogoliubov theory was first proposed by Beliaev in 1958 for a scalar BEC [26, 27]. In this thesis, we develop the spinor version of the Beliaev theory to derive the excitation energy spectrum of spinor BECs, from which numerous properties including the system's stability can be studied. Using the spinor Beliaev theory, we show in Sec. 4.3 that the metastable states that cannot be captured by the Bogoliubov theory indeed appear around the phase boundaries. The presence of a metastable condensate also implies an interesting possibility of a decay of the metastable state into the ground state via macroscopic quantum tunneling (MQT) in which all atoms tunnel simultaneously from one phase to the other. In Sec. 4.4, we evaluate the time scale of the MQT for the cyclic-uniaxial nematic phase transition as it is relevant to experiments of the spin-2 ^{87}Rb BEC.

Besides the first-order phase transitions whose metastable states are induced by quantum fluctuations, we find that there is also in spinor BECs another class of first-order phase transitions that have no metastable state around their phase boundaries. We show that in this case the absence of metastability holds to all orders of approximation. This appears to be contrary to the conventional wisdom that every first order phase transition is accompanied by a metastable state, but in fact there are other examples of this kind of phase transitions such as the ferromagnetic XXZ spin model in which a level crossing happens as the interaction anisotropy is varied [28]. Such phase transitions are characterized by the fact that the Hamiltonian possesses a special symmetry at the phase boundary so that the energy landscape becomes flat. The ground state would then abruptly change to an unstable state without undergoing a transient regime of metastability as the system crosses the phase boundary. This is in contrast to the case of conventional first-order phase transitions where the energy landscape features a double-well structure at the transition point, and therefore, supports the coexistence of two phases [29]. In Sec. 4.5, we investigate in details the symmetry of the Hamiltonian that underlies the flat energy landscape in both spin-1 and spin-2 BECs. It is a high symmetry of the Hamiltonian at the phase boundary that prohibits the metastability to all orders of approximation.

Although first-order phase transitions are usually identified by a finite jump in the first derivative of the ground-state energy with respect to the parameter that drives the transition, the flat energy landscape at the phase boundary suggests the criticality appearing in the dynamics of these phase transitions. In Chap. 5, we investigate the dynamics of a spin-1 BEC in the polar-antiferromagnetic phase transition which is a first-order phase transition without metastable states. Both instantaneous and slow quenches of a system's parameter are studied, and we find that in either case the system's dynamics demonstrates the critical features in a manner similar to second-order phase transitions. In other words, such a phase transition show the properties of either a first-order or a second-order phase transition depending on whether its static or dynamical features are concerned.

Another remarkable effect of quantum fluctuations that we have found is the emergence of a nonzero energy gap of the so-called quasi-Nambu-Goldstone (quasi-NG) modes, which are the extra gapless excitations at the mean-field level that are not generated by spontaneous symmetry breaking [30, 31]. This is similar to the quantum symmetry breaking or quantum anomaly in high-energy physics in which the symmetry of the vacuum's manifold is broken only if the one-loop quantum correction to the tree approximation is taken into account [32].

After first being introduced in the context of gauge theories, quasi-NG modes have become an important element in the theories of technicolor and supersymmetry [33, 34, 35]. They are also predicted to appear in the weak-coupling limit of the A phases of superfluid ^{3}He [36] and spin-1 color superconductors [37]. Despite their prevalence in various fields of physics, no experimental evidence of the quasi-NG modes has hitherto been observed. Recently, it was found that the nematic phase of spin-2 BECs can be a host of quasi-NG modes, leading to a renewed interest in this special kind of excitations [38]. At the mean-field level, all nematic phases are degenerate and quasi-NG modes are gapless. However, the zero-point fluctuations lift this degeneracy in a way similar to the vacuum alignment in quantum field theory. Consequently, it is predicted that with quantum corrections the quasi-NG modes would acquire a nonzero energy gap whose magnitude is of the same order as the zero-point energy. In Chap. 6, we prove explicitly the above conjecture of quasi-NG modes becoming gapful by deriving the analytic expression for the emergent energy gap in terms of the fundamental interaction parameters. Regarding the magnitude of the energy gap, we find that it is not necessarily of the same order as the zero-point energy. In fact, it depends on the relative strengths of the spin-dependent interactions. From the obtained magnitude of the energy gap, we have been able to evaluate the critical temperature above which a topological defect such as a vortex of spin nematicity would decay by emitting thermally excited quasi-NG modes. Conversely, below this temperature the vortex would be stabilized by suppressing the emission of these excitations. In Sec. 6.2, we examine how the propagation velocity of quasi-NG modes is affected by the particle-density fluctuations in the condensate. We find that it decreases as opposed to the enhancement of the sound velocity.

At the level of the Bogoliubov theory, all the quasiparticles in spinor BECs including phonons, magnons, and quasi-NG modes have infinitely long lifetimes. However, by going to the next-order approximation, it can be shown that their lifetimes are actually limited by their decays via the collisions with the condensate atoms. This mechanism is called the Beliaev damping [26, 39]. In Chap. 7, we calculate the damping rates of various types of quasiparticles in a spin-2 condensate. We find that a magnon can decay by forming a quasi-NG mode and another magnon with a rate proportional to $|\mathbf{p}|^3$ where $\hbar\mathbf{p}$ is the momentum. The obtained damping rate, which is a function of the coupling constants, also suggests an alternative approach to measuring precisely the magnitudes of the spin-dependent interactions. We then propose an experimental scheme to measure the lifetime of magnons by temporarily switching on an external magnetic field. On the other hand, the damping of phonons can occur via a number of decay channels, leading to their damping rate being composed of two contributions with different scaling laws with respect to the momentum: one is linear to $|\mathbf{p}|$ and the other is proportional to $|\mathbf{p}|^5$. The former would dominate the damping rate in the low-momentum regime, while the latter is the only contribution in scalar BECs. In contrast, there is no decay channel for quasi-NG modes that satisfies the energy conservation.

This thesis is organized as follows (the flow chart is shown in Fig. 1.2). In Chap. 2 we review the theoretical and experimental aspects of spinor BECs that are based on the mean-field framework. The ground-state phase diagrams of spin-1 and spin-2 BECs at the mean-field level are introduced in Sec. 2.3. The first-order (Bogoliubov) excitation spectra for all possible phases are summarized in Sec. 2.4. In Chap. 3, we introduce the formalism of the Beliaev theory of scalar BECs based on a Green's function approach. We show the second-order (Beliaev) spectrum of phonons in Sec. 3.2, from which it can be seen that the sound velocity is enhanced and a Beliaev damping appears. In Chap. 4, we develop the spinor Beliaev theory and apply it to spin-2 BECs to analyze the stability of each phase in the phase diagram. We find in Sec. 4.3 a class of first-order quantum phase transitions whose accompanied metastable states are induced by quantum fluctuations. The possibility of macroscopic quantum tunneling from

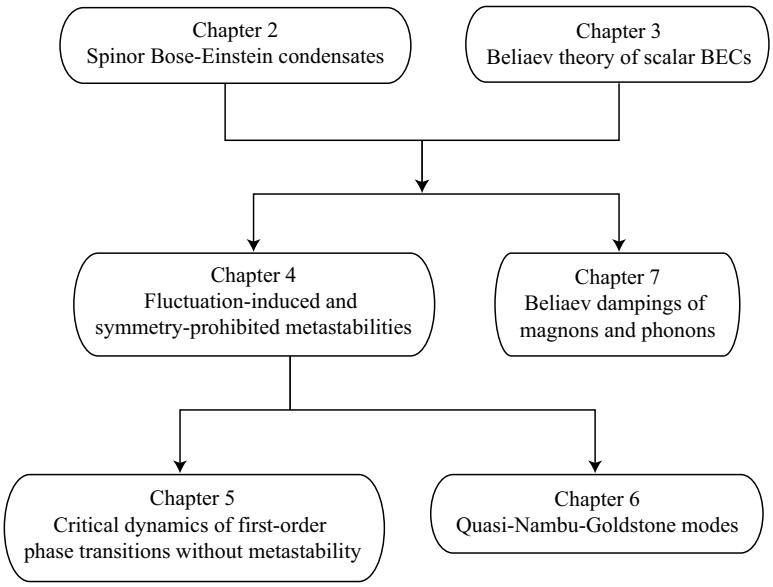

Figure 1.2: Flow chart of the thesis. Chapters 2 and 3 review spinor Bose-Einstein condensates and the Beliaev theory of scalar BECs, respectively. Our results are presented in chapters 4–7.

a metastable state to the ground state is discussed in Sec. 4.4. Another class of first-order quantum phase transitions for which the metastability is prohibited by the high symmetry of the Hamiltonian at the phase boundary is investigated for both spin-1 and spin-2 BECs in Sec. 4.5. In Chap. 5, we study the dynamics of these first-order phase transitions in the context of both instantaneous and slow quenches, in which the criticality is revealed in a manner similar to second-order phase transitions. In Chap. 6, we discuss the modifications of the quasi-NG modes due to quantum fluctuations where the emergent energy gap and the suppression factor of the propagation velocity are analytically derived in Sec. 6.1 and 6.2, respectively. In Chap. 7, we examine in details the Beliaev dampings of various types of quasiparticles in a spin-2 BEC. Finally, in Chap. 8, we summarize this thesis and discuss some outstanding open problems. Some detailed calculations are relegated to the Appendices to avoid digressing from the main subject.

The results in Chaps. 4–7 are based on Refs. [40, 41, 42, 43] which have been done in collaboration with Y. Kawaguchi and M. Ueda.

Chapter 2

Spinor Bose-Einstein condensates

Bose-Einstein condensation (BEC) was predicted by Einstein [44, 45] almost a century ago for a system of bosons cooled to below a critical temperature. A system of noninteracting particles undergoes the BEC as a macroscopic number of particles occupy the single-particle state with the lowest energy. In a homogeneous system, it is the zero-momentum state. For an interacting system, BEC can be formally defined by the presence of a macroscopic eigenvalue of the single-particle reduced density matrix [46]. This macroscopic eigenvalue represents the number of particles in the condensate. The system is then said to have an off-diagonal long-range order (ODLRO).

The first dilute-gas BECs were first observed in 1995 using dilute gases of ^{87}Rb [5], ^{23}Na [6], and ^{7}Li atoms [7]. The atoms were confined in magnetic traps and cooled to temperatures of the order of micro Kelvin by combining laser and evaporative coolings. The appearance of the condensate was evident from the observed velocity distribution of atoms in which a narrow peak at zero momentum arises above a broad background of thermal atoms. Since then, the BECs of other isotopes and atomic species such as ^{85}Rb [47], ^{41}K [48], and ^{133}Cs [49] as well as hydrogen [50] and metastable helium [51] have been achieved.

2.1 Internal degrees of freedom of Bose gases

For alkali-metal atoms with a single electron in the s-orbital of the outermost shell, the eigenvalues of $\hat{\mathbf{F}}$ and $\hat{F}_z$ are the good quantum numbers due to the hyperfine interaction. Here $\hat{\mathbf{F}} = \hat{\mathbf{I}} + \hat{\mathbf{J}}$ is the total angular momentum with $\hat{\mathbf{I}}$ and $\hat{\mathbf{J}}$ are the nuclear and electronic spins, respectively. The hyperfine states $|F, m_F\rangle$ ($m_F = -F, \ldots, F$) then play the role of the internal degrees of freedom. For the atomic species that form stable spinor condensates such as ^{87}Rb and ^{23}Na, $I = 3/2$ and $J = 1/2$ so that the total angular momentum F can takes a value of either $F = 1$ or $F = 2$. However, in a magnetic trap the atoms can only populate the so-called low-field-seeking hyperfine states such as the $|F = 1, m_F = -1\rangle$ and $|F = 2, m_F = 1, 2\rangle$ states [19]. Atoms in the other hyperfine states find a barrier potential at the center of the magnetic trap, and thus escape from the confinement. This leads to the atoms not being able to transfer freely among all of their hyperfine states.

In contrast, in an optical dipole trap [10], the atoms are subject to a potential that is almost independent of the atomic hyperfine state. This potential is due to the electric dipole moment that is induced by the optical electric field on the polarizable atoms. Analogous to the electronic spin, the internal degrees of freedom of the atoms become relevant, leading to their "spinor" behaviors. Since the hyperfine splitting has a magnitude of the order of 1 GHz corresponding to a temperature much higher than the system's temperature in typical experiments of ultracold atoms, there is almost no possibility for atoms in the lower $F = 1$ spin manifold to jump into the

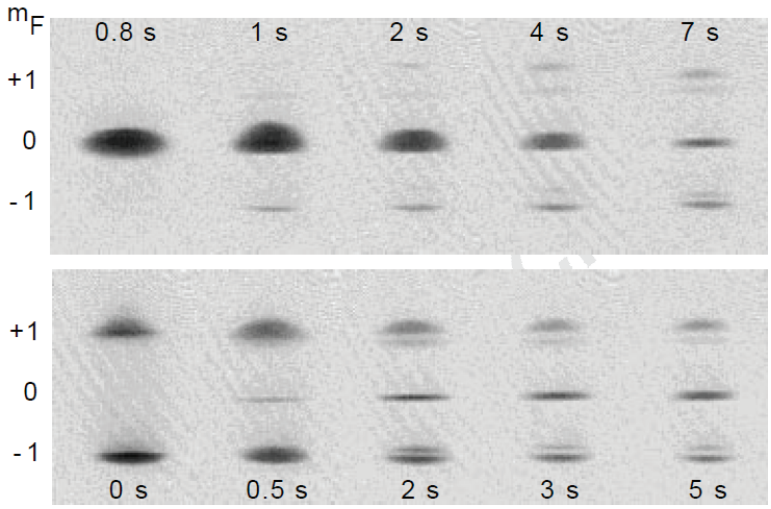

Figure 2.1: Formation of the spin domains in a spin-1 ^{23}Na BEC. Absorption images of ballistically expanding spinor condensates show both the spatial and hypefine distributions. The images of clouds with various dwell times in the trap show the evolution to the same equilibrium state for condensates prepared in either a pure $m_F = 0$ state (upper row) or in equally populated $m_F = \pm 1$ states (lower row). The bias field during the dwell time was $B_0 = 20$ mG, and the field gradient was $B' = 11$ mG cm^{-1}. (Figure reproduced with permission from Ref. [52])

upper $F = 2$ spin manifold. The populations of atoms in the different hyperfine states within a single spin manifold can be measured by using a magnetic field gradient to spatially separate the atoms in the Stern-Gerlach experiment. This method was used to verify the theoretical prediction of the ground-state phase diagram of the ^{23}Na BEC in the $F = 1$ spin manifold (see Fig. 2.1) [52]. To show that all the atoms in the condensate occupy a common single-particle state, the observation of the coherent spin dynamics was performed with the spin-1 ^{23}Na BEC [53, 54]. On the other hand, the ^{23}Na atoms prepared in the $F = 2$ spin manifold have a very short lifetime due to their strong hyperfine relaxations by which the atoms' excessive internal energy is converted to their kinetic energy, accelerating their escape from the trapping potential [55]. In contrast, it was observed that both spin-1 and spin-2 ^{87}Rb BECs are stable in the optical dipole trap [13, 56, 57, 17, 58]. This is due to the fortuitous properties of the molecular potential of the rubidium dimer [59].

2.2 Spin-dependent interactions

In dilute atomic gases with a typical particle-number density of $n \lesssim 10^{15}$ cm^{-3}, the mean atomic distance is much larger than the effective range of interaction which is of the order of an angstrom. Consequently, the details of the interaction become irrelevant, and the effect of the interaction can approximately be described by binary collisions. The typical temperature of the ultracold atoms is of the order of hundreds nano Kelvin to micro Kelvin. This temperature is equivalent to an extremely small energy compared to the energy scale of the effective range of interaction. This means that the two atoms with a nonzero relative orbital angular momentum will confront such a high centrifugal potential barrier that prohibits their approach to a close enough distance for the interaction. Therefore, in dilute weakly interacting ultracold atomic systems, only the s-wave collision channel is relevant, and all the effects of the interaction are encapsulated in a single parameter: the s-wave scattering length.

In general, the interaction of two atoms is sensitive to their atomic states in a complicated manner. However, for ultracold atoms which contain very few uncontrollable impurities, the rotational symmetry simplifies the interaction to a great extent. In the absence of any source of rotational symmetry breaking such as external fields, the sum of the total orbital angular momentum $L_{\rm pair}$ and the total spin angular momentum $F_{\rm pair}$ of a pair of atoms is conserved. Even under a weak enough magnetic field, the above rotational symmetry is essentially valid to a good approximation. Moreover, except for the atomic species with a high spin angular momentum such as ^{52}Cr, the magnetic dipole-dipole interaction is small enough to be ignored. This corresponds to the neglect of the hyperfine relaxation interaction in which a change in $F_{\rm pair}$ is compensated by a change in $L_{\rm pair}$ so that the total is conserved. With this approximation, both $F_{\rm pair}$ and $L_{\rm pair}$ are good quantum numbers.

Furthermore, the parity of $F_{\rm pair}$ is constrained by the quantum statistics of the constituent particles. The total wavefunction of a system of identical spin-F atoms must acquire a factor of $(-1)^{2F}$ under an exchange of any two particles. On the other hand, by the same exchange of particles the orbital and spin parts of the wavefunction acquire factors of $(-1)^{L_{\rm pair}}$ and $(-1)^{F_{\rm pair}+2F}$, respectively. Therefore, to be consistent we must require that $L_{\rm pair}+F_{\rm pair}$ be even. Since only the s-wave scattering channel is relevant, i.e., $L_{\rm pair}=0$, $F_{\rm pair}$ is restricted to even values. The interaction can then be expressed as

$$\hat{V}=\sum_{(i,j)}\delta^{(3)}(\mathbf{r}_i-\mathbf{r}_j)\sum_{\text{even } F_{\rm pair}}\frac{4\pi\hbar^2 a_{F_{\rm pair}}}{M}\hat{P}_{F_{\rm pair}}, \tag{2.1}$$

where M is the atomic mass, $a_{F_{\rm pair}}$ and $\hat{P}_{F_{\rm pair}}$ denote the s-wave scattering length and the projection operator onto the subspace of total spin $F_{\rm pair}$, and the sum is taken over pairs of particles, labeled by i and j. Here, we use the pseudopotential approximation with the contact interaction, which is valid at the mean-field level [60]. At higher-order approximations, the one-loop correction to the interaction is needed. The projection operators $\hat{P}_{F_{\rm pair}}$ are related to the identity and the spin-product operators by

$$\hat{I}_1\otimes\hat{I}_2=\sum_{F_{\rm pair}}\hat{P}_{F_{\rm pair}}, \tag{2.2}$$

$$\hat{\mathbf{F}}_1\cdot\hat{\mathbf{F}}_2=\sum_{F_{\rm pair}}\left[\frac{F_{\rm pair}(F_{\rm pair}+1)}{2}-F(F+1)\right]\hat{P}_{F_{\rm pair}}. \tag{2.3}$$

In the following, we consider the interactions of spin-1 and spin-2 atoms.

2.2.1 Spin-1 atoms

For atoms in the $F=1$ spin manifold, $F_{\rm pair}$ can take the value of either $F_{\rm pair}=0$ or $F_{\rm pair}=2$ since the interaction in the total spin $F_{\rm pair}=1$ channel is irrelevant due to the quantum statistics. Equations (2.2) and (2.3) then reduce to

$$\hat{I}_1\otimes\hat{I}_2=\hat{P}_0+\hat{P}_2, \tag{2.4}$$

$$\hat{\mathbf{F}}_1\cdot\hat{\mathbf{F}}_2=\hat{P}_2-2\hat{P}_0. \tag{2.5}$$

Combined with Eq. (2.1), the interaction of spin-1 bosons can be rewritten as [61, 62]

$$\hat{V}_{F=1}=\sum_{(i,j)}\delta^{(3)}(\mathbf{r}_i-\mathbf{r}_j)\left[c_0\hat{I}_i\otimes\hat{I}_j+c_1\hat{\mathbf{F}}_i\cdot\hat{\mathbf{F}}_j\right], \tag{2.6}$$

where

$$c_0 \equiv \frac{4\pi\hbar^2}{M}\frac{a_0+2a_2}{3}, \tag{2.7a}$$

$$c_1 \equiv \frac{4\pi\hbar^2}{M}\frac{a_2-a_0}{3}. \tag{2.7b}$$

In the second quantization, the interaction Hamiltonian takes the form of

$$\hat{V}_{F=1} = \frac{1}{2}\int \mathrm{d}^3\mathbf{r}\,[c_0 : \hat{n}^2(\mathbf{r}) : + c_1 : \hat{\mathbf{F}}^2(\mathbf{r}) :], \tag{2.8}$$

where the particle-density and spin-density operators are defined as

$$\hat{n}(\mathbf{r}) = \sum_{j=-1}^{1} \hat{\psi}_j^\dagger(\mathbf{r})\hat{\psi}_j(\mathbf{r}), \tag{2.9}$$

$$\hat{\mathbf{F}}(\mathbf{r}) = \sum_{i,j=-1}^{1} \hat{\psi}_i^\dagger(\mathbf{r})\mathbf{f}_{i,j}\hat{\psi}_j(\mathbf{r}) \tag{2.10}$$

with $\hat{\psi}_j(\mathbf{r})$ being the annihilation operator of a particle at position $\mathbf{r}$ in the magnetic sublevel $m_F = j$. The spin-1 matrices are given by

$$f_x = \frac{1}{\sqrt{2}}\begin{pmatrix} 0 & 1 & 0 \\ 1 & 0 & 1 \\ 0 & 1 & 0 \end{pmatrix}, f_y = \frac{i}{\sqrt{2}}\begin{pmatrix} 0 & -1 & 0 \\ 1 & 0 & -1 \\ 0 & 1 & 0 \end{pmatrix}, f_z = \begin{pmatrix} 1 & 0 & 0 \\ 0 & 0 & 0 \\ 0 & 0 & -1 \end{pmatrix}. \tag{2.11}$$

2.2.2 Spin-2 atoms

Similarly, for $F = 2$ atoms $F_{\mathrm{pair}} = 0$, 2, or 4. From the relations

$$\hat{I}_1 \otimes \hat{I}_2 = \hat{P}_0 + \hat{P}_2 + \hat{P}_4, \tag{2.12}$$

$$\hat{\mathbf{F}}_1 \cdot \hat{\mathbf{F}}_2 = -6\hat{P}_0 - 3\hat{P}_2 + 4\hat{P}_4, \tag{2.13}$$

the interaction of spin-2 atoms can be rewritten as [63, 64]

$$\hat{V}_{F=2} = \sum_{(i,j)} \delta^{(3)}(\mathbf{r}_i - \mathbf{r}_j)\left[c_0\hat{I}_i \otimes \hat{I}_j + c_1\hat{\mathbf{F}}_i \cdot \hat{\mathbf{F}}_j + c_2\hat{P}_0^{i,j}\right], \tag{2.14}$$

where

$$c_0 \equiv \frac{4\pi\hbar^2}{M}\frac{4a_2+3a_4}{7}, \tag{2.15a}$$

$$c_1 \equiv \frac{4\pi\hbar^2}{M}\frac{a_4-a_2}{7}, \tag{2.15b}$$

$$c_2 \equiv \frac{4\pi\hbar^2}{M}\frac{7a_0-10a_2+3a_4}{7}. \tag{2.15c}$$

In the second quantization, the interaction Hamiltonian takes the form of

$$\hat{V}_{F=2} = \frac{1}{2}\int \mathrm{d}^3\mathbf{r}\,[c_0 : \hat{n}^2(\mathbf{r}) : + c_1 : \hat{\mathbf{F}}^2(\mathbf{r}) : + c_2\hat{A}_{00}^\dagger(\mathbf{r})\hat{A}_{00}(\mathbf{r})], \tag{2.16}$$

where the particle-density and spin-density operators are defined in a way similar to those of spin-1 atoms, and the spin-singlet-pair amplitude operator is introduced as

$$\hat{A}_{00}(\mathbf{r}) = \frac{1}{\sqrt{5}} \sum_{j=-2}^{2} (-1)^j \hat{\psi}_j(\mathbf{r}) \hat{\psi}_{-j}(\mathbf{r}). \tag{2.17}$$

The spin-2 matrices are given by

$$f_x = \begin{pmatrix} 0 & 1 & 0 & 0 & 0 \\ 1 & 0 & \sqrt{3/2} & 0 & 0 \\ 0 & \sqrt{3/2} & 0 & \sqrt{3/2} & 0 \\ 0 & 0 & \sqrt{3/2} & 0 & 1 \\ 0 & 0 & 0 & 1 & 0 \end{pmatrix}, \; f_y = \begin{pmatrix} 0 & -i & 0 & 0 & 0 \\ i & 0 & -i\sqrt{3/2} & 0 & 0 \\ 0 & i\sqrt{3/2} & 0 & -i\sqrt{3/2} & 0 \\ 0 & 0 & i\sqrt{3/2} & 0 & -i \\ 0 & 0 & 0 & i & 0 \end{pmatrix},$$

$$f_z = \begin{pmatrix} 2 & 0 & 0 & 0 & 0 \\ 0 & 1 & 0 & 0 & 0 \\ 0 & 0 & 0 & 0 & 0 \\ 0 & 0 & 0 & -1 & 0 \\ 0 & 0 & 0 & 0 & -2 \end{pmatrix}. \tag{2.18}$$

2.3 Mean-field ground-state phase diagram

With Bose-Einstein condensation, a macroscopic number of particles occupy a common single-particle state. In the mean-field approximation, quantum fluctuations are neglected and it is assumed that at zero temperature all particles occupy a single spatial mode and a spin state which is generally a superposition of different magnetic sublevels. For a spatially homogeneous system, the spatial mode of the condensate is the zero momentum $\mathbf{p} = \mathbf{0}$ state. Consequently, the normalized state vector is written as

$$|\xi\rangle = \frac{1}{\sqrt{N!}} \left(\sum_{j=-F}^{F} \xi_j \hat{a}_{j,\mathbf{0}} \right)^N |\mathrm{vac}\rangle, \tag{2.19}$$

where $|\mathrm{vac}\rangle$ and N denote the vacuum and the total number of particles, respectively, and the weights ξ_j's are normalized to unity:

$$\sum_{j=-F}^{F} |\xi_j|^2 = 1. \tag{2.20}$$

The operator $\hat{a}_{j,\mathbf{p}}$ which annihilates a particle with momentum $\hbar\mathbf{p}$ in the magnetic sublevel $m_F = j$ is related to the field operator $\hat{\psi}_j(\mathbf{r})$ by a Fourier transformation

$$\hat{a}_{j,\mathbf{p}} = \int \mathrm{d}^3\mathbf{r} \, \frac{e^{-i\mathbf{p}\cdot\mathbf{r}}}{\sqrt{V}} \hat{\psi}_j(\mathbf{r}), \tag{2.21}$$

where V denotes the volume of the system. Using Eqs. (2.19) and (2.21), it is straightforward to obtain the expectation value of different operator products with respect to the state vector

$|\xi\rangle$:

$$\langle\hat{\psi}_j(\mathbf{r})\rangle_{|\xi\rangle} = \langle\hat{\psi}_j^\dagger(\mathbf{r})\rangle_{|\xi\rangle} = 0, \tag{2.22}$$

$$\langle\hat{\psi}_j^\dagger(\mathbf{r})\hat{\psi}_{j'}(\mathbf{r})\rangle_{|\xi\rangle} = n\,\xi_j^*\xi_{j'}, \tag{2.23}$$

$$\langle\hat{\psi}_{j_1}^\dagger(\mathbf{r})\hat{\psi}_{j_2}^\dagger(\mathbf{r})\hat{\psi}_{j_2'}(\mathbf{r})\hat{\psi}_{j_1'}(\mathbf{r})\rangle_{|\xi\rangle} = \left(1-\frac{1}{N}\right) n^2\,\xi_{j_1}^*\xi_{j_2}^*\xi_{j_1'}\xi_{j_2'}, \tag{2.24}$$

where $n = N/V$ is the total particle-number density. For a macroscopic condensate with $N \sim 10^6$, the factor $1/N$ in Eq. (2.24) can be ignored. As a result, the mean-field energy of a BEC can be obtained by replacing the field operators $\hat{\psi}_j$ and $\hat{\psi}_j^\dagger$ in the Hamiltonian with the condensate wavefunction $\boldsymbol{\psi} = \sqrt{n}(\xi_F, \ldots, \xi_{-F})^{\mathrm{T}}$ and its complex conjugate, respectively. In the following, we list the possible mean-field ground states of spin-1 and spin-2 BECs obtained by minimizing the mean-field energy functionals [12].

2.3.1 Spin-1 BECs

In the presence of a homogeneous external magnetic field, the Hamiltonian of a spin-1 BEC is given as

$$\hat{H} = \int \mathrm{d}^3\mathbf{r} \sum_{j=-1}^{1} \left[\hat{\psi}_j^\dagger(\mathbf{r})\left(-\frac{\hbar^2\nabla^2}{2M}\right)\hat{\psi}_j(\mathbf{r}) + qj^2\hat{\psi}_j^\dagger\hat{\psi}_j\right] + \hat{V}_{F=1}, \tag{2.25}$$

where $\hat{V}_{F=1}$ is the interatomic interaction given in Eq. (2.8) and the second term in the square brackets describes the quadratic Zeeman shift of the atomic energy. Here the linear Zeeman energy is suppressed due to the conservation of the total longitudinal magnetization in an isolated system. Since the ultracold atoms are confined in a vacuum chamber, they form an isolated system to a good approximation. The constraint on the magnetization can be mathematically replaced by the introduction of a Lagrange multiplier which cancels the linear Zeeman energy completely for systems prepared in a state with zero total longitudinal magnetization. This is equivalent to going onto a frame rotating at the same frequency as the Larmor precession of the atoms' spin vectors.

Applying the arguments below Eq. (2.24) to the Hamiltonian (2.25), we obtain the mean-field energy functional as

$$\frac{E[\boldsymbol{\psi}]}{V} = \sum_{j=-1}^{1} j^2|\psi_j|^2 + \frac{c_0}{2}n^2 + \frac{c_1}{2}\mathbf{F}^2, \tag{2.26}$$

where the spin density $\mathbf{F}$ is obtained from Eq. (2.10) with $\hat{\psi}_j$ being replaced by ψ_j. The time evolution of the condensate wavefunction $\boldsymbol{\psi}$ is given by the time-dependent Gross-Pitaevskii (GP) equation

$$\begin{aligned} i\hbar\frac{\partial\psi_j}{\partial t} &= \frac{\delta E}{\delta\psi_j^*} \\ &= qj^2\psi_j + c_0 n\psi_j + c_1\sum_{j'=-1}^{1}\mathbf{F}\cdot\mathbf{f}_{j,j'}\psi_{j'}. \end{aligned} \tag{2.27}$$

A stationary state, whose time evolution are given by $\psi_j(t) = \psi_j(0)e^{-i\mu t/\hbar}$ with μ being the

chemical potential, must satisfy the time-independent GP equation [12]

$$qj^2\psi_j + c_0 n\psi_j + c_1 \sum_{j'=-1}^{1} \mathbf{F}\cdot\mathbf{f}_{j,j'}\psi_{j'} = \mu\psi_j, \tag{2.28}$$

or written explicitly as

$$(q + c_0 n + c_1 F_z - \mu)\psi_1 + \frac{c_1}{\sqrt{2}} F_- \psi_0 = 0, \tag{2.29a}$$

$$\frac{c_1}{\sqrt{2}} F_+ \psi_1 + (c_0 n - \mu)\psi_0 + \frac{c_1}{\sqrt{2}} F_- \psi_{-1} = 0, \tag{2.29b}$$

$$\frac{c_1}{\sqrt{2}} F_+ \psi_0 + (q + c_0 n - c_1 F_z - \mu)\psi_{-1} = 0, \tag{2.29c}$$

where $F_\pm \equiv F_x \pm iF_y$.

All possible stationary states are obtained by solving Eqs. (2.29a)–(2.29c), and by comparing their energies, the ground state can be found. Because the system has a rotationally invariant symmetry about the z axis, without loss of generality we can take the transverse magnetization vector to point in the x direction; i.e., we can set $F_y = 0$. This leads to $\mathrm{Im}\psi_1 = \mathrm{Im}\psi_{-1}$. From the U(1) gauge invariant symmetry of the system, we can further choose ψ_0 to be a real number. By writing $\xi_{\pm 1} = \mathrm{Re}\xi_{\pm 1} + i\delta$, Eqs. (2.29a)–(2.29c) reduce to

$$(q + c_1 n F_z - \mu + c_0 n)\xi_1 + c_1 n(\mathrm{Re}\xi_1 + \mathrm{Re}\xi_{-1})\xi_0^2 = 0, \tag{2.30a}$$

$$[\mu - c_0 n - c_1 n(\mathrm{Re}\xi_1 + \mathrm{Re}\xi_{-1})(\mathrm{Re}\xi_1 + \mathrm{Re}\xi_{-1} + 2i\delta)]\xi_0 = 0, \tag{2.30b}$$

$$c_1 n(\mathrm{Re}\xi_1 + \mathrm{Re}\xi_{-1})\xi_0^2 + (q - c_1 n F_z - \mu + c_0 n)\xi_{-1} = 0. \tag{2.30c}$$

From Eq. (2.30b), we have either $\xi_0 = 0$ or $\mu = c_0 n + c_1 n(\mathrm{Re}\xi_1 + \mathrm{Re}\xi_{-1})(\mathrm{Re}\xi_1 + \mathrm{Re}\xi_{-1} + 2i\delta)$. In the former case, we have three stationary states:

Ferromagnetic phase. The spinor order parameter and the energy density are given by either

$$\boldsymbol{\xi}^{\mathrm{FM1}} = (e^{i\chi_1}, 0, 0)^{\mathrm{T}},\ \frac{E}{V} = q + \frac{(c_0 + c_1)n}{2} \tag{2.31}$$

with the maximum longitudinal magnetization pointing in the positive z direction: $F_z/n = 1$, or

$$\boldsymbol{\xi}^{\mathrm{FM2}} = (0, 0, e^{i\chi_{-1}})^{\mathrm{T}},\ \frac{E}{V} = q + \frac{(c_0 + c_1)n}{2} \tag{2.32}$$

with the maximum longitudinal magnetization pointing in the negative z direction: $F_z/n = -1$. The phases $e^{i\chi_{\pm 1}}$ are arbitrary due to the U(1) gauge invariant symmetry of the system.

Antiferromagnetic phase. The spinor order parameter and the energy density are given by

$$\boldsymbol{\xi}^{\mathrm{AFM}} = \left(\frac{e^{i\chi_1}}{\sqrt{2}}, 0, \frac{e^{i\chi_{-1}}}{\sqrt{2}}\right)^{\mathrm{T}},\ \frac{E}{V} = q + \frac{c_0 n}{2}. \tag{2.33}$$

This state is unmagnetized: $\mathbf{F} = \mathbf{0}$.

In the latter case, we have $\delta = 0$ since the chemical potential μ should be a real number. By solving Eqs. (2.30a) and (2.30c), we obtain two other stationary states.

Polar phase. The spinor order parameter and the energy density are given by

$$\boldsymbol{\xi}^{\mathrm{PL}} = (0, e^{i\chi_0}, 0)^{\mathrm{T}},\ \frac{E}{V} = \frac{c_0 n}{2}. \tag{2.34}$$

This phase is also unmagnetized.

Broken-axisymmetry (BA) phase. The spinor order parameter and the energy density are given by [65]

$$\xi_{\pm 1}^{\mathrm{BA}} = \frac{e^{i(\chi_0 \mp \chi_z)}}{2}\sqrt{\frac{q}{2c_1 n} + 1},\ \xi_0^{\mathrm{BA}} = e^{i\chi_0}\sqrt{\frac{1}{2} - \frac{q}{4c_1 n}},\ \frac{E}{V} = \frac{(q + 2c_1 n)^2}{8c_1 n} + \frac{c_0 n}{2}, \tag{2.35}$$

where the phases $e^{i\chi_0}$ and $e^{i\chi_z}$ correspond to the gauge and the rotation about the z axis, respectively. This phase can be stable only if $c_1 < 0$ (see Fig. 2.2). It has a nonzero transverse magnetization:

$$F_+ \equiv F_x + iF_y = e^{i\chi_z}\sqrt{1 - \left(\frac{q}{2|c_1|n}\right)^2},\ F_z = 0. \tag{2.36}$$

The direction of the transverse magnetization in the xy plane, which is determined by the value of χ_z, breaks the rotational symmetry of the Hamiltonian about the z axis.

By comparing the energies of the above stationary states, we obtain the mean-field ground-state phase diagram of spin-1 BECs as shown in Fig. 2.2. The phase diagram is the result of the competition between the spin-dependent interaction with the coupling constant c_1 and the quadratic Zeeman shift with the coefficient q. The spin-dependent interaction can be either ferromagnetic (i.e., $c_1 < 0$, e.g., ^{87}Rb) or antiferromagnetic (i.e., $c_1 > 0$, e.g., ^{23}Na). The sign and the magnitude of the quadratic Zeeman coefficient q can be varied by adjusting the detuning and the power of an applied microwave due to the AC Stark effect [66].

2.3.2 Spin-2 BECs

Similarly, the mean-field energy functional of a homogeneous spin-2 BEC in the absence of external fields is given by

$$\frac{E[\boldsymbol{\psi}]}{V} = \frac{1}{2}(c_0 n^2 + c_1|\mathbf{F}|^2 + c_2|A_{00}|^2), \tag{2.37}$$

where we have introduced the spin-singlet-pair amplitude $A_{00} = (2\psi_2\psi_{-2} - 2\psi_1\psi_{-1} + \psi_0^2)/\sqrt{5}$ which is absent in spin-1 BECs. We then obtain the time-independent GP equation for a stationary state as [63, 12]

$$(4q + c_0 n \pm 2c_1 F_z - \mu)\psi_{\pm 2} + c_1 F_{\mp}\psi_{\pm 1} + \frac{c_2}{\sqrt{5}}A_{00}\psi_{\mp 2}^* = 0, \tag{2.38a}$$

$$(q + c_0 n \pm c_1 F_z - \mu)\psi_{\pm 1} + c_1\left(\frac{\sqrt{6}}{2}F_{\mp}\psi_0 + F_{\pm}\psi_{\pm 2}\right) - \frac{c_2}{\sqrt{5}}A_{00}\psi_{\mp 1}^* = 0, \tag{2.38b}$$

$$(c_0 n - \mu)\psi_0 + \frac{\sqrt{6}}{2}c_1(F_+\psi_1 + F_-\psi_{-1}) + \frac{c_2}{\sqrt{5}}A_{00}\psi_0^* = 0. \tag{2.38c}$$

Similar to the case of spin-1 BECs, by solving Eq. (2.38) we get all possible stationary states. By comparing their energies, we obtain the mean-field ground-state phase diagram of spin-2 BECs shown in Fig. 2.3. Depending on the relative strengths c_1 and c_2 of the two spin-dependent

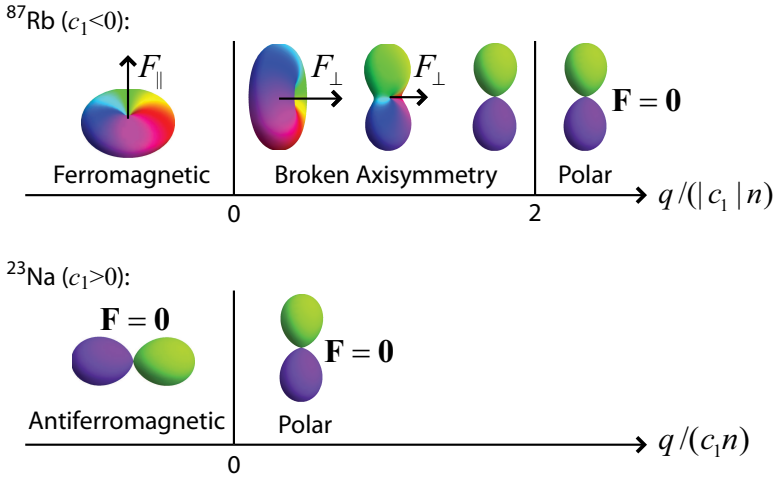

Figure 2.2: Mean-field ground-state phase diagrams of (a) spin-1 ^{87}Rb and (b) spin-1 ^{23}Na BECs, where the spin-dependent interaction is ferromagnetic ($c_1 < 0$) and antiferromagnetic ($c_1 > 0$), respectively. The ground-state phase depends on the ratio of the quadratic Zeeman energy q to the interaction energy $|c_1|n$. The insets show the surface plots of $|\psi(\theta,\phi)|^2 \equiv |\sum_{m=-1}^{1} \xi_m Y_1^m(\theta,\phi)|^2$, where Y_1^m's are the spherical harmonic functions of rank 1. The longitudinal and transverse magnetizations are denoted by $F_\parallel$ and $F_\perp$, respectively. The order parameter $\boldsymbol{\xi}^{\rm BA}$ of the broken-axisymmetry (BA) phase varies continuously as a function of $q/|c_1|n$ [see Eq. (2.35)].

interactions, the ground state is one of the following phases.

Ferromagnetic phase. The representative spinor order parameter and the energy density are given by

$$\boldsymbol{\xi}^{\rm FM} = (1,0,0,0,0)^{\rm T}, \ \frac{E}{V} = \frac{c_0 n}{2} + 2c_1 n \tag{2.39}$$

with the maximum magnitude of magnetization: $|\mathbf{F}|/n = 1$.

Cyclic phase. The representative spinor order parameter and the energy density are given by

$$\boldsymbol{\xi}^{\rm CL} = \left(\sqrt{\frac{1}{3}}, 0, 0, \sqrt{\frac{2}{3}}, 0\right)^{\rm T}, \ \frac{E}{V} = \frac{c_0 n}{2}. \tag{2.40}$$

Both the magnetization and spin-singlet-pair amplitude of this state vanish: $\mathbf{F} = \mathbf{0}$ and $A_{00} = 0$. In the many-body state corresponding to the cyclic phase, every three atoms form a spin-singlet trimer, and these trimers undergo the Bose-Einstein condensation [64, 67]. The energy difference between the cyclic phase and the many-body state of condensed trimers approaches zero in the thermodynamic limit (see, for example, Ref. [19]).

Nematic phase. The representative spinor order parameter of a nematic phase is characterized by an extra parameter η as [67, 68]

$$\boldsymbol{\xi}^{\rm N}(\eta) = \left(\frac{\sin\eta}{\sqrt{2}}, 0, \cos\eta, 0, \frac{\sin\eta}{\sqrt{2}}\right)^{\rm T}. \tag{2.41}$$

At the mean-field level, all nematic phases with different values of η are degenerate with the

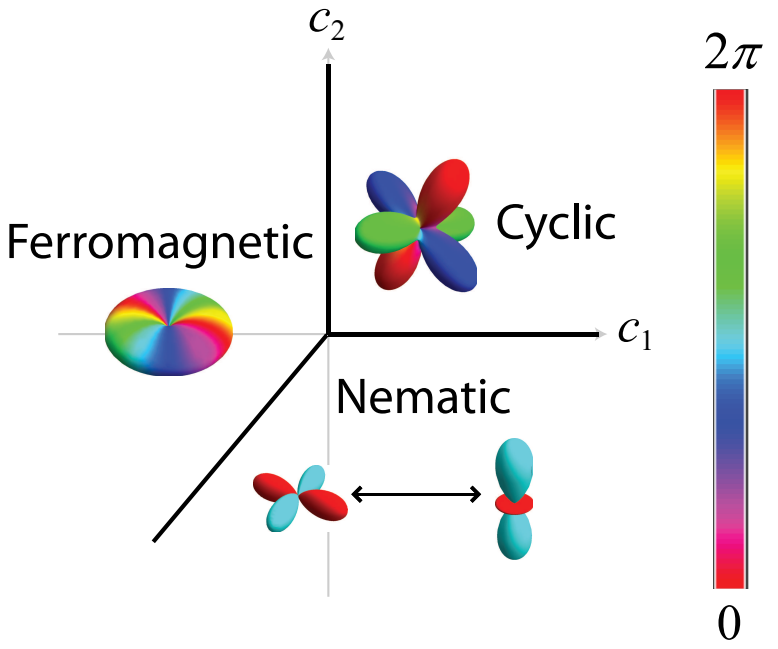

Figure 2.3: Mean-field ground-state phase diagram of spin-2 BECs. The ferromagnetic-nematic phase boundary is given by $c_2 = 20c_1$ and $c_1 < 0$. At the mean-field level, all nematic phases including the uniaxial- and biaxial-nematic phases are degenerate. The insets show the spherical harmonic representations of the spinor order parameters in the same way as Fig. 1.1.

energy density $E/V = c_0 n/2 + c_2 n/10$. A similar degeneracy was found to appear in the d-wave superconductors [63]. These nematic phases are unmagnetized $\mathbf{F} = \mathbf{0}$ but have the maximum value of the spin-singlet-pair amplitude $A_{00}/n = 1/\sqrt{5}$. Similar to the cyclic phase, the many-body state corresponding to the nematic phases involves a Bose-Einstein condensation of the spin-singlet pairs of atoms [64, 67], and the energy difference between the nematic phases and the state of condensed pairs vanishes at the thermodynamic limit.

Since the Hamiltonian (2.16) is invariant under an SO(3) rotation in spin space, the ground-state manifold of each phase contains all states obtained by letting an SO(3) rotational operator $U(\alpha, \beta, \gamma) = e^{-if_z\alpha} e^{-if_y\beta} e^{-if_z\gamma}$ act on the above representative order parameter. Here, α, β, and γ denote the Euler angles of the rotation. For example, the order parameter $(1, 0, i\sqrt{2}, 0, 1)^{\mathrm{T}}/2 = U(\pi/3, \arccos(-1/\sqrt{3}), -\pi/3)(1/\sqrt{3}, 0, 0, \sqrt{2/3}, 0)^{\mathrm{T}}$ also represents one state in the ground-state manifold of the cyclic phase.

2.4 First-order (Bogoliubov) excitation spectrum

Both quantum and thermal fluctuations create elementary excitations above the condensate. In the presence of the condensate, the elementary excitations are superpositions of particle-like and hole-like ones defined by the so-called Bogoliubov transformation [18]. This is a result of the creation of a pair of noncondensed particles out of the condensate and the inverse annihilation process. Due to the macroscopic occupation of atoms in the condensate, the annihilation and creation operators of the condensate mode can be replaced to a good approximation by the condensate wavefunction and its complex conjugate as discussed after Eq. (2.24). The field

operator then can be decomposed into the condensate and noncondensate parts as

$$\begin{aligned}\hat{\psi}_j &= \psi_j + \delta\hat{\psi}_j \\ &= \sqrt{n_0}\xi_j + \sum_{\mathbf{p}\neq 0} \frac{e^{i\mathbf{p}\cdot\mathbf{r}}}{\sqrt{V}}\hat{a}_{j,\mathbf{p}},\end{aligned} \tag{2.42}$$

where n_0 denotes the particle-number density in the condensate. The total number density is given by

$$n = n_0 + \sum_{j,\mathbf{p}\neq 0} \hat{a}^\dagger_{j,\mathbf{p}}\hat{a}_{j,\mathbf{p}}. \tag{2.43}$$

If the excitations are weak enough, e.g., in a weakly interacting dilute Bose gas at zero temperature, the Bogoliubov theory can be applied in which the noncondensate operators $\hat{a}_{j,\mathbf{p}\neq 0}$ and their Hermitian conjugates are retained up to the quadratic terms. The obtained Bogoliubov Hamiltonian can be diagonalized using the Bogoliubov transformation, from which the excitation spectrum is found. The Bogoliubov transformation is canonical in the sense that the operators of the Bogoliubov quasiparticles satisfy the commutator relations for bosons.

2.4.1 Spin-1 BECs

Following the above procedure, the Bogoliubov Hamiltonian of spin-1 BECs is given by [65, 69]

$$\begin{aligned}\hat{H}^{\mathrm{B}}_{F=1} = &\frac{Vn^2}{2}(c_0 + c_1|\mathbf{F}|^2) + qNF_z^2 + \sum_{\mathbf{p}\neq 0}\Bigg[\sum_{j=-1}^{1}(\epsilon^0_{\mathbf{p}} - c_1 n|\mathbf{F}|^2 + qj^2 - qF_z^2)\hat{a}^\dagger_{j,\mathbf{p}}\hat{a}_{j,\mathbf{p}} \\ &+ c_1 n\sum_{j,j'=-1}^{1}\mathbf{F}\cdot\mathbf{f}_{j,j'}\hat{a}^\dagger_{j,\mathbf{p}}\hat{a}_{j',\mathbf{p}} + \frac{c_0 n}{2}(2\hat{D}^\dagger_{\mathbf{p}}\hat{D}_{\mathbf{p}} + \hat{D}_{\mathbf{p}}\hat{D}_{-\mathbf{p}} + \hat{D}^\dagger_{\mathbf{p}}\hat{D}^\dagger_{-\mathbf{p}}) \\ &+ \frac{c_1 n}{2}(2\hat{\mathbf{F}}^\dagger_{\mathbf{p}}\cdot\hat{\mathbf{F}}_{\mathbf{p}} + \hat{\mathbf{F}}_{\mathbf{p}}\cdot\hat{\mathbf{F}}_{-\mathbf{p}} + \hat{\mathbf{F}}^\dagger_{\mathbf{p}}\cdot\hat{\mathbf{F}}^\dagger_{-\mathbf{p}})\Bigg],\end{aligned} \tag{2.44}$$

where $\epsilon^0_{\mathbf{p}} \equiv \hbar^2|\mathbf{p}|^2/(2M)$ is the kinetic energy of a particle with momentum $\hbar\mathbf{p}$ and

$$\mathbf{F} \equiv \sum_{j,j'=-1}^{1}\xi^*_j\mathbf{f}_{j,j'}\xi_{j'}, \tag{2.45}$$

$$\hat{D}_{\mathbf{p}} \equiv \sum_{j=-1}^{1}\xi^*_j\hat{a}_{j,\mathbf{p}}, \tag{2.46}$$

$$\hat{\mathbf{F}}_{\mathbf{p}} \equiv \sum_{j,j'=-1}^{1}\xi^*_j\mathbf{f}_{j,j'}\hat{a}_{j',\mathbf{p}}. \tag{2.47}$$

Here, $\hat{D}_{\mathbf{p}}$ and $\hat{\mathbf{F}}_{\mathbf{p}}$ represent the density and spin fluctuation operators of the condensate, respectively. In the following, we diagonalize the Bogoliubov Hamiltonian (2.44) for the different phases given in Sec. 2.3.1.

Ferromagnetic phase. With the spinor order parameter $\boldsymbol{\xi}^{\mathrm{FM}} = (1, 0, 0)^{\mathrm{T}}$, the Bogoliubov

Hamiltonian is diagonalized as

$$\hat{H}^{\mathrm{B}} = E_0^{\mathrm{FM}} + \sum_{\mathbf{p}\neq 0}[\hbar\omega_{1,\mathbf{p}}\hat{b}_{1,\mathbf{p}}^\dagger\hat{b}_{1,\mathbf{p}} + \hbar\omega_{0,\mathbf{p}}\hat{a}_{0,\mathbf{p}}^\dagger\hat{a}_{0,\mathbf{p}} + \hbar\omega_{-1,\mathbf{p}}\hat{a}_{-1,\mathbf{p}}^\dagger\hat{a}_{-1,\mathbf{p}}], \tag{2.48}$$

where E_0^{FM} is the zero-point energy containing the Lee-Huang-Yang correction to the Hartree mean-field energy [70, 71], and the excitation spectra are given by

$$\hbar\omega_{1,\mathbf{p}} = \sqrt{\epsilon_{\mathbf{p}}^0[\epsilon_{\mathbf{p}}^0 + 2(c_0+c_1)n]}, \tag{2.49}$$

$$\hbar\omega_{0,\mathbf{p}} = \epsilon_{\mathbf{p}}^0 - q, \tag{2.50}$$

$$\hbar\omega_{-1,\mathbf{p}} = \epsilon_{\mathbf{p}}^0 - 2c_1 n. \tag{2.51}$$

The annihilation operator of the Bogoliubov quasiparticle is given by

$$\hat{b}_{1,\mathbf{p}} = u_{1,\mathbf{p}}\hat{a}_{1,\mathbf{p}} + v_{1,\mathbf{p}}\hat{a}_{1,-\mathbf{p}}^\dagger \tag{2.52}$$

with the coefficients

$$u_{1,\mathbf{p}} = \sqrt{\frac{\epsilon_{\mathbf{p}}^0 + (c_0+c_1)n + \hbar\omega_{1,\mathbf{p}}}{2\hbar\omega_{1,\mathbf{p}}}},\ v_{1,\mathbf{p}} = \sqrt{\frac{\epsilon_{\mathbf{p}}^0 + (c_0+c_1)n - \hbar\omega_{1,\mathbf{p}}}{2\hbar\omega_{1,\mathbf{p}}}}. \tag{2.53}$$

Polar phase. Similarly, with the spinor order parameter $\boldsymbol{\xi}^{\mathrm{PL}} = (0,1,0)^{\mathrm{T}}$, the Bogoliubov Hamiltonian for the polar phase is diagonalized as

$$\hat{H}^{\mathrm{B}} = E_0^{\mathrm{PL}} + \sum_{\mathbf{p}\neq 0}[\hbar\omega_{1,\mathbf{p}}\hat{b}_{1,\mathbf{p}}^\dagger\hat{b}_{1,\mathbf{p}} + \hbar\omega_{0,\mathbf{p}}\hat{b}_{0,\mathbf{p}}^\dagger\hat{b}_{0,\mathbf{p}} + \hbar\omega_{-1,\mathbf{p}}\hat{b}_{-1,\mathbf{p}}^\dagger\hat{b}_{-1,\mathbf{p}}], \tag{2.54}$$

with the excitation spectra given by

$$\hbar\omega_{\pm1,\mathbf{p}} = \sqrt{(\epsilon_{\mathbf{p}}^0 + q)(\epsilon_{\mathbf{p}}^0 + q + 2c_1 n)}, \tag{2.55}$$

$$\hbar\omega_{0,\mathbf{p}} = \sqrt{\epsilon_{\mathbf{p}}^0(\epsilon_{\mathbf{p}}^0 + 2c_0 n)}. \tag{2.56}$$

Here there is a twofold degeneracy in the excitation energy (2.55) of the polar phase due to the equivalence of the two magnetic sublevels $m_F = \pm 1$. The Bogoliubov transformations are made for the three excitation modes:

$$\hat{b}_{\pm1,\mathbf{p}} = u_{\pm1,\mathbf{p}}\hat{a}_{\pm1,\mathbf{p}} + v_{\pm1,\mathbf{p}}\hat{a}_{\mp1,-\mathbf{p}}^\dagger, \tag{2.57}$$

$$\hat{b}_{0,\mathbf{p}} = u_{0,\mathbf{p}}\hat{a}_{0,\mathbf{p}} + v_{0,\mathbf{p}}\hat{a}_{0,-\mathbf{p}}^\dagger, \tag{2.58}$$

where

$$u_{\pm1,\mathbf{p}} = \sqrt{\frac{\epsilon_{\mathbf{p}}^0 + q + c_1 n + \hbar\omega_{\pm1,\mathbf{p}}}{2\hbar\omega_{\pm1,\mathbf{p}}}},\ v_{\pm1,\mathbf{p}} = \sqrt{\frac{\epsilon_{\mathbf{p}}^0 + q + c_1 n - \hbar\omega_{\pm1,\mathbf{p}}}{2\hbar\omega_{\pm1,\mathbf{p}}}}, \tag{2.59}$$

$$u_{0,\mathbf{p}} = \sqrt{\frac{\epsilon_{\mathbf{p}}^0 + c_0 n + \hbar\omega_{0,\mathbf{p}}}{2\hbar\omega_{0,\mathbf{p}}}},\ v_{0,\mathbf{p}} = \sqrt{\frac{\epsilon_{\mathbf{p}}^0 + c_0 n - \hbar\omega_{0,\mathbf{p}}}{2\hbar\omega_{0,\mathbf{p}}}}. \tag{2.60}$$

Antiferromagnetic phase. The excitation spectra of the antiferromagnetic phase with the

spinor order parameter $\boldsymbol{\xi}^{\mathrm{AFM}} = (1,0,1)^{\mathrm{T}}$ are calculated to be

$$\hbar\omega_{+,\mathbf{p}} = \sqrt{\epsilon^0_{\mathbf{p}}(\epsilon^0_{\mathbf{p}} + 2c_0 n)}, \tag{2.61}$$

$$\hbar\omega_{0,\mathbf{p}} = \sqrt{(\epsilon^0_{\mathbf{p}} - q)(\epsilon^0_{\mathbf{p}} - q + 2c_1 n)}, \tag{2.62}$$

$$\hbar\omega_{-,\mathbf{p}} = \sqrt{\epsilon^0_{\mathbf{p}}(\epsilon^0_{\mathbf{p}} + 2c_1 n)}. \tag{2.63}$$

The Bogoliubov transformations are given by

$$\hat{b}_{+,\mathbf{p}} = u_{+,\mathbf{p}} \frac{\hat{a}_{1,\mathbf{p}} + \hat{a}_{-1,\mathbf{p}}}{\sqrt{2}} + v_{+,\mathbf{p}} \frac{\hat{a}^\dagger_{1,-\mathbf{p}} + \hat{a}^\dagger_{-1,-\mathbf{p}}}{2}, \tag{2.64}$$

$$\hat{b}_{0,\mathbf{p}} = u_{0,\mathbf{p}} \hat{a}_{0,\mathbf{p}} + v_{0,\mathbf{p}} \hat{a}^\dagger_{0,-\mathbf{p}}, \tag{2.65}$$

$$\hat{b}_{-,\mathbf{p}} = u_{-,\mathbf{p}} \frac{\hat{a}_{1,\mathbf{p}} - \hat{a}_{-1,\mathbf{p}}}{\sqrt{2}} + v_{-,\mathbf{p}} \frac{\hat{a}^\dagger_{1,-\mathbf{p}} - \hat{a}^\dagger_{-1,-\mathbf{p}}}{2} \tag{2.66}$$

with

$$u_{+,\mathbf{p}} = \sqrt{\frac{\epsilon^0_{\mathbf{p}} + c_0 n + \hbar\omega_{+,\mathbf{p}}}{2\hbar\omega_{+,\mathbf{p}}}},\ v_{+,\mathbf{p}} = \sqrt{\frac{\epsilon^0_{\mathbf{p}} + c_0 n - \hbar\omega_{+,\mathbf{p}}}{2\hbar\omega_{+,\mathbf{p}}}}, \tag{2.67}$$

$$u_{0,\mathbf{p}} = \sqrt{\frac{\epsilon^0_{\mathbf{p}} - q + c_1 n + \hbar\omega_{0,\mathbf{p}}}{2\hbar\omega_{0,\mathbf{p}}}},\ v_{1,\mathbf{p}} = \sqrt{\frac{\epsilon^0_{\mathbf{p}} - q + c_1 n - \hbar\omega_{0,\mathbf{p}}}{2\hbar\omega_{0,\mathbf{p}}}}, \tag{2.68}$$

$$u_{-,\mathbf{p}} = \sqrt{\frac{\epsilon^0_{\mathbf{p}} + c_1 n + \hbar\omega_{-,\mathbf{p}}}{2\hbar\omega_{-,\mathbf{p}}}},\ v_{-,\mathbf{p}} = \sqrt{\frac{\epsilon^0_{\mathbf{p}} + c_1 n - \hbar\omega_{-,\mathbf{p}}}{2\hbar\omega_{-,\mathbf{p}}}}. \tag{2.69}$$

BA phase. The Bogoliubov spectra of the BA phase can also be derived in a similar way. Since their derivations and expressions are lengthy, we refer their details to Refs. [12, 68].

2.4.2 Spin-2 BECs

Following a similar procedure, the Bogoliubov Hamiltonian of spin-2 BECs can be written as [68, 69]

$$\begin{aligned}\hat{H}^{\mathrm{B}}_{F=2} = {} & \frac{Vn^2}{2}(c_0 + c_1|\mathbf{F}|^2 + 4c_2|A_{00}|^2) + \sum_{\mathbf{p}\neq 0}\Bigg[\sum_{j=-2}^{2}(\epsilon^0_{\mathbf{p}} - c_1 n|\mathbf{F}|^2 - 4c_2 n|A_{00}|^2)\hat{a}^\dagger_{j,\mathbf{p}}\hat{a}_{j,\mathbf{p}} \\ & + c_1 n\sum_{j,j'=-2}^{2}\mathbf{F}\cdot\mathbf{f}_{j,j'}\hat{a}^\dagger_{j,\mathbf{p}}\hat{a}_{j',\mathbf{p}} + 2c_2 n\hat{A}^\dagger_{\mathbf{p}}\hat{A}_{\mathbf{p}} + c_2 n\sum_{j=-2}^{2}(-1)^j(A_{00}\hat{a}^\dagger_{j,\mathbf{p}}\hat{a}^\dagger_{-j,-\mathbf{p}} + A^*_{00}\hat{a}_{j,\mathbf{p}}\hat{a}_{-j,-\mathbf{p}}) \\ & + \frac{c_0 n}{2}(2\hat{D}^\dagger_{\mathbf{p}}\hat{D}_{\mathbf{p}} + \hat{D}_{\mathbf{p}}\hat{D}_{-\mathbf{p}} + \hat{D}^\dagger_{\mathbf{p}}\hat{D}^\dagger_{-\mathbf{p}}) + \frac{c_1 n}{2}(2\hat{\mathbf{F}}^\dagger_{\mathbf{p}}\cdot\hat{\mathbf{F}}_{\mathbf{p}} + \hat{\mathbf{F}}_{\mathbf{p}}\cdot\hat{\mathbf{F}}_{-\mathbf{p}} + \hat{\mathbf{F}}^\dagger_{\mathbf{p}}\cdot\hat{\mathbf{F}}^\dagger_{-\mathbf{p}})\Bigg],\end{aligned} \tag{2.70}$$

where $\hat{D}_{\mathbf{p}}$ and $\hat{\mathbf{F}}_{\mathbf{p}}$ are defined in the same way as Eqs. (2.46) and (2.47), respectively, and

$$A_{00} \equiv \frac{1}{2}\sum_{j=-2}^{2}(-1)^j \xi_j \xi_{-j}, \tag{2.71}$$

$$\hat{A}_{\mathbf{p}} \equiv \sum_{j=-2}^{2}(-1)^j \xi_j \hat{a}_{-j,\mathbf{p}}. \tag{2.72}$$

Here $\hat{A}_{\mathbf{p}}$ represents the fluctuation operator of the spin-singlet-pair amplitude. By diagonalizing the Bogoliubov Hamiltonian (2.70), we obtain the excitation spectra for different phases of spin-2 BECs as follows. There are a total of five excitation modes.

Ferromagnetic phase. The excitation spectra are given by

$$\sqrt{\epsilon^0_{\mathbf{p}}\left[\epsilon^0_{\mathbf{p}} + 2(c_0 + 4c_1)n\right]}, \tag{2.73a}$$

$$\epsilon^0_{\mathbf{p}}, \tag{2.73b}$$

$$\epsilon^0_{\mathbf{p}} - 4c_1 n, \tag{2.73c}$$

$$\epsilon^0_{\mathbf{p}} - 6c_1 n, \tag{2.73d}$$

$$\epsilon^0_{\mathbf{p}} - (8c_1 - 2c_2/5)n. \tag{2.73e}$$

From Eqs. (2.73c)–(2.73e), it is clear that a Landau instability with a negative excitation energy would occur if either $c_1 > 0$ or $c_2 < 20c_1$. Note that $c_1 = 0, c_2 > 0$ and $c_2 = 20c_1, c_1 < 0$ are the mean-field phase boundaries of the ferromagnetic-cyclic and ferromagnetic-nematic phase transitions, respectively (see Fig. 2.3).

Cyclic phase. The excitation spectra are given by

$$\sqrt{\epsilon^0_{\mathbf{p}}\left(\epsilon^0_{\mathbf{p}} + 2c_0 n\right)}, \tag{2.74a}$$

$$\sqrt{\epsilon^0_{\mathbf{p}}\left(\epsilon^0_{\mathbf{p}} + 4c_1 n\right)}, \tag{2.74b}$$

$$\epsilon^0_{\mathbf{p}} + 2c_2 n/5, \tag{2.74c}$$

$$\sqrt{\epsilon^0_{\mathbf{p}}\left(\epsilon^0_{\mathbf{p}} + 4c_1 n\right)}, \tag{2.74d}$$

$$\sqrt{\epsilon^0_{\mathbf{p}}\left(\epsilon^0_{\mathbf{p}} + 4c_1 n\right)}. \tag{2.74e}$$

From Eq. (2.74c), a Landau instability would occur if $c_2 < 0$. Note that $c_2 = 0$ and $c_1 > 0$ define the mean-field phase boundary of the cyclic-UN phase transition (see Fig. 2.3). On the other hand, Eqs. (2.74b), (2.74d), and (2.74e) imply a dynamical instability in which the excitation energy acquires a nonzero imaginary part if $c_1 < 0$.

Uniaxial-nematic (UN) phase. The spinor order parameter is $\boldsymbol{\xi}^{\mathrm{UN}} = (0, 0, 1, 0, 0)^{\mathrm{T}}$, corre-

sponding to $\eta = 0$ in Eq. (2.41). The excitation spectra are given by

$$\sqrt{\epsilon_{\mathbf{p}}^0 \left[\epsilon_{\mathbf{p}}^0 + 2(c_0 + c_2/5)n\right]}, \tag{2.75a}$$

$$\sqrt{\epsilon_{\mathbf{p}}^0 \left[\epsilon_{\mathbf{p}}^0 + 2(3c_1 - c_2/5)n\right]}, \tag{2.75b}$$

$$\sqrt{\epsilon_{\mathbf{p}}^0 \left[\epsilon_{\mathbf{p}}^0 + 2(3c_1 - c_2/5)n\right]}, \tag{2.75c}$$

$$\sqrt{\epsilon_{\mathbf{p}}^0 \left(\epsilon_{\mathbf{p}}^0 - 2c_2 n/5\right)}, \tag{2.75d}$$

$$\sqrt{\epsilon_{\mathbf{p}}^0 \left(\epsilon_{\mathbf{p}}^0 - 2c_2 n/5\right)}. \tag{2.75e}$$

Equations (2.75b)–(2.75e) indicate a dynamical instability if either $c_2 > 15c_1, c_1 < 0$ or $c_2 > 0$.

Biaxial-nematic (BN) phase. The spinor order parameter is $\boldsymbol{\xi}^{\mathrm{UN}} = (1, 0, 0, 0, 1)^{\mathrm{T}}/\sqrt{2}$, corresponding to $\eta = \pi/6$ in Eq. (2.41). The excitation spectra are given by

$$\sqrt{\epsilon_{\mathbf{p}}^0 \left[\epsilon_{\mathbf{p}}^0 + 2(c_0 + c_2/5)n\right]}, \tag{2.76a}$$

$$\sqrt{\epsilon_{\mathbf{p}}^0 \left[\epsilon_{\mathbf{p}}^0 + 2(4c_1 - c_2/5)n\right]}, \tag{2.76b}$$

$$\sqrt{\epsilon_{\mathbf{p}}^0 \left[\epsilon_{\mathbf{p}}^0 + 2(c_1 - c_2/5)n\right]}, \tag{2.76c}$$

$$\sqrt{\epsilon_{\mathbf{p}}^0 \left[\epsilon_{\mathbf{p}}^0 + 2(c_1 - c_2/5)n\right]}, \tag{2.76d}$$

$$\sqrt{\epsilon_{\mathbf{p}}^0 \left(\epsilon_{\mathbf{p}}^0 - 2c_2 n/5\right)}. \tag{2.76e}$$

From Eqs. (2.76b)–(2.76e), it is clear that a dynamical instability would occur if either $c_2 > 20c_1, c_1 < 0$ or $c_2 > 0$.

Chapter 3

Beliaev theory of scalar BECs

For an interacting Bose gas, even at zero temperature quantum fluctuations cause a depletion of the condensate. The fraction of noncondensed particles which are excited out of the condensate is given by [19]

$$\frac{n^{\rm nc}}{n} \simeq \frac{8}{3\sqrt{\pi}}\sqrt{na^3}. \tag{3.1}$$

It is a function of the only dimensionless parameter na^3 characteristic of a dilute Bose gas with n and a being the total particle-number density and the s-wave scattering length, respectively. The particle density in the condensate therefore decreases to

$$\frac{n_0}{n} \simeq 1 - \frac{8}{3\sqrt{\pi}}\sqrt{na^3}. \tag{3.2}$$

The effects of quantum fluctuations on the excitation spectrum of a scalar (spinless) BEC were studied for the first time by Beliaev [26, 27]. He used a Green's function approach in which the Feynman diagrams up to the second order were considered. In comparison, the Bogoliubov excitation spectrum is reproduced by taking the Feynman diagrams up to the first order. The Bogoliubov and Beliaev spectra thus involve the lowest-order and the next-to-the-lowest-order terms, respectively, in the asymptotic expansion of the excitation spectrum with respect to the dimensionless parameter na^3, which satisfies $na^3 \ll 1$ for dilute Bose gases in typical ultracold atomic experiments. In fermionic systems, we often use a formalism such as the Hartree-Fock approximation in which the motion of a particle and the influence of its interaction with other particles are treated self-consistently. In the language of the Feynman diagrams, the Green's function appearing in each diagrammatic contribution to the self-energy is taken to be the interacting Green's function, which is to be updated by the newly obtained self-energy [20]. However, the situation becomes much more complicated for the case of bosons. A similar approach applied to a BEC leads to an artifact of the excitation spectrum of phonons having a nonzero energy gap [21, 22]. This contradicts the Nambu-Goldstone theorem which states that the phonon excitations arising from the spontaneous symmetry breaking should be gapless [23, 24]. The origin of this discrepancy is that unlike the case of fermions, the Green's function and self-energy of a BEC contain the so-called anomalous component besides the normal one. This anomalous component represents the creation of a pair of noncondensed particles out of the condensate. The replacement of a noninteracting Green's function by an interacting one in the Feynman diagrams of the anomalous self-energy leads to double counting of contributions from different diagrams [25]. Therefore, to avoid double counting and the ensuing artifact of a gapful excitation mode, we need a perturbation theory in which for a given

order of approximation the contribution from each of the Feynman diagrams can be calculated in a fully controlled manner. The Beliaev theory is such a perturbation theory that gives us the beyond-Bogoliubov excitation spectrum of the condensate in an analytic form. In the following, we review the basics of the Beliaev theory for a scalar BEC and show how the spectrum of phonons is modified by quantum fluctuations.

3.1 Formalism

We consider a homogeneous system of spinless bosons, whose Hamiltonian is given as the sum of the kinetic and the interaction energies:

$$\begin{aligned}\hat{H} &= \hat{H}_0 + \hat{V} \\ &= \int \mathrm{d}^3\mathbf{r}\ \hat{\psi}^\dagger(\mathbf{r}) \left(-\frac{\hbar^2\nabla^2}{2M}\right) \hat{\psi}(\mathbf{r}) + \frac{1}{2}\int \mathrm{d}^3\mathbf{r} \int \mathrm{d}^3\mathbf{r}\,' \hat{\psi}^\dagger(\mathbf{r})\hat{\psi}^\dagger(\mathbf{r}')V(\mathbf{r}-\mathbf{r}')\hat{\psi}(\mathbf{r}')\hat{\psi}(\mathbf{r}). \end{aligned} \tag{3.3}$$

As in the Bogoliubov theory, the field operator is decomposed into the condensate part which can be replaced by a c-number and the noncondensate part which contains only the nonzero-momentum components:

$$\hat{\psi}(\mathbf{r}) = \sqrt{n_0} + \hat{\delta}(\mathbf{r}). \tag{3.4}$$

Substituting Eq. (3.4) in Eq. (3.3), we obtain

$$\hat{V} = E_0 + \sum_{n=1}^{7} \hat{V}_n, \tag{3.5}$$

where

$$E_0 = \frac{1}{2}n_0^2 \int \mathrm{d}^3\mathbf{r} \int \mathrm{d}^3\mathbf{r}\,' V(\mathbf{r}-\mathbf{r}'), \tag{3.6a}$$

$$\hat{V}_1 = \frac{1}{2}n_0 \int \mathrm{d}^3\mathbf{r} \int \mathrm{d}^3\mathbf{r}\,' V(\mathbf{r}-\mathbf{r}')\hat{\delta}(\mathbf{r}')\hat{\delta}(\mathbf{r}), \tag{3.6b}$$

$$\hat{V}_2 = \frac{1}{2}n_0 \int \mathrm{d}^3\mathbf{r} \int \mathrm{d}^3\mathbf{r}\,' \hat{\delta}^\dagger(\mathbf{r})\hat{\delta}^\dagger(\mathbf{r}')V(\mathbf{r}-\mathbf{r}'), \tag{3.6c}$$

$$\hat{V}_3 = n_0 \int \mathrm{d}^3\mathbf{r} \int \mathrm{d}^3\mathbf{r}\,' \hat{\delta}^\dagger(\mathbf{r}')V(\mathbf{r}-\mathbf{r}')\hat{\delta}(\mathbf{r}), \tag{3.6d}$$

$$\hat{V}_4 = n_0 \int \mathrm{d}^3\mathbf{r} \int \mathrm{d}^3\mathbf{r}\,' \hat{\delta}^\dagger(\mathbf{r})V(\mathbf{r}-\mathbf{r}')\hat{\delta}(\mathbf{r}), \tag{3.6e}$$

$$\hat{V}_5 = n_0^{1/2} \int \mathrm{d}^3\mathbf{r} \int \mathrm{d}^3\mathbf{r}\,' \hat{\delta}^\dagger(\mathbf{r})\hat{\delta}^\dagger(\mathbf{r}')V(\mathbf{r}-\mathbf{r}')\hat{\delta}(\mathbf{r}), \tag{3.6f}$$

$$\hat{V}_6 = n_0^{1/2} \int \mathrm{d}^3\mathbf{r} \int \mathrm{d}^3\mathbf{r}\,' \hat{\delta}^\dagger(\mathbf{r})V(\mathbf{r}-\mathbf{r}')\hat{\delta}(\mathbf{r}')\hat{\delta}(\mathbf{r}), \tag{3.6g}$$

$$\hat{V}_7 = \frac{1}{2}\int \mathrm{d}^3\mathbf{r} \int \mathrm{d}^3\mathbf{r}\,' \hat{\delta}^\dagger(\mathbf{r})\hat{\delta}^\dagger(\mathbf{r}')V(\mathbf{r}-\mathbf{r}')\hat{\delta}(\mathbf{r}')\hat{\delta}(\mathbf{r}). \tag{3.6h}$$

These interactions are classified by the number of noncondensed particles involved and are schematically illustrated by the Feynman diagrams in Fig. 3.1. Note that in Eqs. (3.6a)–(3.6h)

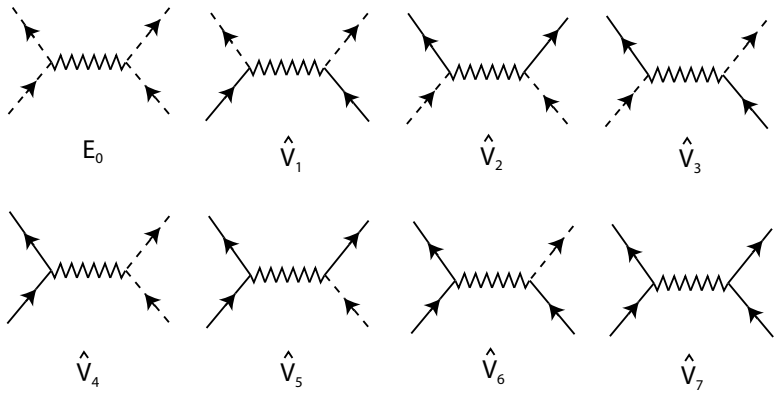

Figure 3.1: Feynman diagrams representing the terms (3.6a)–(3.6h) in the interaction Hamiltonian. The dashed, solid, and wavy lines represent condensate particles, noncondensate particles, and the interaction, respectively.

there is no term of the first order in $\hat{\delta}(\mathbf{r})$ since

$$\int \mathrm{d}^3\mathbf{r}\, \hat{\delta}(\mathbf{r}) = \sum_{\mathbf{p}\neq 0} \int \mathrm{d}^3\mathbf{r}\, \frac{e^{i\mathbf{p}\cdot\mathbf{r}}}{\sqrt{V}} \hat{a}_{\mathbf{p}} = 0. \tag{3.7}$$

We consider a grand canonical ensemble of the above system, and introduce the generalized Hamiltonian

$$\hat{K} \equiv \hat{H} - \mu\hat{N}, \tag{3.8}$$

where μ denotes the chemical potential and $\hat{N}$ is the total particle number operator

$$\hat{N} = \int \mathrm{d}^3\mathbf{r}\ \hat{\psi}^\dagger(\mathbf{r})\hat{\psi}(\mathbf{r}). \tag{3.9}$$

Using Eqs. (3.3),(3.4),(3.5), and (3.8), we have

$$\hat{K} = E_0 - \mu N_0 + \hat{K}', \tag{3.10}$$

where E_0 given by Eq. (3.6a) and $N_0 = Vn_0$ are the interaction energy and the total number of the condensate particles, respectively, and

$$\hat{K}' \equiv \hat{K}_0 + \hat{K}_1 \tag{3.11}$$

is the corresponding Hamiltonian for the noncondensed particles with

$$\hat{K}_0 \equiv \sum_{\mathbf{p}\neq 0} (\epsilon^0_{\mathbf{p}} - \mu)\hat{a}^\dagger_{\mathbf{p}}\hat{a}_{\mathbf{p}}, \tag{3.12}$$

$$\hat{K}_1 \equiv \sum_{n=1}^{7} \hat{V}_n. \tag{3.13}$$

Here $\epsilon^0_{\mathbf{p}} \equiv \hbar^2|\mathbf{p}|^2/(2M)$. In the following, $\hat{K}_0$ and $\hat{K}_1$ are referred to as the noninteracting Hamiltonian and the interaction of the noncondensed particles, respectively. For a weakly interacting system, $\hat{K}_1$ can be treated as a perturbation to $\hat{K}_0$.

3.1.1 Green's function

The Green's function can also be decomposed into the condensate and noncondensate parts as [20, 27]

$$iG(x,y) = n_0 + iG'(x,y), \tag{3.14}$$

where $x = (\mathbf{r}, t), y = (\mathbf{r}', t')$ are spatial-temporal four-vectors. The noncondensate part of the Green's function is defined as

$$iG'(x,y) \equiv \frac{\langle \mathbf{O}|\mathcal{T}\hat{\delta}_{\mathrm{H}}(x)\hat{\delta}^{\dagger}_{\mathrm{H}}(y)|\mathbf{O}\rangle}{\langle \mathbf{O}|\mathbf{O}\rangle}. \tag{3.15}$$

Here $|\mathbf{O}\rangle$ is the ground state of the Hamiltonian (3.11), and $\mathcal{T}$ and H denote the time-ordering operator and the Heisenberg representation, respectively.

In the presence of the condensate, we must take into account the creation of a pair of noncondensed particles out of the condensate and the inverse pair annihilation process. To this end, in addition to the normal Green's function $G'(x,y)$ in Eq. (3.15), it is necessary to introduce the so-called anomalous Green's functions defined by

$$iG^{12}(x,y) \equiv \frac{\langle \mathbf{O}|\mathcal{T}\hat{\delta}^{\dagger}_{\mathrm{H}}(x)\hat{\delta}^{\dagger}_{\mathrm{H}}(y)|\mathbf{O}\rangle}{\langle \mathbf{O}|\mathbf{O}\rangle}, \tag{3.16}$$

$$iG^{21}(x,y) \equiv \frac{\langle \mathbf{O}|\mathcal{T}\hat{\delta}_{\mathrm{H}}(x)\hat{\delta}_{\mathrm{H}}(y)|\mathbf{O}\rangle}{\langle \mathbf{O}|\mathbf{O}\rangle}. \tag{3.17}$$

In energy-momentum space, the Dyson's equation for the noncondensate Green's function is given in terms of the proper self-energy Σ and the noninteracting Green's function G^0 as

$$\hat{G}(p) = \hat{G}^0(p) + \hat{G}^0(p)\hat{\Sigma}(p)\hat{G}(p), \tag{3.18}$$

where $p \equiv (\omega_{\mathbf{p}}, \mathbf{p})$ denotes a frequency-wavenumber four-vector, and $\hat{G}$, $\hat{G}^0$, and $\hat{\Sigma}$ are 2×2 matrices:

$$\hat{G}(p) \equiv \begin{bmatrix} G^{11}(p) & G^{12}(p) \\ G^{21}(p) & G^{22}(p) \end{bmatrix}, \hat{\Sigma}(p) \equiv \begin{bmatrix} \Sigma^{11}(p) & \Sigma^{12}(p) \\ \Sigma^{21}(p) & \Sigma^{22}(p) \end{bmatrix}. \tag{3.19}$$

Here $G^{11}(p) \equiv G'(p)$, $G^{22}(p) \equiv G'(-p)$, and $\Sigma^{22}(p) \equiv \Sigma^{11}(-p)$. The Dyson's equation (3.18) is represented by the Feynman diagrams in Fig. 3.2.

The solution to Eq. (3.18) can be written as

$$\hat{G}(p) = \left[1 - \hat{G}^0(p)\hat{\Sigma}(p)\right]^{-1}\hat{G}^0(p). \tag{3.20}$$

The noninteracting Green's function is defined as

$$iG^0(x,y) \equiv \frac{\langle 0|\mathcal{T}\hat{\delta}_0(x)\hat{\delta}^{\dagger}_0(y)|0\rangle}{\langle 0|0\rangle}, \tag{3.21}$$

where $\hat{\delta}_0$ indicates the free evolution of $\hat{\delta}$ for the noninteracting Hamiltonian $\hat{K}_0$ given by Eq. (3.12), and $|0\rangle$ represents the noninteracting ground state, which is the vacuum with respect to the noncondensate operators; i.e., $\hat{a}_{\mathbf{p}}|0\rangle = 0$ for any $\mathbf{p} \neq 0$. Substituting Eq. (3.12) in

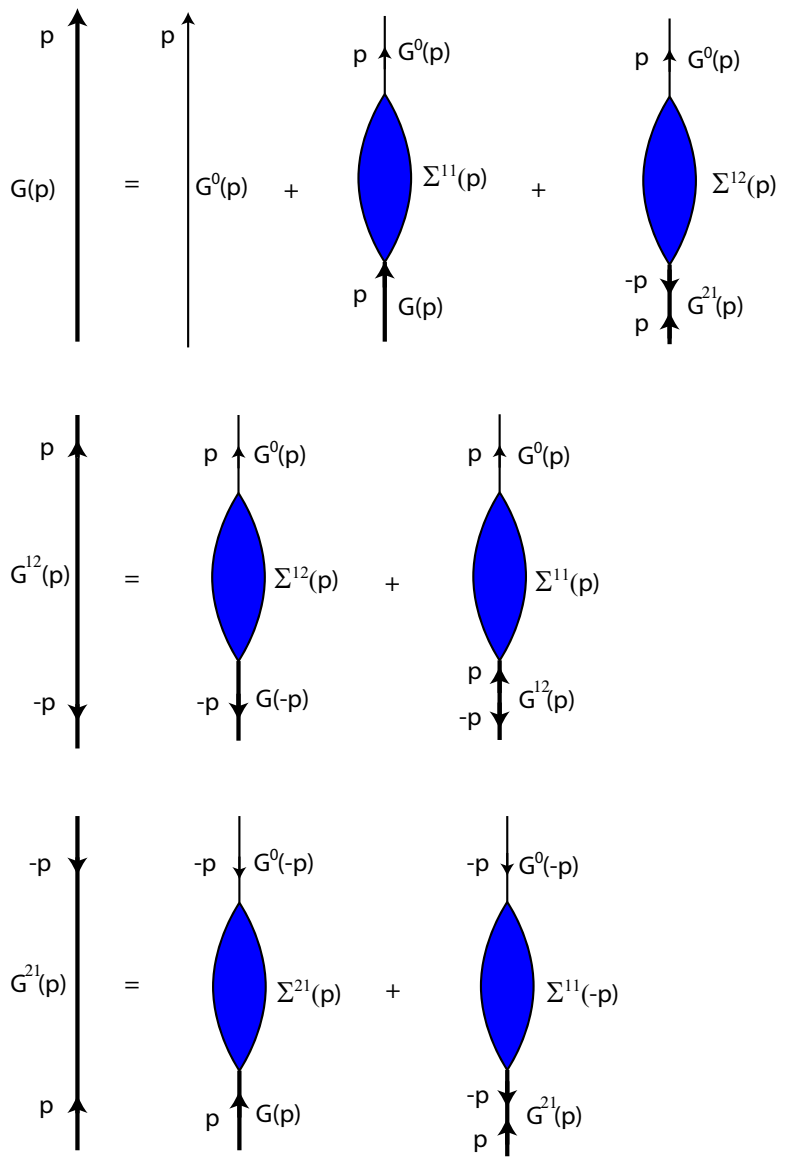

Figure 3.2: Dyson's equations for the normal and anomalous Green's functions (see Eq. (3.18)). The thick, thin lines, and the oval represent the interacting Green's functions, the noninteracting Green's functions, and the proper self-energy, respectively. Here G and Σ^{11} denote the normal components, while $G^{12;21}$ and $\Sigma^{12;21}$ denote the anomalous components.

Eq. (3.21), we obtain the Fourier transform of $G^0(x,y)$ as

$$\begin{aligned} G^0(p) &= \int \mathrm{d}^4x\, e^{-ip(x-y)} G^0(x,y) \\ &= \frac{1}{\omega_{\mathbf{p}} - (\epsilon^0_{\mathbf{p}} - \mu)/\hbar + i\eta}, \end{aligned} \tag{3.22}$$

where η is an infinitesimal positive number. Note that the anomalous Green's functions in a noninteracting system vanish invariably, and thus the matrix $\hat{G}^0(p)$ in Eq. (3.20) is diagonal with the matrix elements given by Eq. (3.22).

Substituting Eq. (3.22) in Eq. (3.20), the normal and anomalous Green's functions can be expressed in terms of the self-energies as

$$G^{11}(p) = \frac{-[G^0(-p)]^{-1} + \Sigma^{11}(-p)}{D} = \frac{\omega_{\mathbf{p}} + (\epsilon^0_{\mathbf{p}} - \mu)/\hbar + \Sigma^{11}(-p)}{D}, \tag{3.23a}$$

$$G^{12}(p) = -\frac{\Sigma^{12}(p)}{D},\ G^{21}(p) = -\frac{\Sigma^{21}(p)}{D}, \tag{3.23b}$$

where

$$\begin{aligned} D =& -[G^0(p)]^{-1}[G^0(-p)]^{-1} + \Sigma^{11}(p)[G^0(-p)]^{-1} + \Sigma^{22}(p)[G^0(p)]^{-1} - \Sigma^{11}(p)\Sigma^{22}(p) \\ &+ \Sigma^{21}(p)\Sigma^{12}(p) \\ =& \omega^2_{\mathbf{p}} - \left[\Sigma^{11}(p) - \Sigma^{22}(p)\right]\omega_{\mathbf{p}} + \Sigma^{21}(p)\Sigma^{12}(p) - \left[\frac{\epsilon^0_{\mathbf{p}} - \mu}{\hbar} + \frac{\Sigma^{11}(p) + \Sigma^{22}(p)}{2}\right]^2 \\ &+ \left[\frac{\Sigma^{11}(p) - \Sigma^{22}(p)}{2}\right]^2 + i\eta. \end{aligned} \tag{3.24}$$

3.1.2 T-matrix

For a weakly interacting dilute Bose gas, the contributions from all ladder-type diagrams to the self-energy have been shown to be of the same order of magnitude [20, 26], and thus all of them must be taken into account. The T-matrix is defined as the sum of an infinite number of ladder-type diagrams as illustrated in Fig. 3.3. It is written explicitly as

$$\begin{aligned} \Gamma(p_1,p_2;p_3,p_4) =& V(\mathbf{p}_1 - \mathbf{p}_3) + \frac{i}{\hbar}\int \frac{\mathrm{d}^4q}{(2\pi)^4} G^0(p_1 - q)G^0(p_2 + q)V(\mathbf{q})V(\mathbf{p}_1 - \mathbf{q} - \mathbf{p}_3) + \dots \\ =& V(\mathbf{p}_1 - \mathbf{p}_3) + \int \frac{\mathrm{d}^3\mathbf{q}}{(2\pi)^3} \frac{1}{\hbar(\omega_{\mathbf{p}_1} + \omega_{\mathbf{p}_2}) - \epsilon^0_{\mathbf{p}_1-\mathbf{q}} - \epsilon^0_{\mathbf{p}_2+\mathbf{q}} + 2\mu + i\eta} \\ &\times V(\mathbf{q})V(\mathbf{p}_1 - \mathbf{q} - \mathbf{p}_3) + \dots \end{aligned} \tag{3.25}$$

Here, in deriving the second equality in Eq. (3.25), we used Eq. (3.22) to carry out the integral $\int \mathrm{d}\omega_{\mathbf{q}}$. The T-matrix describes a two-body scattering under the influence of the medium containing the other particles which is implied by the chemical potential in Eq. (3.25).

The T-matrix $\Gamma(p_1,p_2;p_3,p_4)$ can be expressed in terms of the vacuum scattering amplitude

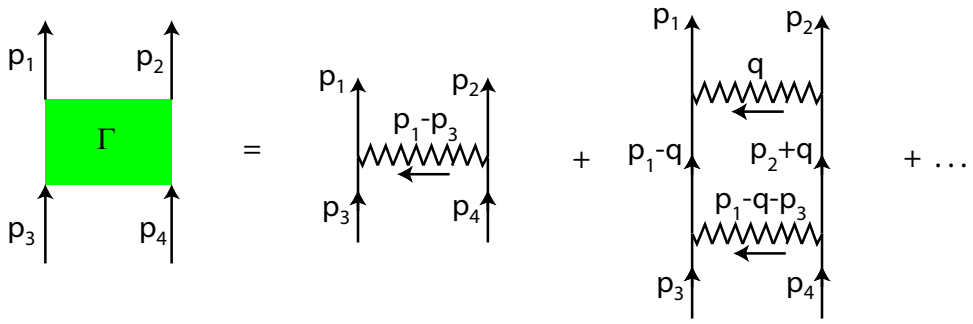

Figure 3.3: T-matrix of the two-body scattering. The interaction of two atoms with momenta $\hbar\mathbf{p}_3$ and $\hbar\mathbf{p}_4$ causes a change in momenta to $\hbar\mathbf{p}_1$ and $\hbar\mathbf{p}_2$. The T-matrix is defined as the sum of an infinite number of ladder-type diagrams which describe multiple virtual scatterings [see Eq. (3.25)].

as (see Appendix A)

$$\begin{aligned}\Gamma(p_1,p_2;p_3,p_4) &= \Gamma(\mathbf{p},\mathbf{p}',P)\\ &= \tilde{f}(\mathbf{p},\mathbf{p}') + \int \frac{\mathrm{d}^3\mathbf{q}}{(2\pi)^3}\,\tilde{f}(\mathbf{p},\mathbf{q})\left(\frac{1}{\hbar\omega_{\mathbf{P}} - \frac{\hbar^2\mathbf{P}^2}{4M} + 2\mu - \frac{\hbar^2\mathbf{q}^2}{M} + i\eta}\right.\\ &\quad\left. + \frac{1}{\frac{\hbar^2\mathbf{q}^2}{M} - \frac{\hbar^2\mathbf{p}'^2}{M} - i\eta}\right)\tilde{f}^*(\mathbf{p}',\mathbf{q}).\end{aligned} \tag{3.26}$$

Here $-M\tilde{f}(\mathbf{p},\mathbf{p}')/(4\pi\hbar^2)$ is the vacuum scattering amplitude of the two-body collision in which the relative momentum changes from $\hbar\mathbf{p}'$ to $\hbar\mathbf{p}$. As seen in Eq. (3.26), it can be shown that $\Gamma(p_1,p_2;p_3,p_4)$ depends only on the center-of-mass four-vector $\hbar P \equiv \hbar p_1 + \hbar p_2 = \hbar p_3 + \hbar p_4$ and the relative momenta $\hbar\mathbf{p} \equiv (\hbar\mathbf{p}_1 - \hbar\mathbf{p}_2)/2$, $\hbar\mathbf{p}' \equiv (\hbar\mathbf{p}_3 - \hbar\mathbf{p}_4)/2$, and neither on $\omega_{\mathbf{p}} \equiv [\omega_{\mathbf{p}_1} - \omega_{\mathbf{p}_2}]/2$ nor $\omega_{\mathbf{p}'} \equiv [\omega_{\mathbf{p}_3} - \omega_{\mathbf{p}_4}]/2$.

3.1.3 First-order (Bogoliubov) energy spectrum

In the following, we make the asymptotic expansions of Σ and μ with respect to the characteristic dimensionless parameter na^3, which is much smaller than unity for typical ultracold atomic experiments. These expansions are represented by the sums of the Feynman diagrams at different orders of approximation:

$$\Sigma^{\alpha\beta} = \sum_{n=1}^{\infty}\Sigma^{\alpha\beta(n)}, \tag{3.27a}$$

$$\mu = \sum_{n=1}^{\infty}\mu^{(n)}, \tag{3.27b}$$

where $\Sigma^{\alpha\beta(n)}$ and $\mu^{(n)}$ are the contributions to the self-energy and the chemical potential from the nth-order Feynman diagrams. The Bogoliubov and Beliaev theories consist of the contributions from the Feynman diagrams up to the first order (Fig. 3.4) and the second order (Figs. 3.5–3.8), respectively.

In the first-order approximation, we can neglect the $\int \mathrm{d}^3\mathbf{q}$ integral in Eq. (3.26) since its contribution is of the second order whose magnitude is smaller than the first order by a factor of

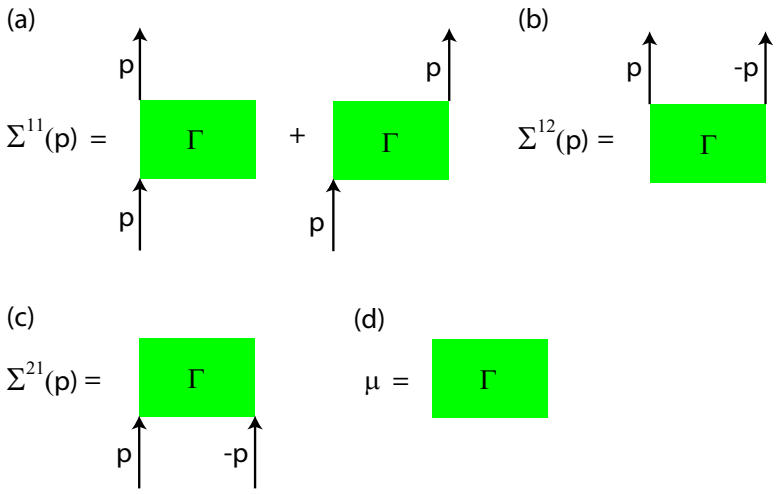

Figure 3.4: First-order diagrams of the proper self-energies (a)-(c) and the chemical potential (d). The squares represent the T-matrix, and we choose the convention that the condensate particles are not explicitly shown. In fact, in (a) there are one condensate particle moving in and another moving out; in (b) and (c) there are two condensate particles moving in and two moving out, respectively; in (d) all four particles belong to the condensate. This convention would help simplify the second-order diagrams in Sec. 3.2.

$\sqrt{na^3} \ll 1$ (see Sec. 3.2). On the other hand, in the low-energy regime $|\mathbf{p}| \ll 1/a$, the momentum dependence of the vacuum scattering amplitude is negligible, and $\tilde{f}(\mathbf{p}, \mathbf{p}')$ approaches $g \equiv 4\pi\hbar^2 a/M$ in the limit of zero momenta $\mathbf{p}, \mathbf{p}' \to 0$. The T-matrix then reduces to

$$\Gamma(\mathbf{p}, \mathbf{p}', P) \simeq g. \tag{3.28}$$

The proper self-energies and the chemical potential at the first-order approximation, whose Feynman diagrams are shown in Fig. 3.4, are given by

$$\begin{aligned}
\hbar\Sigma^{11(1)}(p) &= \Gamma(\mathbf{p}/2, \mathbf{p}/2, p)n_0 + \Gamma(\mathbf{p}/2, -\mathbf{p}/2, p)n_0 \\
&\simeq 2gn_0, && \text{(3.29a)} \\
\hbar\Sigma^{12(1)}(p) = \hbar\Sigma^{21(1)}(p) &= \Gamma(\mathbf{p}, \mathbf{0}, 0)n_0 \\
&\simeq gn_0, && \text{(3.29b)} \\
\mu^{(1)} &= \Gamma(\mathbf{0}, \mathbf{0}, 0)n_0 \\
&\simeq gn_0. && \text{(3.29c)}
\end{aligned}$$

By substituting Eqs. (3.29a)–(3.29c) in Eqs. (3.23a) and (3.23b), we obtain the first-order Green's functions as

$$G^{11(1)}(p) = \frac{\omega_{\mathbf{p}} + (\epsilon^0_{\mathbf{p}} + gn_0)/\hbar}{\omega^2_{\mathbf{p}} - [\omega^{(1)}_{\mathbf{p}}]^2 + i\eta}, \tag{3.30a}$$

$$G^{12(1)}(p) = G^{21(1)}(p) = -\frac{gn_0/\hbar}{\omega^2_{\mathbf{p}} - [\omega^{(1)}_{\mathbf{p}}]^2 + i\eta}, \tag{3.30b}$$

where the excitation spectrum, which can be determined from the pole of the Green's functions

according to the Lehmann representation [80], is given by

$$\hbar\omega_{\mathbf{p}}^{(1)} = \sqrt{\epsilon_{\mathbf{p}}^0[\epsilon_{\mathbf{p}}^0 + 2gn_0]}. \tag{3.31}$$

This is the energy spectrum of phonons obtained by using the Bogoliubov theory [18]. Therefore, the first-order approximation reproduces the Bogoliubov excitation spectrum. In the low-momentum regime $\epsilon_{\mathbf{p}}^0 \ll gn$, the dispersion relation is linear

$$\begin{aligned}\hbar\omega_{\mathbf{p}}^{(1)} \simeq& \sqrt{2gn_0\epsilon_{\mathbf{p}}^0} \\ \simeq& \sqrt{2gn\epsilon_{\mathbf{p}}^0} \\ =& v_{\mathrm{s}}^{(1)}\hbar|\mathbf{p}|,\end{aligned} \tag{3.32}$$

where $v_{\mathrm{s}}^{(1)} = \sqrt{gn/M}$ is the sound velocity. Here we used relation (3.2) between n_0 and n and ignored terms of the order of $\sqrt{na^3} \ll 1$.

To faciliate the second-order calculations in Sec. 3.2, we rewrite the first-order Green's functions in Eqs. (3.30a) and (3.30b) as

$$G^{11(1)}(p) = \frac{A_{\mathbf{p}}}{\omega_{\mathbf{p}} - \omega_{\mathbf{p}}^{(1)} + i\eta} - \frac{B_{\mathbf{p}}}{\omega_{\mathbf{p}} + \omega_{\mathbf{p}}^{(1)} - i\eta}, \tag{3.33a}$$

$$G^{12(1)}(p) = G_{11}^{21(1)}(p) = -C_{\mathbf{p}}\left(\frac{1}{\omega_{\mathbf{p}} - \omega_{\mathbf{p}}^{(1)} + i\eta} - \frac{1}{\omega_{\mathbf{p}} + \omega_{\mathbf{p}}^{(1)} - i\eta}\right), \tag{3.33b}$$

where

$$A_{\mathbf{p}} = \frac{\hbar\omega_{\mathbf{p}}^{(1)} + \epsilon_{\mathbf{p}}^0 + gn_0}{2\hbar\omega_{\mathbf{p}}^{(1)}}, \tag{3.34a}$$

$$B_{\mathbf{p}} = \frac{-\hbar\omega_{\mathbf{p}}^{(1)} + \epsilon_{\mathbf{p}}^0 + gn_0}{2\hbar\omega_{\mathbf{p}}^{(1)}}, \tag{3.34b}$$

$$C_{\mathbf{p}} = \frac{gn_0}{2\hbar\omega_{\mathbf{p}}^{(1)}}. \tag{3.34c}$$

3.2 Second-order (Beliaev) energy spectrum

The second-order contributions to the proper self-energies and the chemical potential consist of two components. The first one results from the second-order contribution to the T-matrix in the first-order diagrams (Fig. 3.4). It is obtained by substituting the $\int \mathrm{d}^3\mathbf{q}$ integral and the

imaginary part of $\tilde{f}(\mathbf{p},\mathbf{p}')$ in Eq. (3.26) in the first lines of Eqs. (3.29a)–(3.29c). We then have

$$\hbar\Sigma^{11}(p) : i\,\mathrm{Im}\tilde{f}(\mathbf{p}/2,\mathbf{p}/2)n_0 + i\,\mathrm{Im}\tilde{f}(\mathbf{p}/2,-\mathbf{p}/2)n_0 + 2n_0g^2\int\frac{\mathrm{d}^3\mathbf{q}}{(2\pi)^3}\left(\frac{1}{\hbar\omega_{\mathbf{p}}+2gn_0-\epsilon^0_{\mathbf{q}}-\epsilon^0_{\mathbf{k}}+i\eta}-\frac{1}{\epsilon^0_{\mathbf{p}}-\epsilon^0_{\mathbf{q}}-\epsilon^0_{\mathbf{k}}+i\eta}\right), \tag{3.35a}$$

$$\hbar\Sigma^{12,21}(p) : n_0g^2\int\frac{\mathrm{d}^3\mathbf{q}}{(2\pi)^3}\left(\frac{1}{2gn_0-2\epsilon^0_{\mathbf{q}}+i\eta}+\frac{1}{2\epsilon^0_{\mathbf{q}}}\right), \tag{3.35b}$$

$$\mu : n_0g^2\int\frac{\mathrm{d}^3\mathbf{q}}{(2\pi)^3}\left(\frac{1}{2gn_0-2\epsilon^0_{\mathbf{q}}+i\eta}+\frac{1}{2\epsilon^0_{\mathbf{q}}}\right), \tag{3.35c}$$

where Im denotes the imaginary part and $\mathbf{k}\equiv\mathbf{q}-\mathbf{p}$. Using the optical theorem for scattering, the imaginary part of the on-shell vacuum scattering amplitude $\tilde{f}(\mathbf{p},\mathbf{p}')$ ($|\mathbf{p}|=|\mathbf{p}'|$) is given by [20]

$$\begin{aligned}\mathrm{Im}\tilde{f}(\mathbf{p},\mathbf{p}') =& -\frac{\pi M}{\hbar^2}\int\frac{\mathrm{d}^3\mathbf{q}}{(2\pi)^3}\,\tilde{f}(\mathbf{p},\mathbf{q})\tilde{f}^*(\mathbf{p}',\mathbf{q})\delta(\mathbf{p}^2-\mathbf{q}^2)\\ =&\frac{-|\mathbf{p}|M}{16\pi^2\hbar^2}\int d\Omega_{\mathbf{q}}\tilde{f}(\mathbf{p},\mathbf{q})\tilde{f}^*(\mathbf{p}',\mathbf{q}),\end{aligned} \tag{3.36}$$

where $\Omega_{\mathbf{q}}$ denotes the solid angle of the on-shell momentum $\mathbf{q}$ ($|\mathbf{q}|=|\mathbf{p}|=|\mathbf{p}'|$). Therefore, we obtain the imaginary part of $\tilde{f}(\mathbf{p}/2,\pm\mathbf{p}/2)$ in Eq. (3.35a) to the second-order approximation as

$$\mathrm{Im}\tilde{f}(\mathbf{p}/2,\pm\mathbf{p}/2) =\frac{-|\mathbf{p}|M}{8\pi\hbar^2}g^2, \tag{3.37}$$

where we replaced $\tilde{f}(\mathbf{p},\mathbf{q})$ and $\tilde{f}(\mathbf{p}',\mathbf{q})$ on the right-hand side of Eq. (3.36) by their zero-momentum limit g.

The second component of the second-order contributions to the proper self-energies and the chemical potential arises from the second-order Feynman diagrams shown in Figs. 3.5–3.8. It is calculated straightforwardly by using Eqs. (3.33a) and (3.33b) for the first-order Green's functions. By summing the obtained two components, we find the second-order contributions to the self-energies and the chemical potential to be

$$\begin{aligned}\hbar\Sigma^{11(2)}(p) =&\hbar\Sigma^{22(2)}(-p)\\ =&\frac{-i|\mathbf{p}|Mn_0g^2}{4\pi\hbar^2}+2n_0g^2\int\frac{\mathrm{d}^3\mathbf{q}}{(2\pi)^3}\left(\frac{1}{\hbar\omega_{\mathbf{p}}+2gn_0-\epsilon^0_{\mathbf{q}}-\epsilon^0_{\mathbf{k}}+i\eta}-\frac{1}{\epsilon^0_{\mathbf{p}}-\epsilon^0_{\mathbf{q}}-\epsilon^0_{\mathbf{k}}+i\eta}\right)\\ &+n_0g^2\int\frac{\mathrm{d}^3\mathbf{q}}{(2\pi)^3}\left(\frac{2\{A_{\mathbf{q}},B_{\mathbf{k}}\}+4C_{\mathbf{q}}C_{\mathbf{k}}-4\{A_{\mathbf{q}},C_{\mathbf{k}}\}+2A_{\mathbf{q}}A_{\mathbf{k}}}{\hbar\left[\omega_{\mathbf{p}}-\omega^{(1)}_{\mathbf{q}}-\omega^{(1)}_{\mathbf{k}}\right]+i\eta}\right.\\ &\left.-\frac{2\{A_{\mathbf{q}},B_{\mathbf{k}}\}+4C_{\mathbf{q}}C_{\mathbf{k}}-4\{B_{\mathbf{q}},C_{\mathbf{k}}\}+2B_{\mathbf{q}}B_{\mathbf{k}}}{\hbar\left[\omega_{\mathbf{p}}+\omega^{(1)}_{\mathbf{q}}+\omega^{(1)}_{\mathbf{k}}\right]-i\eta}-\frac{2}{\hbar\omega_{\mathbf{p}}-\epsilon^0_{\mathbf{q}}-\epsilon^0_{\mathbf{k}}+2gn_0+i\eta}\right)\\ &+2g\int\frac{\mathrm{d}^3\mathbf{q}}{(2\pi)^3}\,B_{\mathbf{q}},\end{aligned} \tag{3.38}$$

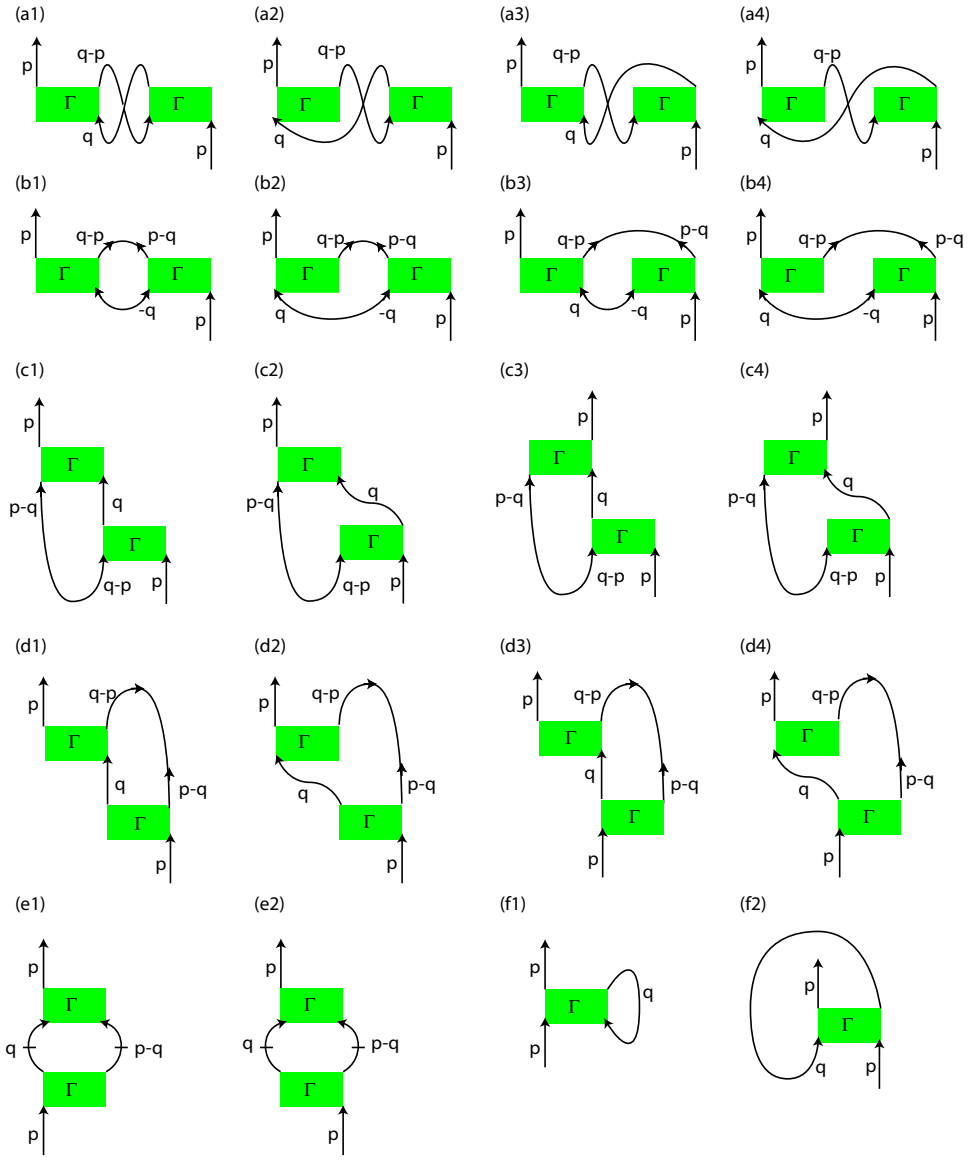

Figure 3.5: Second-order diagrams for the proper self-energy $\Sigma^{11}(p)$. The intermediate propagators are classified into three different categories, depending on the number of noncondensed atoms moving into and out of the condensate. They are represented by curves with one arrow ($\longrightarrow$), two pointing-out arrows ($\longleftarrow$), and two pointing-in arrows ($\rightarrow\leftarrow$), and are described by the first-order normal Green's function $G^{11(1)}(p)$ and anomalous Green's functions $G^{12(1)}(p)$ and $G^{21(1)}(p)$, respectively. Here, the two horizontal dashes in diagrams (e1) and (e2) indicate that we need to subtract from these diagrams the terms involving the noninteracting Green's function to avoid double counting of the contributions that have already been taken into account in the T-matrix and the first-order diagrams. As in Fig. 3.4, we use the convention that the condensate particles in diagrams (a1)–(e2) are not explicitly shown.

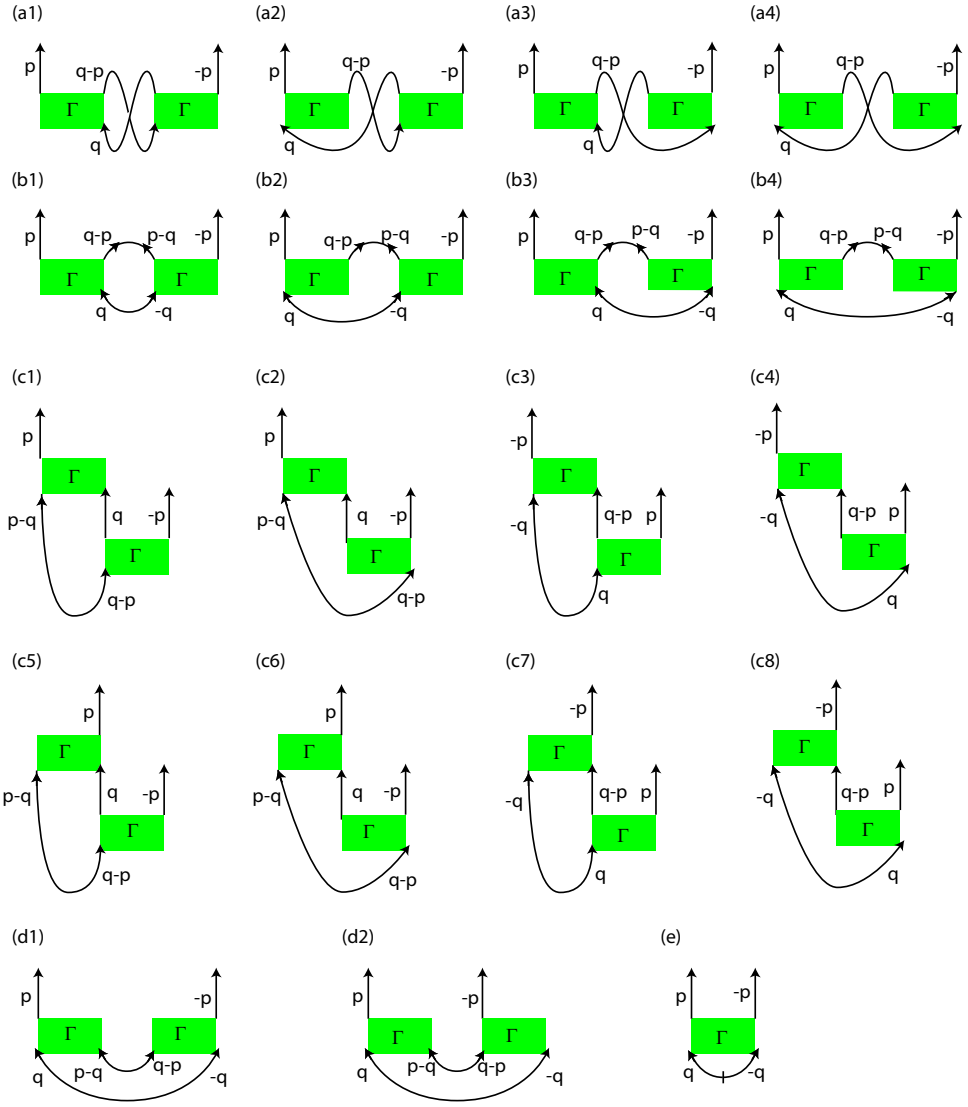

Figure 3.6: Second-order diagrams for the proper self-energy $\Sigma^{12}(p)$.

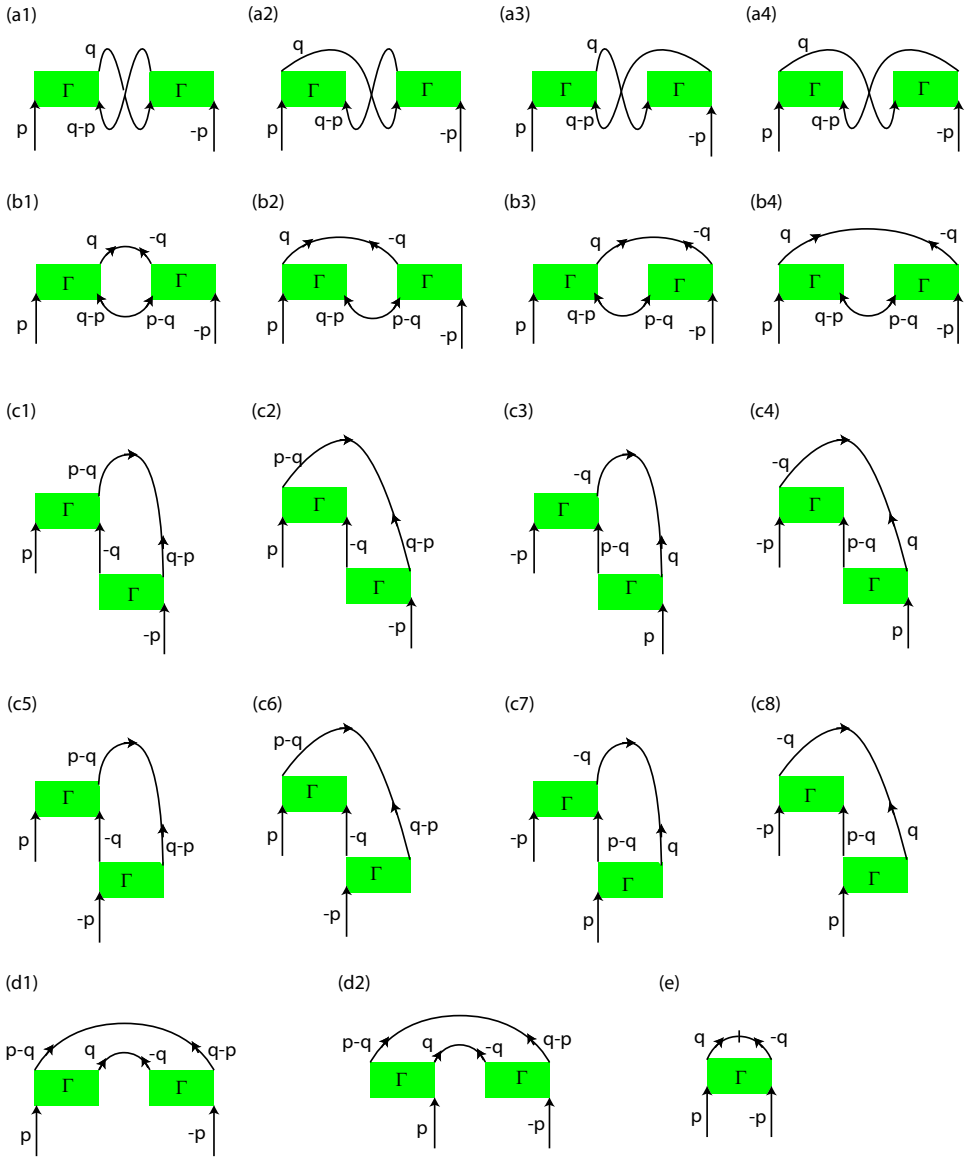

Figure 3.7: Second-order diagrams for the proper self-energy $\Sigma^{21}(p)$.

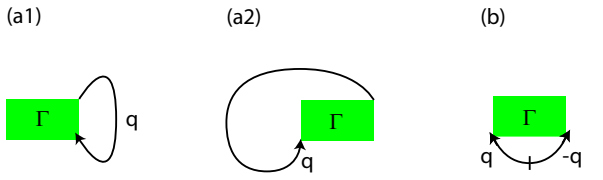

Figure 3.8: Second-order diagrams for the chemical potential μ.

$$\begin{aligned}\hbar\Sigma^{12(2)}(p) =& \hbar\Sigma^{21(2)}(p)\\ =& n_0 g^2 \int \frac{\mathrm{d}^3\mathbf{q}}{(2\pi)^3}\left(\frac{1}{2gn_0 - 2\epsilon_{\mathbf{q}}^0 + i\eta} + \frac{1}{2\epsilon_{\mathbf{q}}^0}\right) + n_0 g^2 \int \frac{\mathrm{d}^3\mathbf{q}}{(2\pi)^3}\left[\Big(2\left\{A_{\mathbf{q}}, B_{\mathbf{k}}\right\} + 6C_{\mathbf{q}}C_{\mathbf{k}}\right.\\ &\left. - 2\left\{A_{\mathbf{q}} + B_{\mathbf{q}}, C_{\mathbf{k}}\right\}\Big)\left(\frac{1}{\hbar\left[\omega_{\mathbf{p}} - \omega_{\mathbf{q}}^{(1)} - \omega_{\mathbf{k}}^{(1)}\right] + i\eta} - \frac{1}{\hbar\left[\omega_{\mathbf{p}} + \omega_{\mathbf{q}}^{(1)} + \omega_{\mathbf{k}}^{(1)}\right] - i\eta}\right)\right]\\ &+ g\int \frac{\mathrm{d}^3\mathbf{q}}{(2\pi)^3}\left(-C_{\mathbf{q}} + \frac{gn_0}{2\epsilon_{\mathbf{q}}^0 - 2gn_0 - i\eta}\right),\end{aligned} \tag{3.39}$$

$$\begin{aligned}\mu^{(2)} =& n_0 g^2 \int \frac{\mathrm{d}^3\mathbf{q}}{(2\pi)^3}\left(\frac{1}{2gn_0 - 2\epsilon_{\mathbf{q}}^0 + i\eta} + \frac{1}{2\epsilon_{\mathbf{q}}^0}\right) + 2g\int \frac{\mathrm{d}^3\mathbf{q}}{(2\pi)^3} B_{\mathbf{q}}\\ &+ c_0 \int \frac{\mathrm{d}^3\mathbf{q}}{(2\pi)^3}\left(-C_{\mathbf{q}} + \frac{gn_0}{2\epsilon_{\mathbf{q}}^0 - 2gn_0 - i\eta}\right),\end{aligned} \tag{3.40}$$

where $\omega_{\mathbf{q}}^{(1)}$ and $A_{\mathbf{q}}, B_{\mathbf{q}}, C_{\mathbf{q}}$ are given by Eqs. (3.31) and (3.34a)–(3.34c), and $\{A_{\mathbf{q}}, B_{\mathbf{k}}\} \equiv A_{\mathbf{q}}B_{\mathbf{k}} + A_{\mathbf{k}}B_{\mathbf{q}}$.

Since the shift of the energy spectrum of phonons from its first-order value is expected to be small: $|\omega_{\mathbf{p}}/\omega_{\mathbf{p}}^{(1)} - 1| \ll 1$ for a weakly interacting dilute Bose gas, which can be justified *a posteriori* from the final result, we can make Taylor series expansions of $\Sigma^{11(2)}$, $\Sigma^{22(2)}$, and $\Sigma^{12(2)}$ in powers of $\omega_{\mathbf{p}} - \omega_{\mathbf{p}}^{(1)}$ as

$$\Sigma^{11(2)}(p) = A^{11} + B^{11}(\omega_{\mathbf{p}} - \omega_{\mathbf{p}}^{(1)}) + \mathcal{O}[(\omega_{\mathbf{p}} - \omega_{\mathbf{p}}^{(1)})^2], \tag{3.41a}$$

$$\Sigma^{22(2)}(p) = A^{22} + B^{22}(\omega_{\mathbf{p}} - \omega_{\mathbf{p}}^{(1)}) + \mathcal{O}[(\omega_{\mathbf{p}} - \omega_{\mathbf{p}}^{(1)})^2], \tag{3.41b}$$

$$\Sigma^{12(2)}(p) = A^{12} + B^{12}(\omega_{\mathbf{p}} - \omega_{\mathbf{p}}^{(1)}) + \mathcal{O}[(\omega_{\mathbf{p}} - \omega_{\mathbf{p}}^{(1)})^2], \tag{3.41c}$$

where

$$A^{\alpha\beta} = \Sigma^{\alpha\beta(2)}(\omega_{\mathbf{p}} = \omega_{\mathbf{p}}^{(1)}, \mathbf{p}), \tag{3.42}$$

$$B^{\alpha\beta} = \left.\frac{\partial\Sigma^{\alpha\beta(2)}}{\partial\omega_{\mathbf{p}}}\right|_{\omega_{\mathbf{p}}=\omega_{\mathbf{p}}^{(1)}}. \tag{3.43}$$

In the low-momentum regime $\epsilon_{\mathbf{p}}^0 \ll gn$, the coefficients $A^{\alpha\beta}$ and $B^{\alpha\beta}$ can be further expanded in powers of $\hbar\omega_{\mathbf{p}}^{(1)}/(gn_0) \ll 1$. Substituting Eqs. (3.31) and (3.34a)–(3.34c) in Eqs. (3.38)–(3.40), we obtain [25]

$$\hbar\mathrm{Re}A^{11} = \frac{8\sqrt{n_0 a^3}gn_0}{\sqrt{\pi}}\left[\left(\frac{14}{3} - 2D_1\right) + \left(2D_1 - \frac{1}{2}\right)\frac{\hbar\omega_{\mathbf{p}}^{(1)}}{gn_0} + \left(\frac{161}{1440} - \frac{D_1}{2} - \frac{3D_3}{32}\right)\left(\frac{\hbar\omega_{\mathbf{p}}^{(1)}}{gn_0}\right)^2\right], \tag{3.44}$$

$$\hbar\mathrm{Re}A^{22} = \frac{8\sqrt{n_0 a^3}gn_0}{\sqrt{\pi}}\left[\left(\frac{14}{3} - 2D_1\right) - \left(2D_1 - \frac{1}{2}\right)\frac{\hbar\omega_{\mathbf{p}}^{(1)}}{gn_0} + \left(\frac{161}{1440} - \frac{D_1}{2} - \frac{3D_3}{32}\right)\left(\frac{\hbar\omega_{\mathbf{p}}^{(1)}}{gn_0}\right)^2\right], \tag{3.45}$$

$$\hbar \mathrm{Re}A^{12} = \frac{8\sqrt{n_0 a^3} g n_0}{\sqrt{\pi}} \left[(3 - 2D_1) + \left(-\frac{79}{1440} + \frac{D_1}{2} - \frac{3D_3}{32} \right) \left(\frac{\hbar\omega_{\mathbf{p}}^{(1)}}{g n_0} \right)^2 \right], \tag{3.46}$$

$$\hbar \mathrm{Im}A^{11} = -\sqrt{\pi n_0 a^3} g n_0 \left[1 - \frac{\hbar\omega_{\mathbf{p}}^{(1)}}{g n_0} - \frac{1}{24} \left(\frac{\hbar\omega_{\mathbf{p}}^{(1)}}{g n_0} \right)^2 + \frac{7}{24} \left(\frac{\hbar\omega_{\mathbf{p}}^{(1)}}{g n_0} \right)^3 + \frac{13}{1920} \left(\frac{\hbar\omega_{\mathbf{p}}^{(1)}}{g n_0} \right)^4 - \frac{193}{1920} \left(\frac{\hbar\omega_{\mathbf{p}}^{(1)}}{g n_0} \right)^5 + \frac{307}{35840} \left(\frac{\hbar\omega_{\mathbf{p}}^{(1)}}{g n_0} \right)^6 \right], \tag{3.47}$$

$$\hbar \mathrm{Im}A^{22} = -\sqrt{\pi n_0 a^3} g n_0 \left[1 + \frac{\hbar\omega_{\mathbf{p}}^{(1)}}{g n_0} - \frac{1}{24} \left(\frac{\hbar\omega_{\mathbf{p}}^{(1)}}{g n_0} \right)^2 - \frac{7}{24} \left(\frac{\hbar\omega_{\mathbf{p}}^{(1)}}{g n_0} \right)^3 + \frac{13}{1920} \left(\frac{\hbar\omega_{\mathbf{p}}^{(1)}}{g n_0} \right)^4 + \frac{193}{1920} \left(\frac{\hbar\omega_{\mathbf{p}}^{(1)}}{g n_0} \right)^5 + \frac{307}{35840} \left(\frac{\hbar\omega_{\mathbf{p}}^{(1)}}{g n_0} \right)^6 \right], \tag{3.48}$$

$$\hbar \mathrm{Im}A^{12} = -\sqrt{\pi n_0 a^3} g n_0 \left[1 - \frac{13}{24} \left(\frac{\hbar\omega_{\mathbf{p}}^{(1)}}{g n_0} \right)^2 + \frac{293}{1920} \left(\frac{\hbar\omega_{\mathbf{p}}^{(1)}}{g n_0} \right)^4 - \frac{1255}{21504} \left(\frac{\hbar\omega_{\mathbf{p}}^{(1)}}{g n_0} \right)^6 \right], \tag{3.49}$$

$$\mathrm{Re}B^{11} = \frac{8\sqrt{n_0 a^3}}{\sqrt{\pi}} \left[-\left(\frac{1}{2} - 2D_1 \right) - \left(\frac{1}{15} + \frac{D_1}{4} + 16D_3 \right) \frac{\hbar\omega_{\mathbf{p}}^{(1)}}{g n_0} \right], \tag{3.50}$$

$$\mathrm{Re}B^{22} = \frac{8\sqrt{n_0 a^3}}{\sqrt{\pi}} \left[\left(\frac{1}{2} - 2D_1 \right) - \left(\frac{1}{15} + \frac{D_1}{4} + 16D_3 \right) \frac{\hbar\omega_{\mathbf{p}}^{(1)}}{g n_0} \right], \tag{3.51}$$

$$\mathrm{Re}B^{12} = \frac{8\sqrt{n_0 a^3}}{\sqrt{\pi}} \left(\frac{7D_1}{4} - 16D_3 - \frac{1}{15} \right) \frac{\hbar\omega_{\mathbf{p}}^{(1)}}{g n_0}, \tag{3.52}$$

$$\mathrm{Im}B^{11} = -\sqrt{\pi n_0 a^3} \left[-1 - \frac{1}{2} \frac{\hbar\omega_{\mathbf{p}}^{(1)}}{g n_0} + \frac{25}{24} \left(\frac{\hbar\omega_{\mathbf{p}}^{(1)}}{g n_0} \right)^2 + \frac{13}{48} \left(\frac{\hbar\omega_{\mathbf{p}}^{(1)}}{g n_0} \right)^3 - \frac{1133}{1920} \left(\frac{\hbar\omega_{\mathbf{p}}^{(1)}}{g n_0} \right)^4 - \frac{97}{768} \left(\frac{\hbar\omega_{\mathbf{p}}^{(1)}}{g n_0} \right)^5 \right], \tag{3.53}$$

$$\mathrm{Im}B^{22} = -\sqrt{\pi n_0 a^3} \left[1 - \frac{1}{2} \frac{\hbar\omega_{\mathbf{p}}^{(1)}}{g n_0} - \frac{25}{24} \left(\frac{\hbar\omega_{\mathbf{p}}^{(1)}}{g n_0} \right)^2 + \frac{13}{48} \left(\frac{\hbar\omega_{\mathbf{p}}^{(1)}}{g n_0} \right)^3 + \frac{1133}{1920} \left(\frac{\hbar\omega_{\mathbf{p}}^{(1)}}{g n_0} \right)^4 - \frac{97}{768} \left(\frac{\hbar\omega_{\mathbf{p}}^{(1)}}{g n_0} \right)^5 \right], \tag{3.54}$$

$$\mathrm{Im}B^{12} = -\sqrt{\pi n_0 a^3}\left[-\frac{3}{2}\frac{\hbar\omega_{\mathbf{p}}^{(1)}}{gn_0} + \frac{13}{16}\left(\frac{\hbar\omega_{\mathbf{p}}^{(1)}}{gn_0}\right)^3 - \frac{613}{1280}\left(\frac{\hbar\omega_{\mathbf{p}}^{(1)}}{gn_0}\right)^5\right], \tag{3.55}$$

$$\mu^{(2)} = \frac{40\sqrt{n_0 a^3}gn_0}{3\sqrt{\pi}}, \tag{3.56}$$

where

$$D_1 \equiv \int_0^\infty \mathrm{d}x \frac{1}{x(x^2+4)^{3/2}}, \tag{3.57}$$

$$D_3 \equiv \int_0^\infty \mathrm{d}x \frac{1}{x^3(x^2+4)^{7/2}}. \tag{3.58}$$

Although D_1 and D_3 are infrared divergent, their divergences do not affect the final result of the excitation spectrum since they cancel each other as shown below. These infrared divergences, which result from the gapless excitation mode, is characteristic of Bose-Einstein condensates.

The excitation spectrum determined from the poles of the Green's function is obtained by equating the right-hand side of Eq. (3.24) to zero. The two roots of the quadratic equation result in the two poles of the Green's function with the same absolute value and the opposite signs in the Lehmann representation, which correspond to the particle and hole excitations, respectively. Unlike fermionic systems, since an elementary excitation of a Bose-Einstein condensate can be constituted from a superposition of a particle and a hole excitations, we only need to take one out of the two roots for each count of excitation modes. The excitation spectrum is then written in terms of the second-order self-energies as

$$\begin{aligned}
\omega_{\mathbf{p}} =& \frac{\Sigma^{11}-\Sigma^{22}}{2} + \sqrt{\left[\frac{\epsilon_{\mathbf{p}}^0-\mu}{\hbar} + \left(\frac{\Sigma^{11}+\Sigma^{22}}{2}\right)\right]^2 - \Sigma^{12}\Sigma^{21}} \\
=& \frac{\Sigma^{11(2)}-\Sigma^{22(2)}}{2} + \left\{\left[\frac{\epsilon_{\mathbf{p}}^0+gn_0}{\hbar} + \left(\frac{\Sigma^{11(2)}+\Sigma^{22(2)}}{2}\right) - \frac{\mu^{(2)}}{\hbar}\right]^2 - \left(\frac{gn_0}{\hbar}+\Sigma^{12(2)}\right)^2\right\}^{1/2} \\
\simeq& \frac{\Sigma^{11(2)}-\Sigma^{22(2)}}{2} + \left\{\left[\omega_{\mathbf{p}}^{(1)}\right]^2 + \frac{\left(\Sigma^{11(2)}+\Sigma^{22(2)}-2\mu^{(2)}/\hbar\right)\left(\epsilon_{\mathbf{p}}^0+gn_0\right)}{\hbar} - 2\frac{gn_0}{\hbar}\Sigma^{12(2)}\right\}^{1/2} \\
\simeq& \frac{\Sigma^{11(2)}-\Sigma^{22(2)}}{2} + \left[\omega_{\mathbf{p}}^{(1)} + \frac{\left(\Sigma^{11(2)}+\Sigma^{22(2)}-2\mu^{(2)}/\hbar\right)\left(\epsilon_{\mathbf{p}}^0+gn_0\right)}{2\hbar\omega_{\mathbf{p}}^{(1)}} - \frac{gn_0}{\hbar\omega_{\mathbf{p}}^{(1)}}\Sigma^{12(2)}\right] \\
=& \omega_{\mathbf{p}}^{(1)} + \Lambda,
\end{aligned} \tag{3.59}$$

where

$$\Lambda \equiv \frac{\left(\epsilon_{\mathbf{p}}^0+gn_0\right)\left(\Sigma^{11(2)}+\Sigma^{22(2)}-2\mu^{(2)}/\hbar\right)}{2\hbar\omega_{\mathbf{p}}^{(1)}} - \frac{gn_0\Sigma^{12(2)}}{\hbar\omega_{\mathbf{p}}^{(1)}} + \frac{\Sigma^{11(2)}-\Sigma^{22(2)}}{2}. \tag{3.60}$$

Note that Λ is an implicit function of both $\mathbf{p}$ and $\omega_{\mathbf{p}}$ via the self-energies. Substituting Eqs. (3.41a)–(3.41c) and (3.44)–(3.56) in Eqs. (3.59) and (3.60), we obtain the second-order

energy spectrum of phonons in the low-momentum regime as

$$\begin{aligned}\hbar\omega_{\mathbf{p}}^{(2)} &= \left(1+\frac{28\sqrt{n_0a^3}}{3\sqrt{\pi}}\right)\sqrt{2gn_0\epsilon_{\mathbf{p}}^0}-i\frac{3\sqrt{\pi}\sqrt{n_0a^3}(\epsilon_{\mathbf{p}}^0)^{5/2}}{80(n_0g)^{3/2}}\\ &= \left(1+\frac{8\sqrt{na^3}}{\sqrt{\pi}}\right)\sqrt{2gn\epsilon_{\mathbf{p}}^0}-i\frac{3\sqrt{\pi}\sqrt{na^3}(\epsilon_{\mathbf{p}}^0)^{5/2}}{80(ng)^{3/2}}\\ &= \left(1+\frac{8\sqrt{na^3}}{\sqrt{\pi}}\right)\hbar v_{\mathrm{s}}^{(1)}|\mathbf{p}|-i\frac{3\hbar^2|\mathbf{p}|^5}{640\pi Mn}. \end{aligned} \tag{3.61}$$

Here in deriving the second equality, we used relation (3.2) between n_0 and n. Comparing this result with the Bogoliubov first-order spectrum [Eq. (3.32)], it is evident that the sound velocity increases by a factor of

$$v_{\mathrm{s}}^{(2)} = \left(1+\frac{8\sqrt{na^3}}{\sqrt{\pi}}\right)v_{\mathrm{s}}^{(1)}, \tag{3.62}$$

and a nonzero imaginary part of the excitation energy appears, describing a finite lifetime of the phonons with a damping rate

$$P_{\mathrm{damp}} = \frac{3\hbar|\mathbf{p}|^5}{320\pi Mn}. \tag{3.63}$$

Here we used the relation $P_{\mathrm{damp}} = -2\mathrm{Im}\,\hbar\omega_{\mathbf{p}}^{(2)}$ resulting from the fact that the probability of finding a quasiparticle is proportional to the square of its wavefunction.

Chapter 4

Fluctuation-induced and symmetry-prohibited metastabilities

Since the order parameters and the associated symmetries of the different phases of spin-2 BECs in Fig. 2.3 cannot be transformed continuously at the phase boundary, these phase transitions must be first order. This can be justified by a finite jump in the first derivative of the ground-state energy with respect to the parameter that drives the transition (see Appendix C). First-order phase transitions are usually accompanied by metastable states. However, the Bogoliubov analysis predicts either a dynamical instability with a complex excitation energy or a Landau instability with a negative excitation energy at the mean-field phase boundaries as shown in Sec. 2.4.2. This implies no metastability. Such discrepancy is due to the fact that the Bogoliubov spectrum is obtained by considering a small amplitude expansion of the order parameter around the mean field. This is carried out by linearizing the Gross-Pitatevskii energy functional which, for a homogeneous system with contact interactions, consists of only terms up to the fourth order in the order parameter [19]. We note that the Gross-Pitaevskii energy functional is equivalent to that of Landau's $\phi^2 + \phi^4$ model which plays the key role in the treatment of second-order phase transitions. However, to describe the first-order phase transitions, terms of higher orders in ϕ are needed [29], and in gaseous BECs these higher-order terms can only be obtained by taking into account quantum fluctuations. In other words, in spin-2 BECs the metastability, if it exists, is induced by quantum fluctuations. In Sec. 4.3, we show that metastable states indeed appear as we go to the next-order approximation, i.e., the spinor Beliaev theory [40].

In this chapter, we first construct the beyond-mean-field ground-state phase diagram of spin-2 BECs at the level of the Lee-Huang-Yang (LHY) correction (Sec. 4.1). We then develop the Beliaev theory of spin-2 BECs, from which the excitation spectra of the ferromagnetic and uniaxial-nematic (UN) phases are derived (Sec. 4.2). From the obtained spectra, we show that the fluctuation-induced metastable states appear around the ferromagnetic-BN and UN-cyclic phase boundaries (Sec. 4.3). With the presence of a metastable condensate, we then discuss the possibility of macroscopic quantum tunneling (Sec. 4.4). On the other hand, we find no metastability at the other two phase boundaries. We will show that the absence of metastability holds to all orders of approximation since the metastable state is prohibited by the high symmetry of the Hamiltonian at the phase boundary (Sec. 4.5). Therefore, the spinor Beliaev theory gives fully consistent results for all of the first-order phase transitions in spin-2 BECs.

4.1 Beyond-mean-field ground-state phase diagram

The ground-state phase diagram with the Lee-Huang-Yang (LHY) correction is shown in Fig. 4.1. The LHY correction is the leading-order correction to the Hartree mean-field energy, which arises from quantum fluctuations of the condensate [70, 71]. Recent experiments on ultracold atoms have demonstrated that the LHY correction can accurately account for the deviation of the ground-state energy from the Hartree energy up to the strongest interaction available for a stable condensate [72]. The LHY corrections were calculated for the different phases in spin-1 and spin-2 BECs in Refs. [68, 73, 74]. Using the LHY corrections, we find that the ground-state phase diagram is modified from that in Fig. 2.3 as follows. The detailed calculations are given in Appendix B.

Uniaxial nematic (UN) - biaxial nematic (BN) phase boundary. As shown in Refs. [73, 74], zero-point fluctuations lift the degeneracy in the nematic phase, rendering the ground state either the UN phase ($\eta = n\pi/3$) for $c_1 > 0$ or the BN phase ($\eta = \pi/6 + n\pi/3$) for $c_1 < 0$. Here η is the parameter characterizing the nematic phases as introduced in Sec. 2.3.2. Therefore, the UN-BN phase transition occurs at $c_1 = 0$. Note that all the states whose order parameters are characterized by different values of $n = 0, \ldots, 5$ are degenerate and belong to the same ground-state manifold. For example, the BN phase includes the states with the order parameters $(\sqrt{2}, 0, 2\sqrt{3}, 0, \sqrt{2})^{\mathrm{T}}/4$ ($\eta = \pi/6$) and $(1, 0, 0, 0, 1)^{\mathrm{T}}/\sqrt{2}$ ($\eta = \pi/2$).

Ferromagnetic-BN phase boundary. By comparing the ground-state energies with the LHY corrections of the ferromagnetic and BN phases [see Eqs. (B.2)-(B.4) in Appendix B], we find that the ferromagnetic-BN phase boundary is shifted from its mean-field counterpart at $c_2 = 20c_1$ to

$$c_2^{\mathrm{FM-BN}} \simeq 20c_1 - 1521 \left(\frac{|c_1|}{c_0}\right)^{3/2} \sqrt{na^3}\, |c_1|; \tag{4.1}$$

i.e., the region of the ferromagnetic phase is enlarged. Here $a \equiv (4a_2 + 3a_4)/7$ so that $c_0 = 4\pi\hbar^2 a/M$.

UN-cyclic phase boundary. Similarly, the phase boundary between the UN and cyclic phases is given by [see Eqs. (B.5)–(B.7) in Appendix B]

$$c_2^{\mathrm{UN-CL}} \simeq -342 \left(\frac{c_1}{c_0}\right)^{3/2} \sqrt{na^3}\, c_1. \tag{4.2}$$

Comparing this with the mean-field UN-cyclic phase boundary given by $c_2 = 0$ and $c_1 > 0$, we know that the region of the cyclic phase is enlarged.

Ferromagnetic-cyclic phase boundary. The LHY correction does not shift the ferromagnetic-cyclic phase boundary. In fact, this phase boundary stays at $c_1 = 0$ to all orders of approximation. Indeed, from the order parameters $\boldsymbol{\xi}^{\mathrm{FM}} = (1, 0, 0, 0, 0)^{\mathrm{T}}$ and $\boldsymbol{\xi}^{\mathrm{CL}} = (1, 0, 0, \sqrt{2}, 0)^{\mathrm{T}}/\sqrt{3}$, it is evident that the ground-state energies of the ferromagnetic and cyclic phases are independent of c_2 since the excitations caused by c_2 vanish due to the absence of spin-singlet pairs in both of these phases. Because c_0 is the coupling constant of the spin-independent interaction, the energies of these two phases should be equal at $c_1 = 0$. Therefore, the phase boundary is not shifted by quantum fluctuations (see also Sec. 4.5.2).

Note that the failure of the Bogoliubov theory in capturing the metastability leads to a disagreement with the ground-state phase diagram (Fig. 4.1). For example, the ground state is the ferromagnetic phase for $c_2 > c_2^{\mathrm{F-BN}}$ and $c_1 < 0$ [see Eq. (4.1)], whereas the Bogoliubov spectrum indicates an instability of the ferromagnetic phase for $c_2^{\mathrm{F-BN}} < c_2 < 20c_1$ (see Sec. 2.4.2). In Secs. 4.3 and 4.5 below, we will show that the spinor Beliaev theory gives results which are

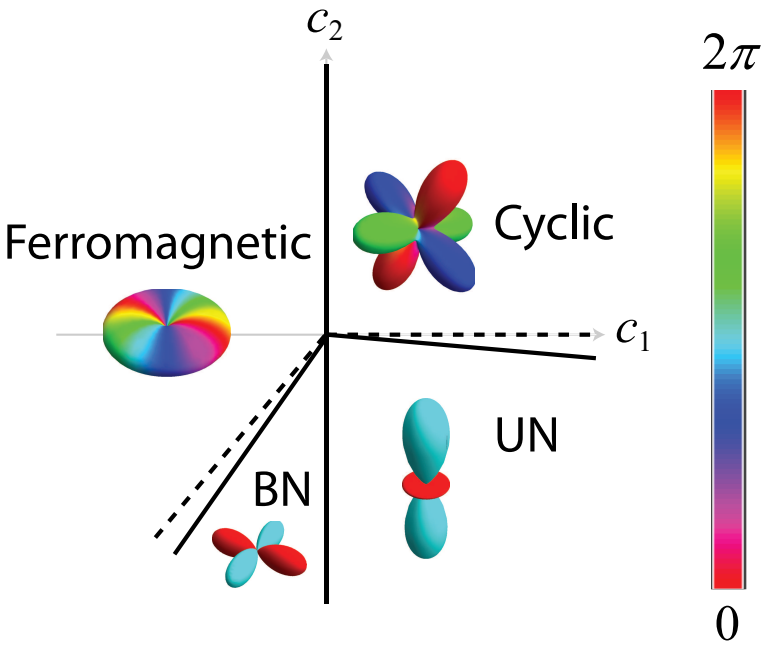

Figure 4.1: Ground-state phase diagram of spin-2 BECs obtained with the Lee-Huang-Yang (LHY) correction (solid lines). The dashed lines indicate the phase boundaries obtained with the Hartree mean-field approximation (Fig. 2.3). The representative spinor order parameters of the ferromagnetic, cyclic, uniaxial-nematic (UN), and biaxial-nematic (BN) phases are given by $\boldsymbol{\xi}^{\mathrm{FM}} = (1,0,0,0,0)^{\mathrm{T}}$, $\boldsymbol{\xi}^{\mathrm{CL}} = (1,0,0,\sqrt{2},0)^{\mathrm{T}}/\sqrt{3}$, $\boldsymbol{\xi}^{\mathrm{UN}} = (0,0,1,0,0)^{\mathrm{T}}$, and $\boldsymbol{\xi}^{\mathrm{BN}} = (\sqrt{2},0,2\sqrt{3},0,\sqrt{2})^{\mathrm{T}}/4$, respectively. The insets show the spherical harmonic representations of the spinor order parameters as explained in Fig. 1.1. Note that the ground-state manifold of each phase includes all the states obtained by applying SO(3) rotations in spin space to the representative order parameter; e.g., the order parameters $\boldsymbol{\xi}^{\mathrm{BN}} = (1,0,0,0,1)^{\mathrm{T}}/\sqrt{2}$ and $\boldsymbol{\xi}^{\mathrm{CL}} = (1,0,i\sqrt{2},0,1)^{\mathrm{T}}/2$ belong to the BN and cyclic phases, respectively. The LHY correction due to quantum fluctuations lifts the degeneracy in the manifold of the nematic phases, rendering the ground state either the UN phase for $c_1 > 0$ or the BN phase for $c_1 < 0$. Quantum fluctuations also shift the cyclic-UN and ferromagnetic-BN phase boundaries as indicated by the solid lines. However, the ferromagnetic-cyclic phase boundary is not affected to all orders of approximation (see text). (Figure reproduced from Ref. [40])

fully consistent with the ground-state phase diagram of spin-2 BECs with the LHY correction.

In the presence of an external magnetic field, the quadratic Zeeman shift with the coefficient q may compete with the shift due to the LHY correction whose order of magnitude is $\Delta E \sim M^{3/2}c_1^{5/2}n^{3/2}/\pi^2\hbar^3$ (see Appendix B). The phase diagram, therefore, depends on the relative strength of these two effects. In the limit of high magnetic field $q \gg \Delta E$, the effect of quantum fluctuations can be ignored, and the ground-state phase diagram is obtained by the Hartree mean-field theory [75]. This is the condition for the experiments of the spin-2 ^{87}Rb BEC described in Ref. [17]. For ^{87}Rb under a high magnetic field, the ground state is the BN phase, while the dynamics starting from the unstable UN phase could populate all magnetic sublevels. In the opposite limit of low magnetic field $q \ll \Delta E$, quantum fluctuations dominate, and the quadratic Zeeman energy becomes negligible. In this case, the ground-state phase diagram is shown in Fig. 4.1. The crossover between these two distinct regimes occurs at $q \sim \Delta E$, which corresponds to a magnetic field of the order of 7 mG for the parameters of ^{87}Rb [76, 77] with an atomic density $n = 10^{15}\,\mathrm{cm}^{-3}$. All these regimes can, in principle, be studied since the lowest magnetic field that has been achieved in ultracold atomic experiments is as small as 0.1 mG [78]. In the next section, however, we only consider the case of spin-2 BECs in the absence of a magnetic field.

4.2 Beliaev theory of spin-2 BECs

In this section, we develop the spinor Beliaev theory for spin-2 BECs based on a Green's function approach, and then apply it to calculate the excitation spectra of the ferromagnetic and UN states. The formalism is a generalization of the scalar Beliaev theory introduced in Sec. 3.1 to spin-2 condensates. It also shares many similarities with the spin-1 Beliaev theory developed in Ref. [79]. From the obtained excitation spectra, we can determine the points in the phase diagram at which instabilities set in.

The Dyson equation for the Green's function is given by Eq. (3.18) as for scalar BECs, but now $\hat{G}$, $\hat{G}^0$, and $\hat{\Sigma}$ are 10×10 matrices with the superscripts labeling the normal (11 and 22) and anomalous (12 and 21) components and the subscripts indicating the magnetic sublevels. For the ferromagnetic and UN states with order parameters $\boldsymbol{\xi}^{\mathrm{FM}} = (1,0,0,0,0)^{\mathrm{T}}$ and $\boldsymbol{\xi}^{\mathrm{UN}} = (0,0,1,0,0)^{\mathrm{T}}$, the self-energies are given by

$$\hat{\Sigma}^{\mathrm{FM}} = \begin{bmatrix} \Sigma^{11}_{2,2} & 0 & 0 & 0 & 0 & \Sigma^{12}_{2,2} & 0 & 0 & 0 & 0 \\ 0 & \Sigma^{11}_{1,1} & 0 & 0 & 0 & 0 & 0 & 0 & 0 & 0 \\ 0 & 0 & \Sigma^{11}_{0,0} & 0 & 0 & 0 & 0 & 0 & 0 & 0 \\ 0 & 0 & 0 & \Sigma^{11}_{-1,-1} & 0 & 0 & 0 & 0 & 0 & 0 \\ 0 & 0 & 0 & 0 & \Sigma^{11}_{-2,-2} & 0 & 0 & 0 & 0 & 0 \\ \Sigma^{21}_{2,2} & 0 & 0 & 0 & 0 & \Sigma^{22}_{2,2} & 0 & 0 & 0 & 0 \\ 0 & 0 & 0 & 0 & 0 & 0 & \Sigma^{22}_{1,1} & 0 & 0 & 0 \\ 0 & 0 & 0 & 0 & 0 & 0 & 0 & \Sigma^{22}_{0,0} & 0 & 0 \\ 0 & 0 & 0 & 0 & 0 & 0 & 0 & 0 & \Sigma^{22}_{-1,-1} & 0 \\ 0 & 0 & 0 & 0 & 0 & 0 & 0 & 0 & 0 & \Sigma^{22}_{-2,-2} \end{bmatrix} \tag{4.3}$$

and

$$\hat{\Sigma}^{\mathrm{UN}} = \begin{bmatrix} \Sigma^{11}_{2,2} & 0 & 0 & 0 & 0 & 0 & 0 & 0 & 0 & \Sigma^{12}_{2,-2} \\ 0 & \Sigma^{11}_{1,1} & 0 & 0 & 0 & 0 & 0 & 0 & \Sigma^{12}_{1,-1} & 0 \\ 0 & 0 & \Sigma^{11}_{0,0} & 0 & 0 & 0 & 0 & \Sigma^{12}_{0,0} & 0 & 0 \\ 0 & 0 & 0 & \Sigma^{11}_{-1,-1} & 0 & 0 & \Sigma^{12}_{-1,1} & 0 & 0 & 0 \\ 0 & 0 & 0 & 0 & \Sigma^{11}_{-2,-2} & \Sigma^{12}_{-2,2} & 0 & 0 & 0 & 0 \\ 0 & 0 & 0 & 0 & \Sigma^{21}_{2,-2} & \Sigma^{22}_{2,2} & 0 & 0 & 0 & 0 \\ 0 & 0 & 0 & \Sigma^{21}_{1,-1} & 0 & 0 & \Sigma^{22}_{1,1} & 0 & 0 & 0 \\ 0 & 0 & \Sigma^{21}_{0,0} & 0 & 0 & 0 & 0 & \Sigma^{22}_{0,0} & 0 & 0 \\ 0 & \Sigma^{21}_{-1,1} & 0 & 0 & 0 & 0 & 0 & 0 & \Sigma^{22}_{-1,-1} & 0 \\ \Sigma^{21}_{-2,2} & 0 & 0 & 0 & 0 & 0 & 0 & 0 & 0 & \Sigma^{22}_{-2,-2} \end{bmatrix}. \quad (4.4)$$

Here $\Sigma^{22}_{jj'}(p) \equiv \Sigma^{11}_{jj'}(-p)$, and $\Sigma^{12}_{jj'}(p) = \Sigma^{21}_{jj'}(p)$ because the corresponding diagrams are the same. In $\hat{\Sigma}^{\mathrm{UN}}$, only the anomalous components $\Sigma^{12;21}_{j,-j}$ $(j = 2, \cdots, -2)$ are nonzero due to the spin conservation applied to the creation of a pair of noncondensed particles out of a condensate in the spin state $m_F = 0$. The Green's functions $\hat{G}^{\mathrm{FM}}$ and $\hat{G}^{\mathrm{UN}}$ have the same forms of matrix as $\hat{\Sigma}^{\mathrm{FM}}$ and $\hat{\Sigma}^{\mathrm{UN}}$, respectively, i.e., $G^{\alpha\beta}_{j,j'} = 0$ provided $\Sigma^{\alpha\beta}_{j,j'} = 0$.

By solving the Dyson equation, we can express the Green's functions in terms of the self-energies, and according to the Lehmann representation [80, 20], the excitation spectra are obtained from the poles of the Green's functions. Since the low-energy long-wavelength excitation modes give rise to the instabilities near the phase boundaries, we will focus on the zero-momentum excitation energies. The results for the ferromagnetic and UN states are summarized as follows.

Ferromagnetic state. The $m_F = 2$ excitation mode, which is in the same spin state as the condensate, correspond to the phonon excitation. It features the nonzero anomalous self-energies $\Sigma^{12;21}_{2,2}$ in Eq. (4.3) and thus has a linear dispersion relation in the low-momentum regime characterized by the sound velocity as in scalar BECs. The sound velocity is always positive as long as $c_0 \gg |c_1|, |c_2|$, which is the case of atomic species such as ^{87}Rb and ^{23}Na; therefore, no instability should occur with this mode. In contrast, the $m_F = j \neq 2$ modes are single-particle-like excitations due to the vanishing of the anomalous self-energies, and their Green's functions are given by

$$G^{11}_{j,j}(p) = \frac{1}{[G^0_j(p)]^{-1} - \Sigma^{11}_{j,j}(p)}, \quad (4.5)$$

where the noninteracting Green's function $G^0_j(p)$ in the absence of an external magnetic field is independent of j and given by the right-hand side of Eq. (3.22). From Eq. (4.5), the zero-momentum energy of the $m_F = j$ excitation mode satisfies

$$\omega_{j,\mathbf{p}=\mathbf{0}} = \Sigma^{11}_{j,j}\left(\omega_{j,\mathbf{p}=\mathbf{0}}, \mathbf{p} = \mathbf{0}\right) - \mu/\hbar. \quad (4.6)$$

UN state. The Green's function of the $m_F = 0$ mode describes the phonon excitation which does not bring about any instability for $c_0 \gg |c_1|, |c_2|$. For the other $m_F \neq 0$ modes, the corresponding Green's functions are given by

$$G^{11}_{j,j}(p) = \frac{-[G^0_j(-p)]^{-1} + \Sigma^{11}_{j,j}(-p)}{D_j}, \quad (4.7)$$

where

$$D_j = -[G_j^0(p)]^{-1}[G_{-j}^0(-p)]^{-1} + \Sigma_{j,j}^{11}(p)[G_{-j}^0(-p)]^{-1} + \Sigma_{-j,-j}^{22}(p)[G_j^0(p)]^{-1} - \Sigma_{j,j}^{11}(p)\Sigma_{-j,-j}^{22}(p) + \Sigma_{-j,j}^{21}(p)\Sigma_{j,-j}^{12}(p) + i\eta. \tag{4.8}$$

The zero of D_j gives the excitation energy spectrum, which is calculated for $\mathbf{p} = \mathbf{0}$ to be

$$\omega_{j,\mathbf{p}=\mathbf{0}} = \frac{\left(\Sigma_{j,j}^{11} - \Sigma_{-j,-j}^{22}\right)}{2} + \left\{ -\Sigma_{j,-j}^{12}\Sigma_{-j,j}^{21} + \left[-\frac{\mu}{\hbar} + \frac{\left(\Sigma_{j,j}^{11} + \Sigma_{-j,-j}^{22}\right)}{2} \right]^2 \right\}^{1/2}. \tag{4.9}$$

Here, with the same argument as given above Eq. (3.59), we take only the plus sign in front of the square root in Eq. (4.9). For the UN phase with a symmetric order parameter $\boldsymbol{\xi}^{\mathrm{UN}} = (0,0,1,0,0)^{\mathrm{T}}$, there is an equivalence between the $m_F = \pm j$ magnetic sublevels, leading to

$$\Sigma_{j,j}^{11} = \Sigma_{-j,-j}^{11},\ \Sigma_{j,j}^{22} = \Sigma_{-j,-j}^{22}, \tag{4.10a}$$

$$\Sigma_{j,-j}^{12} = \Sigma_{-j,j}^{12} = \Sigma_{j,-j}^{21} = \Sigma_{-j,j}^{21}, \tag{4.10b}$$

$$D_j = D_{-j}. \tag{4.10c}$$

Equation (4.10c) implies twofold degeneracies in the excitation energies given by Eq. (4.9) with $j = \pm 1$ and ± 2.

In the next section, we make expansions of Σ and μ with respect to na^3, which is the characteristic dimensionless parameter of a dilute weakly interacting Bose gas. These expansions are represented by the sums of Feynman diagrams similar to Figs. 3.4–3.8. Compared with the Feynman diagrams of scalar BECs, we need to add the spin degrees of freedom to each propagator in the diagrams of spinor BECs. Furthermore, the T-matrix, which represents the two-body scattering in a medium composed of the other particles, now have the contributions from both the spin-independent and spin-dependent interactions with the coupling constants c_0, c_1, and c_2 defined in Eq. (2.15). The Bogoliubov and Beliaev theories are constucted from the contributions of the Feynman diagrams up to the first and second order, respectively. In comparison, there appear virtual excitations, i.e., quantum fluctuations, of the condensate with momenta q and $p-q$ in the second-order diagrams, which are absent in the first-order ones (see Figs. 3.4–3.8). It is these quantum fluctuations that generate the higher-order terms beyond ϕ^4 in the energy functional which play an essential role in the first-order phase transitions of spin-2 BECs, as discussed at the beginning of this chapter.

4.3 Fluctuation-induced metastability

With the excitation energies obtained in the previous section, we can identify the points in the phase diagram at which instabilities set in. Combined with the conditions on the phase boundaries discussed in Sec. 4.1, we find that the fluctuation-induced metastable states appear in the ferromagnetic-BN and UN-cyclic phase transitions, while there is no metastability associated with the ferromagnetic-cyclic and UN-BN phase transitions. In the latter case, the absence of metastability holds to all orders of approximation due to the symmetry of the Hamiltonian as will be discussed in Sec. 4.5.

Ferromagnetic-BN phase transition. From the order parameters of the ferromagnetic [$\boldsymbol{\xi}^{\mathrm{FM}} = (1,0,0,0,0)^{\mathrm{T}}$] and BN [$\boldsymbol{\xi}^{\mathrm{BN}} = (1,0,0,0,1)^{\mathrm{T}}/\sqrt{2}$] states, it is clear that starting from the ferromagnetic phase, the excitation mode that drives this phase transition is the one with $m_F = -2$. We thus examine the zero-momentum energy of this mode. The expansion of Eq. (4.6) up to

the first-order Feynman diagrams reproduces the Bogoliubov result:

$$\begin{aligned}\hbar\omega^{(1)}_{-2,\mathbf{p}=\mathbf{0}} &\simeq \hbar\Sigma^{11(1)}_{-2,-2} - \mu^{(1)} \\ &= \left(-8c_1 + \frac{2c_2}{5}\right) n_0. \end{aligned} \tag{4.11}$$

By summing all the contributions to $\Sigma^{11}_{-2,-2}$ and μ from the second-order diagrams, we obtain [see Eq. (D.12) in Appendix D]

$$\hbar\Sigma^{11(2)}_{-2,-2} - \mu^{(2)} \simeq \frac{(36\sqrt{3}+64)|c_1|^{5/2}(Mn_0)^{3/2}}{2\sqrt{2}\pi\hbar^3} \tag{4.12}$$

near the ferromagnetic-BN phase boundary where $c_1 < 0$ and $c_2 \simeq 20c_1$ [see Eq. (4.1)]. From Eqs. (4.6), (4.11), and (4.12), the zero-momentum energy of the $m_F = -2$ excitation mode of the ferromagnetic phase is obtained up to the second order as

$$\hbar\omega^{(2)}_{-2,\mathbf{p}=\mathbf{0}} \simeq \left(-8c_1 + \frac{2c_2}{5}\right) n_0 + \frac{(36\sqrt{3}+64)|c_1|^{5/2}(Mn_0)^{3/2}}{2\sqrt{2}\pi\hbar^3}. \tag{4.13}$$

From Eq. (4.13), we find that the Landau instability of the ferromagnetic phase arises if $\hbar\omega^{(2)}_{-2,\mathbf{p}=\mathbf{0}} < 0$, or equivalently, if

$$\begin{aligned} c_2 < c_2^{\mathrm{FM-unstable}} &\equiv 20c_1 - \frac{5(36\sqrt{3}+64)M^{3/2}n_0^{1/2}c_1^{5/2}}{4\sqrt{2}\pi\hbar^3} \\ &\simeq 20c_1 - 1584\left(\frac{|c_1|}{c_0}\right)^{3/2}\sqrt{n_0a^3}\,|c_1| \\ &\simeq 20c_1 - 1584\left(\frac{|c_1|}{c_0}\right)^{3/2}\sqrt{na^3}\,|c_1|. \end{aligned} \tag{4.14}$$

In the last (approximate) equality in Eq. (4.14), we used the relation between the condensate's particle density and the total atomic density $n_0/n = 1 - 8\sqrt{na^3}/(3\sqrt{\pi})$, and retained only terms up to the order of $\sqrt{na^3}$, which is the order of magnitude under consideration in the Beliaev theory. It follows from Eqs. (4.1) and (4.14) that the ferromagnetic phase is metastable for

$$-1584 < \frac{c_2 - 20c_1}{\left(\frac{|c_1|}{c_0}\right)^{3/2}\sqrt{na^3}|c_1|} < -1521. \tag{4.15}$$

From the hysteretic feature of a first-order phase transition, the BN phase is also expected to be metastable for $c_2^{\mathrm{FM-BN}} < c_2 < c_2^{\mathrm{BN-unstable}}$.

UN-cyclic phase transition. As shown in Sec. 4.2, for the UN phase with a symmetric order parameter $\boldsymbol{\xi}^{\mathrm{UN}} = (0,0,1,0,0)^{\mathrm{T}}$, there are two degenerate excitation modes which are superpositions of the magnetic sublevels $m_F = \pm 2$. Since the order parameter $(1,0,i\sqrt{2},0,1)^{\mathrm{T}}/2$, which has equal weights of $m_F = \pm 2$ components, describes a state of the cyclic phase (see Sec. 2.3.2), it is evident that the instability in the $m_F = \pm 2$ modes causes the UN-cyclic phase transition. By separating the contributions to Σ and μ in Eq. (4.9) from the first- and second-order Feynman diagrams, the zero-momentum excitation energies of these modes are given up

to the second order by

$$\omega_{\pm 2,\mathbf{p}=\mathbf{0}} = \frac{\Sigma_{22}^{11(2)} - \Sigma_{22}^{22(2)}}{2} + \left\{ -\left[\frac{c_2 n_0}{5\hbar} + \Sigma_{2,-2}^{12(2)}\right]^2 + \left[-\frac{c_2 n_0}{5\hbar} - \frac{\mu^{(2)}}{\hbar} + \frac{\Sigma_{22}^{11(2)} + \Sigma_{22}^{22(2)}}{2}\right]^2 \right\}^{1/2}, \tag{4.16}$$

where Eqs. (4.10a) and (4.10b) were used. Since it is expected that $\hbar\omega_{\pm 2,\mathbf{p}=\mathbf{0}} \ll c_1 n_0$ near the phase boundary which can be justified *a posteriori* from the final result, we can make Taylor series expansions of $\Sigma_{2,2}^{11(2)}$, $\Sigma_{2,2}^{22(2)}$, and $\Sigma_{2,-2}^{12(2)}$ in powers of $\hbar\omega_{\pm 2,\mathbf{p}=\mathbf{0}}/(c_1 n_0)$ as (see Appendix D)

$$\hbar\Sigma_{2,2}^{11(2)} = A + B\hbar\omega_{\pm 2,\mathbf{p}=\mathbf{0}} + \mathcal{O}\left[\left(\frac{\hbar\omega_{\pm 2,\mathbf{p}=\mathbf{0}}}{c_1 n_0}\right)^2\right], \tag{4.17}$$

$$\hbar\Sigma_{2,2}^{22(2)} = A - B\hbar\omega_{\pm 2,\mathbf{p}=\mathbf{0}} + \mathcal{O}\left[\left(\frac{\hbar\omega_{\pm 2,\mathbf{p}=\mathbf{0}}}{c_1 n_0}\right)^2\right], \tag{4.18}$$

$$\hbar\Sigma_{2,-2}^{12(2)} = C + \mathcal{O}\left[\left(\frac{\hbar\omega_{\pm 2,\mathbf{p}=\mathbf{0}}}{c_1 n_0}\right)^2\right], \tag{4.19}$$

where we ignored the quadratic and higher-order terms. Substituting Eqs. (4.17)-(4.19) into Eq. (4.16), we obtain

$$\hbar\omega_{\pm 2,\mathbf{p}=\mathbf{0}} \simeq \frac{\sqrt{\left[-\frac{c_2 n_0}{5} + A - \mu^{(2)}\right]^2 - \left[\frac{c_2 n_0}{5} + C\right]^2}}{1 - B}. \tag{4.20}$$

Therefore, a dynamical instability will arise if $\omega_{\pm 2,\mathbf{p}=\mathbf{0}}$ is a complex number with a nonzero imaginary part, i.e., if

$$\begin{aligned} 0 &> \left[-\frac{c_2 n_0}{5} + A - \mu^{(2)}\right]^2 - \left[\frac{c_2 n_0}{5} + C\right]^2 \\ &= \left[A - \mu^{(2)} + C\right]\left[-\frac{2c_2 n_0}{5} + A - \mu^{(2)} - C\right]. \end{aligned} \tag{4.21}$$

By summing all the contributions to Σ and μ from the second-order Feynman diagrams, we find that around the UN-cyclic phase boundary where $c_1 > 0, c_2 < 0$ and $|c_2| \ll c_1$ [see Eq. (4.2)], the coefficients A, B, and C in Eqs. (4.17)–(4.19) are given by [see Eqs. (D.32)–(D.34) in Appendix D]

$$\frac{A - \mu^{(2)}}{(M n_0)^{3/2}} \simeq -\frac{4\sqrt{3}c_1^{5/2}}{\pi^2\hbar^3} + \frac{\left(42\sqrt{3}c_1^{3/2} - 10c_0^{3/2}\right)c_2}{15\pi^2\hbar^3} + \mathcal{O}\left[\left(\frac{|c_2|}{c_1}\right)^2\right], \tag{4.22}$$

$$\frac{B}{M^{3/2} n_0^{1/2}} \simeq -\frac{\left(c_0^{3/2} + 3\sqrt{3}c_1^{3/2}\right)}{3\pi^2\hbar^3} - \frac{\left(c_0^{1/2} + \sqrt{3}c_1^{1/2}\right)c_2}{30\pi^2\hbar^3} + \mathcal{O}\left[\left(\frac{|c_2|}{c_1}\right)^2\right], \tag{4.23}$$

$$\frac{C}{(M n_0)^{3/2}} \simeq \frac{12\sqrt{3}c_1^{5/2}}{\pi^2\hbar^3} + \frac{\left(10c_0^{3/2} - 30\sqrt{3}c_1^{3/2}\right)c_2}{15\pi^2\hbar^3} + \mathcal{O}\left[\left(\frac{|c_2|}{c_1}\right)^2\right]. \tag{4.24}$$

By substituting Eqs. (4.22)–(4.24) in Eq. (4.21), we find that the UN phase becomes dynamically unstable and the system makes a transition to the cyclic phase if

$$c_2 > c_2^{\mathrm{UN-unstable}} \equiv -\frac{40\sqrt{3}M^{3/2}n^{1/2}c_1^{5/2}}{\pi^2\hbar^3} \simeq -313\left(\frac{c_1}{c_0}\right)^{3/2}\sqrt{na^3}\,c_1. \tag{4.25}$$

It follows from Eqs. (4.2) and (4.25) that the UN phase is metastable for

$$-342 < \frac{c_2}{\left(\frac{c_1}{c_0}\right)^{3/2}\sqrt{na^3}\,c_1} < -313. \tag{4.26}$$

From the hysteretic feature of a first-order phase transition, the cyclic phase is also expected to be metastable for $c_2^{\mathrm{UN-CL}} > c_2 > c_2^{\mathrm{CL-unstable}}$. Therefore, by using the spinor Beliaev theory, we have shown explicitly the existence of the metastable states that are induced by quantum fluctuations. This result also finds a qualitative agreement with the slow dynamics of the spin-2 ^{87}Rb condensate that has been observed in spin-dynamics measurements [17].

4.4 Macroscopic quantum tunneling

The presence of a metastable condensate as shown in the previous section suggests an interesting possibility of a decay of the metastable state into the lower energy state via macroscopic quantum tunneling (MQT); i.e., all atoms tunnel simultaneously from one phase to the other. We consider this possibility for the metastable state near the UN-cyclic phase boundary, as the parameters of the spin-2 ^{87}Rb BEC are thought to lie in the vicinity of this phase boundary [76, 77, 81]. Equation (4.26) shows that there is a parameter regime for which the UN phase is metastable and the cyclic phase is the ground state. By neglecting the quantum depletion, these state vectors are expressed by

$$|\mathrm{UN}\rangle \simeq \left(\hat{a}^\dagger_{0,\mathbf{p}=\mathbf{0}}\right)^N |\mathrm{vac}\rangle, \tag{4.27a}$$

$$|\mathrm{Cyclic}\rangle \simeq \left(\frac{\hat{a}^\dagger_{2,\mathbf{p}=\mathbf{0}}}{2} + \frac{\hat{a}^\dagger_{0,\mathbf{p}=\mathbf{0}}}{\sqrt{2}} + \frac{\hat{a}^\dagger_{-2,\mathbf{p}=\mathbf{0}}}{2}\right)^N |\mathrm{vac}\rangle. \tag{4.27b}$$

Since these states are not the exact eigenstates of the many-body Hamiltonian (2.16), they will undergo quantum diffusions in spin space [82, 83, 84, 85] and induce MQT. We now estimate the time scale of MQT by using the two-level model in which the Hilbert space is restricted to the two states at the local energy minima. The time scale of MQT is then given by $\tau = \hbar/\Delta$ with $\Delta = 2\langle \mathrm{Cyclic}|\hat{V}|\mathrm{UN}\rangle$ being the off-diagonal element of the Hamiltonian. Substituting Eqs. (4.27a) and (4.27b) in Eq. (2.16), we obtain

$$\tau \simeq \hbar\frac{2^{N/2}}{c_0 n(N-1)}, \tag{4.28}$$

where N is the total number of particles. The exponentially large factor of $2^{N/2}$ reflects bosonic stimulation in a BEC. To observe MQT, τ must be equal to or smaller than the lifetime of the BEC, which is typically of the order of a second. Using the parameters of ^{87}Rb [81], we can estimate the upper bound for the total number of particles: $N_{\max} \simeq 36$ for $\tau \lesssim 1$ s. Such

microcondensates have been extensively studied recently [86, 87, 88]. A similar time scale is expected for MQT in the ferromagnetic-BN transition.

4.5 Symmetry-prohibited metastability

In Sec. 4.3, we have shown the existence of the metastable states that are induced by quantum fluctuations in the ferromagnetic-BN and UN-cyclic phase transitions. Now we examine the possibility of metastability at the level of Beliaev approximation in the remaining ferromagnetic-cyclic and UN-BN phase transitions of spin-2 BECs.

Ferromagnetic-cyclic phase transition. From the order parameters of the ferromagnetic [$\boldsymbol{\xi}^{\rm FM} = (1,0,0,0,0)^{\rm T}$] and cyclic [$\boldsymbol{\xi}^{\rm CL} = (1,0,0,\sqrt{2},0)^{\rm T}/\sqrt{3}$] phases, it is clear that the excitation mode that causes the ferromagnetic-cyclic phase transition is the one with $m_F = -1$. Expanding the right-hand side of Eq. (4.6) up to the first-order Feynman diagrams, we reproduce the Bogoliubov result:

$$\begin{aligned}\hbar\omega^{(1)}_{-1,\mathbf{p}=\mathbf{0}} &\simeq \hbar\Sigma^{11(1)}_{-1,-1} - \mu^{(1)} \\ &= -6c_1 n_0. \end{aligned} \tag{4.29}$$

By summing all the contributions to Σ and μ from the second-order Feynman diagrams, we obtain [see Eq. (D.15) in Appendix D]

$$\hbar\Sigma^{11(2)}_{-1,-1} - \mu^{(2)} \simeq -\frac{18c_1 c_0^{3/2}(Mn_0)^{3/2}}{\pi^2\hbar^3}. \tag{4.30}$$

Substituting Eqs. (4.29) and (4.30) in Eq. (4.6), we find the zero-momentum energy of the $m_F = -1$ excitation mode as

$$\hbar\omega^{(2)}_{-1,\mathbf{p}=\mathbf{0}} = -6c_1 n_0 - \frac{18c_1 c_0^{3/2}(Mn_0)^{3/2}}{\pi^2\hbar^3}. \tag{4.31}$$

Equation (4.31) indicates that a Landau instability of the ferromagnetic phase sets in, i.e., $\omega_{-1,\mathbf{p}=\mathbf{0}} < 0$, for $c_1 > 0$. This implies that there is no parameter regime for a metastable ferromagnetic state since the ferromagnetic-cyclic phase boundary lies at $c_1 = 0$. However, although the ferromagnetic state is unstable for $c_1 > 0$, it becomes an excited state, indicating that a level crossing occurs at the ferromagnetic-cyclic phase boundary.

UN-BN phase transition. Similar to the UN-cyclic phase transition, since the order parameter $\boldsymbol{\xi}^{\rm BN} = (1,0,0,0,1)^{\rm T}/\sqrt{2}$ with equal weights of the $m_F = \pm 2$ components describes a BN state (see Sec. 4.1), we know that a dynamical instability in the degenerate $m_F = \pm 2$ excitation modes of the UN state would bring about the UN-BN phase transition. The condition for this instability is given by Eqs. (4.20) and (4.21). Around the UN-BN phase boundary where $c_2 < 0$ and $|c_2| \gtrsim |c_1|$, the coefficients in Eq. (4.21) are calculated to be (see Appendix D)

$$\frac{A - \mu^{(2)} + C}{(Mn_0)^{3/2}} = \frac{1}{\pi^2\hbar^3}\left(8\sqrt{3}\tilde{c}_1^{5/2} - \frac{32}{\sqrt{3}}\tilde{c}_1^{3/2}\tilde{c}_2 + \frac{16}{3}\tilde{c}_1\tilde{c}_2^{3/2} + \frac{8}{\sqrt{3}}\tilde{c}_1^{1/2}\tilde{c}_2^2 - \frac{16}{9}\tilde{c}_2^{5/2}\right) \tag{4.32}$$

and

$$-\frac{2c_2 n_0}{5} + A - \mu^{(2)} - C \simeq -\frac{2c_2 n_0}{5}, \tag{4.33}$$

where $\tilde{c}_2 \equiv -c_2/5$ and $\tilde{c}_1 \equiv c_1 - c_2/15$. It follows from Eqs. (4.21), (4.32), and (4.33) that a

dynamical instability arises if

$$f(x) \equiv 8\sqrt{3}x^{5/2} - \frac{32}{\sqrt{3}}x^{3/2} + \frac{16}{3}x + \frac{8}{\sqrt{3}}x^{1/2} - \frac{16}{9} < 0, \tag{4.34}$$

where $x \equiv \tilde{c}_1/\tilde{c}_2$. The function $f(x)$ on the left-hand side of Eq. (4.34) is plotted in Fig. 4.2, from which we find that the UN state becomes dynamically unstable and the system is driven towards the BN phase if $x < 1/3$, or equivalently, if $c_1 < 0$. That the UN-BN phase boundary lies at $c_1 = 0$ implies that there is no parameter regime for which the UN state is metastable. However, it should be noted that for $c_1 < 0$, where the BN phase is the ground state, the UN state becomes dynamically unstable and cannot exist as an excited state since the excitation modes would grow exponentially. In other words, in contrast to the ferromagnetic-cyclic phase transition there is no level crossing in the UN-BN phase transition. It should be stressed that this result, which has been derived from a stability analysis, is stronger than the previous result obtained in Refs. [73, 74] since it implies not only that the UN phase is no longer the ground state for $c_1 < 0$ but also that it is not even an excited state due to the dynamical instability.

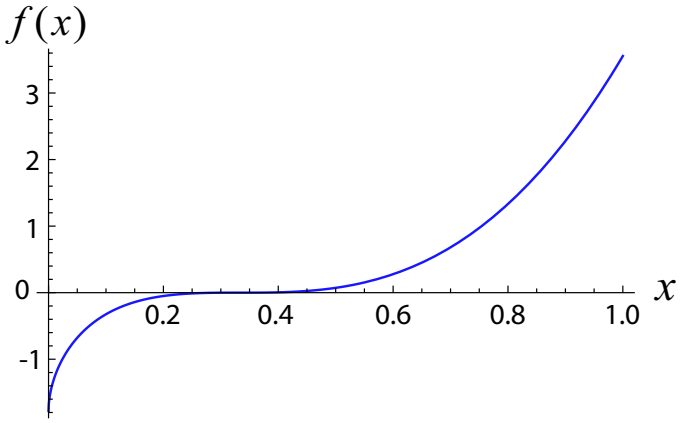

Figure 4.2: Plot of $f(x)$ defined in Eq. (4.34). (Figure reproduced from Ref. [40])

The above stability analysis based on the spinor Beliaev theory shows that the ferromagnetic-cyclic and UN-BN phase transitions are not accompanied by metastable states. In the following two subsections, we show that the absence of metastability holds not only at the level of the Beliaev approximation but to all orders of approximation since the metastable state is prohibited by the high symmetry of the Hamiltonian at the phase boundary. We investigate these underlying symmetries which result in flat energy landscapes at the phase boundaries in both spin-1 and spin-2 BECs. It is these flat energy landscapes that prohibit a coexistence of two phases as opposed to the double-well structure that supports metastability in conventional first-order phase transitions.

4.5.1 Spin-1 BECs

The mean-field ground-state phase diagram of spin-1 BECs is shown in Fig. 2.2. Due to the discontinuity in the transformation of the order parameter and the associated symmetry at the phase boundary, the ferromagnetic-BA and antiferromagnetic-polar phase transitions are first order. This can also be confirmed by a finite jump in the first derivative of the ground-state energy with respect to the quadratic Zeeman coefficient q that drives these transitions (see Appendix C). In contrast, the BA-polar phase transition is second order at the mean-field level.

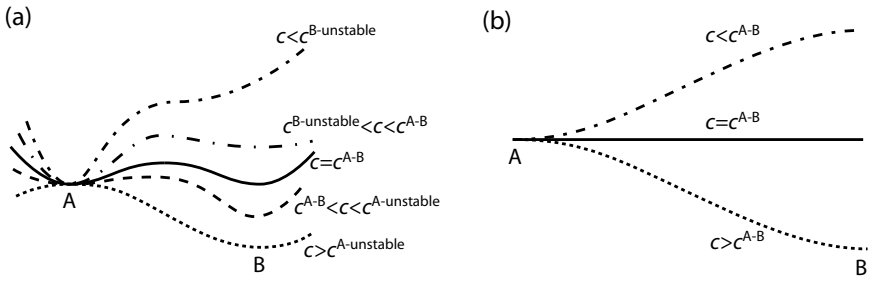

Figure 4.3: Energy landscape in the first-order quantum phase transitions (a) with and (b) without metastability [see Eq. (4.35)]. The transition between A and B phases is controlled by a parameter c (e.g., the interaction c_1 or c_2 in Fig. 4.1 or the quadratic Zeeman coefficient q in Fig. 2.2). Here, $c^{\mathrm{A-B}}$ indicates the phase boundary between the two phases, while $c^{\mathrm{A-unstable}}$ represents the value of c at which the A phase becomes unstable. The energy landscape in (a) features a double-well structure at $c = c^{A-B}$, supporting metastable states around the transition point, whereas the energy landscape in (b) becomes flat at $c = c^{A-B}$, allowing no metastable state. (Figure reproduced from Ref. [40])

We now show that the first-order quantum phase transitions in spin-1 BECs are not accompanied by metastable states, and this holds to all orders of approximation. For nonzero q, the Hamiltonian has the $\mathrm{U}(1)_\phi\times\mathrm{SO}(2)_{f_z}$ symmetry involving the gauge and rotational invariances about the z axis in spin space. Only at $q = 0$ does the Hamiltonian possess a larger symmetry of $\mathrm{U}(1)_\phi\times\mathrm{SO}(3)_{\mathbf{f}}$, corresponding to a full rotational invariance in spin space. On the other hand, at $q = 0$ the order parameters of each pair of phases in the above first-order phase transitions can be transformed between each other via an SO(3) rotation, $\boldsymbol{\xi}^{\mathrm{BA}}(q=0) = e^{if_y\pi/2}\boldsymbol{\xi}^{\mathrm{FM}}$, $\boldsymbol{\xi}^{\mathrm{PL}} = e^{if_y\pi/2}\boldsymbol{\xi}^{\mathrm{AFM}}$. Therefore, the two phases are degenerate at $q = 0$ at any order of approximation. Namely, the phase boundary at $q = 0$ remains unchanged even if quantum corrections are added to the ground-state energy. Furthermore, if we use a parameter θ to represent the order parameters of the intermediate states in the transformation from the ferromagnetic (antiferromagnetic) to the BA (polar) phase: $e^{if_y\theta}\boldsymbol{\xi}^{\mathrm{FM}} = (\cos^2(\theta/2), \sin\theta/\sqrt{2}, \sin^2(\theta/2))^{\mathrm{T}}$ ($e^{if_y\theta}\boldsymbol{\xi}^{\mathrm{AFM}} = (\sin\theta/\sqrt{2}, \cos\theta, \sin\theta/\sqrt{2})^{\mathrm{T}}$) ($0 \leqslant \theta \leqslant \pi/2$), all of these intermediate states are degenerate, i.e., $E(\theta)$ is independent of θ, resulting in a flat energy landscape at $q = 0$. As q traverses the phase boundary from the negative to the positive side, the ferromagnetic (antiferromagnetic) phase abruptly changes from the ground state to an unstable state, leading to no parameter regime of metastability. Similarly, no metastable regime exists for the BA (polar) phase as q crosses the phase boundary from the positive to the negative side. This can be understood by looking at the mean-field energy landscapes

$$E^{\mathrm{FM-BA}}(\theta)/V = \frac{(c_0+c_1)n^2}{2} + qn\left(1-\frac{\sin^2\theta}{2}\right), \tag{4.35}$$

$$E^{\mathrm{AFM-PL}}(\theta)/V = \frac{c_0 n^2}{2} + qn\sin^2\theta, \tag{4.36}$$

where their maximum and minimum at $\theta = 0$ and $\theta = \pi/2$ are exchanged as q crosses the phase boundary. A comparison with the conventional first-order phase transitions, whose energy landscapes feature double-well structures and thus support metastability, is illustrated in Fig. 4.3. Note that the absence of metastability holds not only at the mean-field level but to all orders of approximation since the above argument of the flat energy landscapes at the phase boundaries is based on the consideration of the system's symmetry.

4.5.2 Spin-2 BECs

Now we show that the absence of metastability in the ferromagnetic-cyclic and UN-BN phase transitions, which was proved up to the second-order approximation at the beginning of Sec. 4.5, holds to all orders of approximation due to the symmetry of the Hamiltonian. For finite c_1, the Hamiltonian of spin-2 BECs [Eq. (2.16)] has the $\mathrm{U}(1)_\phi \times \mathrm{SO}(3)_{\mathbf{f}}$ invariant symmetry. Only at $c_1 = 0$ is its symmetry enlarged to $\mathrm{U}(1)_\phi \times \mathrm{SO}(5)_{\mathbf{f}}$ due to the invariance of the interaction $c_2 : \hat{A}_{00}^\dagger \hat{A}_{00} :$ under SO(5) rotations in $F = 2$ spin space [68]. On the other hand, from the order parameters $\boldsymbol{\xi}^{\mathrm{FM}} = (1, 0, 0, 0, 0)^{\mathrm{T}}$ and $\boldsymbol{\xi}^{\mathrm{CL}} = (1, 0, 0, \sqrt{2}, 0)^{\mathrm{T}}/\sqrt{3}$, the ferromagnetic and cyclic phases both have zero spin-singlet-pair amplitude $\langle \hat{A}_{00} \rangle = 0$. Conversely, the UN ($\boldsymbol{\xi}^{\mathrm{UN}} = (0, 0, 1, 0, 0)^{\mathrm{T}}$) and BN ($\boldsymbol{\xi}^{\mathrm{BN}} = (1, 0, 0, 0, 1/)^{\mathrm{T}}/\sqrt{2}$) phases both have the maximum value of the spin-singlet-pair amplitude $\langle \hat{A}_{00} \rangle = n_0/\sqrt{5}$. In other words, the ferromagnetic and cyclic phases (UN and BN phases) belong to the same group of the minimum (maximum) value of the spin-singlet-pair amplitude whose elements can be transformed between each other by SO(5) rotations. Therefore, these pairs of phases are degenerate at $c_1 = 0$ where the Hamiltonian possesses the same symmetry. That the degeneracy strictly holds makes the phase boundaries stay at $c_1 = 0$ even when quantum corrections are taken into account. Furthermore, similar to spin-1 BECs, if the order parameters of the intermediate states in the transformation from the ferromagnetic (UN) to the cyclic (BN) phase are parametrized as $U(\eta)\boldsymbol{\xi}^{\mathrm{FM}} = (\cos\eta, 0, 0, \sin\eta, 0)^{\mathrm{T}}$ [$U'(\eta)\boldsymbol{\xi}^{\mathrm{UN}} = (\sin\eta/\sqrt{2}, 0, \cos\eta, 0, \sin\eta/\sqrt{2})^{\mathrm{T}}$], where $U(\eta)$ [$U'(\eta)$] is an SO(5) rotation operator, all of these intermediate states are energy degenerate, resulting in a flat energy landscape at the phase boundary (see Fig. 4.4). This is evident by, for example, looking at the energy landscape of the nematic phases [Eq. (C.1)] [74, 68]

$$\frac{E^{\mathrm{UN-BN}}(\eta)}{V} = \omega \sum_{j=0}^{2} \left[1 - \frac{2c_1}{2c_1 - c_2/5} \cos\left(2\eta + \frac{2\pi j}{3} \right) \right]^{\frac{5}{2}} + \eta\text{-independent terms}, \tag{4.37}$$

where $\omega \equiv 8M^{3/2}[n(2c_1 - c_2/5)]^{5/2}/(15\pi^2\hbar^3)$. $E^{\mathrm{UN-BN}}(\eta)$ is η-independent for $c_1 = 0$. Equation (4.37) has the minimum (maximum) at $\eta = n\pi/3$ ($\eta = \pi/6 + n\pi/3$) ($n = 0, 1, \dots$) corresponding to the UN (BN) phase for $c_1 > 0$ and vice versa for $c_1 < 0$. It means that the UN phase changes abruptly from the ground state to an unstable state as c_1 traverses the phase boundary, implying no parameter regime of metastable states. Since the above argument of the flat energy landscape is based on the symmetry of the Hamiltonian, the absence of metastability is valid to all orders of approximation.

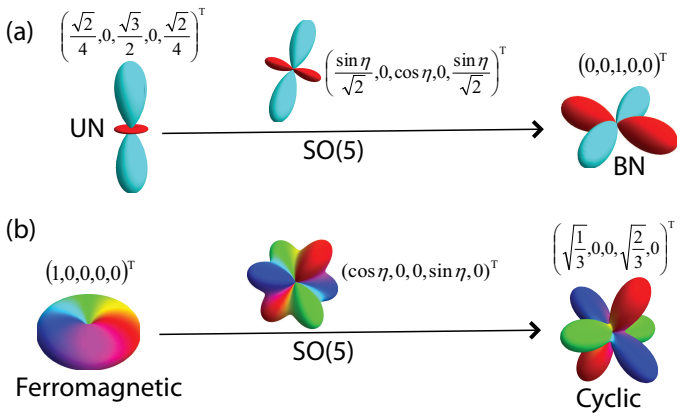

Figure 4.4: SO(5) rotations connecting (a) UN and BN phases and (b) ferromagnetic and cyclic phases. The order parameters and the spherical harmonic representations of the initial, final, and intermediate states are displayed. (Figure reproduced from Ref. [40])

Chapter 5

Critical dynamics of a first-order quantum phase transition without metastability

As seen in Sec. 4.5, the first-order quantum phase transitions that are not accompanied by metastable states are characterized by a flat energy landscape at the phase boundary. This energy landscape implies that it costs no energy for the system to be excited. Therefore, it is expected that the criticality that arises from the flat energy landscape can be observed. In this chapter, we show that the dynamics of a spinor BEC through such a first-order quantum phase transition exhibits critical features similar to second-order phase transitions.

There are a total of four first-order quantum phase transitions in spin-1 and spin-2 BECs that are not accompanied by metastable states. They are classified into two categories as shown in Table 5.1. The first one consists of the ferromagnetic-BA (spin-1) and ferromagnetic-cyclic (spin-2) phase transitions. In these phase transitions, as the system's parameter (q for spin-1 and c_1 for spin-2 BECs) crosses the phase boundary, the ground state changes to an excited state with a local maximum energy. Despite being an unstable state, the excited state can have a long lifetime in an isolated system where energy dissipation is suppressed. The higher energy of this state is exhibited in the excitation spectrum where a Landau instability is associated with a negative excitation energy. In other words, a level crossing occurs in these phase transitions as illustrated in Fig. 5.1. Since the excited state is an energy eigenstate, the dynamics of the system would be closed within the subspace spanned by that state as the wavefunction merely acquires a phase. In contrast, there is no level crossing in the second category which involves the antiferromagnetic-polar (spin-1) and UN-BN (spin-2) phase transitions. As the system's parameter traverses the phase boundary, a dynamical instability arises with the excitation spectrum becoming a complex number with a nonzero imaginary part. The excitation modes therefore grow exponentially and drive the system away from the initial state, leading to a nontrivial dynamics. In the following we study the dynamics of a spin-1 condensate through the antiferromagnetic-polar phase transition. This phase transition has been observed in Refs. [89, 90] using ^{23}Na atoms.

5.1 Instantaneous quench

First, let us consider an instantaneous quench of a spin-1 BEC with an antiferromagnetic interaction, i.e., $c_1 > 0$, through the polar-antiferromagnetic phase transition (see Fig. 2.2). The condensate is initially prepared in the ground state of the polar phase by setting the quadratic Zeeman coefficient q to a positive value. It is then suddenly switched to a negative value in close

	Phase transition	Instability	Level crossing	Dynamics
Spin-1 BECs	FM-BA	Landau	Yes	Closed
	AFM-PL	Dynamical	No	Nontrivial
Spin-2 BECs	FM-CL	Landau	Yes	Closed
	UN-BN	Dynamical	No	Nontrivial

Table 5.1: Classification of the first-order quantum phase transitions in spin-1 and spin-2 BECs that are not accompanied by metastable states. FM, BA, AFM, PL, CL, UN, and BN stand for ferromagnetic, broken-axisymmetry, antiferromagnetic, polar, cyclic, uniaxial-nematic, and biaxial-nematic phases, respectively.

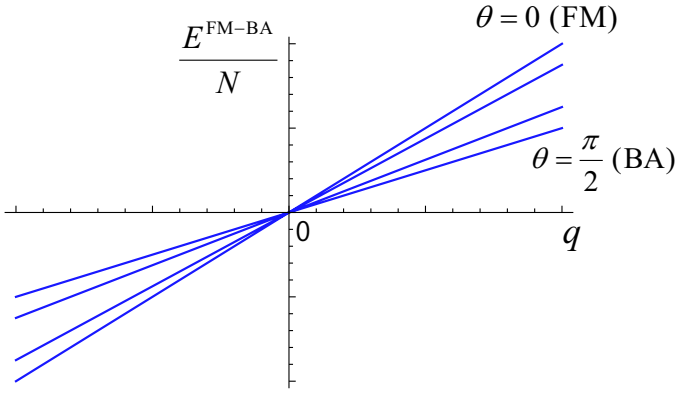

Figure 5.1: Energy level crossing in the ferromagnetic-BA phase transition of a spin-1 BEC. The mean-field energy per particle $E^{\mathrm{FM-BA}}/N$ given by Eq. (4.35) is plotted against the quadratic Zeeman coefficient q. The phase transition occurs at $q = 0$. The intermediate states in the transformation from the ferromagnetic phase to the BA phase is characterized by a parameter θ ($0 \leq \theta \leq \pi/2$) as discussed in the text above Eq. (4.35). The ferromagnetic and BA phases correspond to $\theta = 0$ and $\theta = \pi/2$, respectively.

proximity to the phase boundary $q = 0$. From the energy spectrum of the degenerate $m_F = \pm 1$ excitation modes of the polar phase given by Eq. (2.55), it is evident that a dynamical instability would arise if $\omega_{\pm 1,\mathbf{p}}$ become complex numbers with nonzero imaginary parts. This results in an exponential growth of atoms in the $m_F = \pm 1$ magnetic sublevels at the beginning of the dynamics when the populations of atoms in these hyperfine spin states are still small compared to the number of condensate atoms. As long as $n_{\pm 1} \ll n_0$, we can apply the Bogoliubov theory (see Sec. 2.4), in which the system is approximated by the Bogoliubov Hamiltonian [Eq. (2.44)]. The Heisenberg equations of motion for the operators $\hat{a}_{\pm 1,\mathbf{p}}$ are then given by

$$i\hbar \frac{d\hat{a}_{\pm 1,\mathbf{p}}(t)}{dt} = \left(\epsilon^0_{\mathbf{p}} + q + c_1 n\right) \hat{a}_{\pm 1,\mathbf{p}}(t) + c_1 n \hat{a}^\dagger_{\mp 1,-\mathbf{p}}(t). \tag{5.1}$$

They form closed sets of equations for the pairs of operators $\hat{a}_{\pm 1,\mathbf{p}}$ and $\hat{a}^\dagger_{\mp 1,-\mathbf{p}}$. The corresponding solutions are [91]

$$\hat{a}_{\pm 1,\mathbf{p}}(t) = \left[\cosh\left(\frac{D_{\mathbf{p}} t}{\hbar}\right) - i\frac{\epsilon^0_{\mathbf{p}} + q + c_1 n}{D_{\mathbf{p}}} \sinh\left(\frac{D_{\mathbf{p}} t}{\hbar}\right)\right] \hat{a}_{\pm 1,\mathbf{p}}(0) - i\frac{c_1 n}{D_{\mathbf{p}}} \sinh\left(\frac{D_{\mathbf{p}} t}{\hbar}\right) \hat{a}^\dagger_{\mp 1,-\mathbf{p}}(0), \tag{5.2}$$

where $D_{\mathbf{p}} \equiv \sqrt{-(\epsilon^0_{\mathbf{p}} + q)(\epsilon^0_{\mathbf{p}} + q + 2c_1 n)}$. Here q ($|q| \ll c_1 n$) indicates the final value of the quadratic Zeeman coefficient after the quench. It is clear from the hyperbolic functions in Eq. (5.2) that the population of atoms in the $m_F = \pm 1$ spin states will grow exponentially. This growing number of atoms would create a finite transverse magnetization in the system. Using Eq. (2.10), the transverse spin-density operator $\hat{F}_+(\mathbf{r}, t) \equiv \hat{F}_x(\mathbf{r}, t) + i\hat{F}_y(\mathbf{r}, t)$ is expressed in terms of the field operators as

$$\begin{aligned}
\hat{F}_+(\mathbf{r}, t) &= \sqrt{2}\left[\hat{\psi}^\dagger_1(\mathbf{r}, t)\hat{\psi}_0(\mathbf{r}, t) + \hat{\psi}^\dagger_0(\mathbf{r}, t)\hat{\psi}_{-1}(\mathbf{r}, t)\right] \\
&\simeq \sqrt{2n}\left[\hat{\psi}^\dagger_1(\mathbf{r}, t) + \hat{\psi}_{-1}(\mathbf{r}, t)\right] \\
&= \sqrt{2n}\left[\sum_{\mathbf{p}} \frac{e^{-i\mathbf{p}\cdot\mathbf{r}}}{\sqrt{V}} \hat{a}^\dagger_{1,\mathbf{p}}(t) + \sum_{\mathbf{p}} \frac{e^{i\mathbf{p}\cdot\mathbf{r}}}{\sqrt{V}} \hat{a}_{-1,\mathbf{p}}(t)\right],
\end{aligned} \tag{5.3}$$

where in deriving the second equality we have replaced $\hat{\psi}_0$ and $\hat{\psi}^\dagger_0$ by n due to the macroscopic occupation of the condensate and $n_{\pm 1} \ll n_0$. Substituting Eq. (5.2) in Eq. (5.3), we have

$$\begin{aligned}
\hat{F}_+(\mathbf{r}, t) =& \frac{\sqrt{2n_0}}{\sqrt{V}} \sum_{|\mathbf{p}|<p_c} e^{-i\mathbf{p}\cdot\mathbf{r}} \left\{ \left[i\frac{\epsilon^0_{\mathbf{p}} + q}{D_{\mathbf{p}}} \sinh\left(\frac{D_{\mathbf{p}} t}{\hbar}\right) + \cosh\left(\frac{D_{\mathbf{p}} t}{\hbar}\right) \right] \hat{a}^\dagger_{1,\mathbf{p}}(0) \right. \\
&\left. + \left[-i\frac{\epsilon^0_{\mathbf{p}} + q}{D_{\mathbf{p}}} \sinh\left(\frac{D_{\mathbf{p}} t}{\hbar}\right) + \cosh\left(\frac{D_{\mathbf{p}} t}{\hbar}\right) \right] \hat{a}_{-1,-\mathbf{p}}(0) \right\}.
\end{aligned} \tag{5.4}$$

Here, since the dynamical instability results in an exponential growth, in the sum on the right-hand side of Eq. (5.4) we took only the contributions from the dynamically unstable excitation modes whose momenta satisfy $|\mathbf{p}| < p_c \equiv \sqrt{2M|q|}/\hbar$ and ignored those from stable modes. Similarly, we obtain the expression for $\hat{F}_-(\mathbf{r}, t) = \hat{F}^\dagger_+(\mathbf{r}, t)$. From these expressions, we can evaluate the time evolution of the transverse spin correlation function $\hat{F}_+(\mathbf{r}, t)\hat{F}_-(\mathbf{r}', t) = \hat{F}_x(\mathbf{r}, t)\hat{F}_x(\mathbf{r}', t) + \hat{F}_y(\mathbf{r}, t)\hat{F}_y(\mathbf{r}', t)$. Even if there is initially no atom in the $m_F = \pm 1$ magnetic sublevels at $t = 0$, the atomic seeds due to quantum fluctuations would trigger the dynamical

instability, leading to the formation of a finite transverse spin correlation function. This is parametric amplification of quantum fluctuations [92, 93]. Since the growth is exponential, we can ignore the small fraction of atoms in the $m_F = \pm 1$ spin states due to quantum depletion at $t = 0$. The transverse spin correlation function at time t is then found to be

$$\langle \hat{F}_+(\mathbf{r}, t)\hat{F}_-(\mathbf{r}', t)\rangle = \frac{2n}{V}\sum_{|\mathbf{p}|<p_c}\left[\frac{(\epsilon^0_{\mathbf{p}} + q)^2}{D^2_{\mathbf{p}}}\sinh^2\left(\frac{D_{\mathbf{p}}t}{\hbar}\right) + \cosh^2\left(\frac{D_{\mathbf{p}}t}{\hbar}\right)\right]e^{i\mathbf{p}\cdot(\mathbf{r}'-\mathbf{r})}. \tag{5.5}$$

At time t such that $D_{\mathbf{p}}t/\hbar \gg 1$, it reduces to

$$\langle \hat{F}_+(\mathbf{r}, t)\hat{F}_-(\mathbf{r}', t)\rangle = \frac{2n}{V}\sum_{|\mathbf{p}|<p_c}\frac{\epsilon^0_{\mathbf{p}} + q + c_1 n}{\epsilon^0_{\mathbf{p}} + q + 2c_1 n}e^{2D_{\mathbf{p}}t/\hbar}e^{i\mathbf{p}\cdot(\mathbf{r}'-\mathbf{r})}. \tag{5.6}$$

The maximally unstable mode is determined by the maximum value of $D_{\mathbf{p}}$, which is that with zero wavenumber $\mathbf{p} = 0$. Since the fraction in Eq. (5.6) is a smooth function of $\mathbf{p}$ compared with the exponential function $e^{2D_{\mathbf{p}}t/\hbar}$, we can replace the wavenumber in the fraction by $\mathbf{p} = 0$ for which the exponent has the maximum value. The fraction then reduces to $(q+c_1n)/(q+2c_1n) \simeq 1/2$, where we used $|q| \ll c_1 n$. On the other hand, the exponent $2D_{\mathbf{p}}t/\hbar$ can be expanded around $\mathbf{p} = 0$ as [91]

$$\frac{2D_{\mathbf{p}}t}{\hbar} = \frac{t}{\tau}\left(1 - \frac{\xi^2\mathbf{p}^2}{4}\right) + \mathcal{O}(\mathbf{p}^4), \tag{5.7}$$

where

$$\tau \equiv \frac{\hbar}{\sqrt{(-q)(q + 2c_1 n)}}, \tag{5.8}$$

$$\xi \equiv \sqrt{\frac{2(q + c_1 n)\hbar^2}{(-q)(q + 2c_1 n)M}}. \tag{5.9}$$

In the thermodynamic limit the sum in Eq. (5.6) can be replaced by an integral, and by carrying out the three-dimensional integral, we obtain

$$\langle \hat{F}_+(\mathbf{r}, t)\hat{F}_-(\mathbf{r}', t)\rangle = \frac{n}{4\pi^2|\mathbf{r} - \mathbf{r}'|}\int_0^{\sqrt{2}/\xi} \mathrm{d}p\, p e^{(t/\tau)(1-\xi^2p^2/4)}\sin(p|\mathbf{r} - \mathbf{r}'|). \tag{5.10}$$

Here the upper wavenumber p_c was expressed in terms of ξ by $p_c\xi = 2\sqrt{(q + c_1 n)/(q + 2c_1 n)} \simeq \sqrt{2}$. It is evident from Eq. (5.10) that the transverse spin correlation is a function of the dimensionless quantities t/τ and $|\mathbf{r} - \mathbf{r}'|/\xi$. The correlations at $t/\tau = 1$ and $t/\tau = 10$ are plotted in Fig. 5.2 where the quadratic Zeeman coefficient is chosen to be $q = (-2+\sqrt{3})c_1 n$ so that the correlation length ξ becomes equal to l, where $l \equiv \hbar/\sqrt{c_1 n M}$ is the so-called spin coherence length which is the characteristic length scale associated with the spin-dependent interaction c_1. Since at $t/\tau = 10$ the ratio of the spin correlation to n^2 is less than $60/(nl^3) = 480(\pi c_1/c_0)^{3/2}\sqrt{na^3} \ll 1$, the Bogoliubov approximation used in the foregoing arguments remains valid for a relatively long time. This also justifies the assumption of t used in Eq. (5.6).

Since $\langle \hat{F}_+(\mathbf{r}, t)\hat{F}_-(\mathbf{r}', t)\rangle$ is a function of only t/τ and $|\mathbf{r} - \mathbf{r}'|/\xi$, it is evident that τ characterizes the time scale of the exponential growth of spin correlation induced by a dynamical instability, i.e., the system's response time, and ξ represents the system's correlation length.

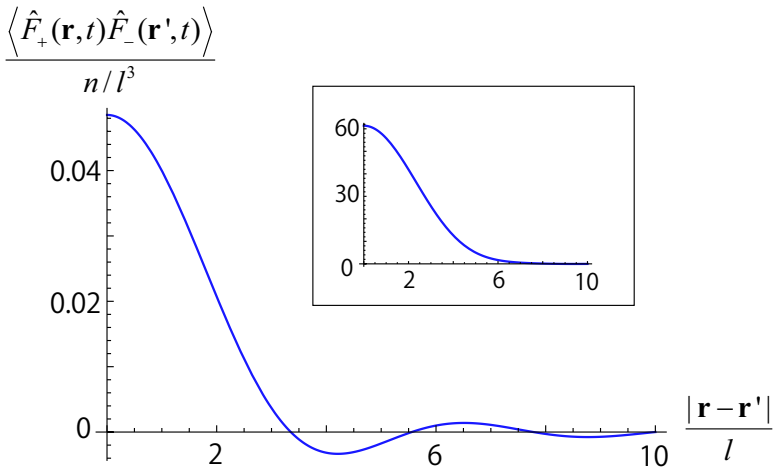

Figure 5.2: Transverse spin correlation at time $t = \tau$, where τ is defined by Eq. (5.8). The spin correlation $\langle \hat{F}_+(\mathbf{r},t)\hat{F}_-(\mathbf{r}',t)\rangle$ and the distance $|\mathbf{r}-\mathbf{r}'|$ are expressed in units of n/l^3 and l, respectively, where $l \equiv \hbar/\sqrt{c_1 n M}$ is the spin coherence length. The quadratic Zeeman coefficient is chosen so that the correlation length ξ becomes equal to l. The inset shows the spin correlation at $t = 10\tau$.

From Eqs. (5.8) and (5.9), it is clear that both τ and ξ diverge as q approaches the phase boundary $q = 0$. This is similar to the case of second-order phase transitions where the phase boundary is a critical point. This can be interpreted as a consequence of the flat energy landscape at the phase boundary of a first-order quantum phase transition that is not accompanied by a metastable state. The vanishing cost of excitation energy at the transition point would lead to a divergently long response time as shown above.

5.2 Slow quench

Now let us consider a slow quench, in which the quadratic Zeeman coefficient q is linearly varied with time as $q(t)/(c_1 n) = -t/\tau_{\rm Q}$ so that it acquires the value of $-c_1 n$ at time $t = \tau_{\rm Q}$. As shown in Sec. 5.1, the order of magnitude of the system's response time τ is inversely proportional to the energy gap of excitations. It becomes divergently large as the excitations become gapless at the transition point $q = 0$ [see Eq. (5.8)]. For $q < 0$ the ground state is the antiferromagnetic phase, and the excitation spectra are given by Eqs. (2.61)–(2.63). Among them, $\omega_{+,\mathbf{p}}$ indicates the phonon mode, while $\omega_{-,\mathbf{p}}$ represents a spatially periodic modulation of the quantization axis of the antiferromagnetic phase in the xy-plane. These two excitation modes are gapless since they arise from spontaneous symmetry breaking of the Hamiltonian. In contrast, $\omega_{0,\mathbf{p}}$ gives the energy spectrum of the magnon excitation and has a finite energy gap given by

$$\Delta(t) = \sqrt{q(t)[q(t) - 2c_1 n]}. \tag{5.11}$$

It is a function of time via the time-dependent quadratic Zeeman coefficient $q(t)$. As a result, the system's response time varies with time as $\tau(t) \sim \hbar/\Delta(t)$. On the other hand, the time scale of the variation of the system's parameter can be evaluated via the time-dependent energy gap by $\tilde{\tau}(t) \sim \Delta(t)/(\mathrm{d}\Delta/\mathrm{d}t)$. Right after crossing the phase boundary as $t \simeq 0$, we have $\tau(t) \gg \tilde{\tau}(t)$ due to the small energy gap $\Delta(t)$, and thus the system is dynamically frozen in response to the change of parameter [94, 95, 96]. After that the system's response time $\tau(t)$ decreases with time, and the system starts to adiabatically follow the variation of the parameter from the time

t^* determined by equating the orders of magnitude of $\tau(t)$ and $\tilde{\tau}(t)$:

$$\frac{\hbar}{\Delta(t^*)} \sim \frac{\Delta(t^*)}{(\mathrm{d}\Delta/\mathrm{d}t)_{t^*}}. \tag{5.12}$$

Using Eq. (5.11) for the energy gap $\Delta(t)$, we obtain

$$\frac{\hbar}{c_1 n\sqrt{(t^*/\tau_\mathrm{Q})(t^*/\tau_\mathrm{Q}+2)}} \sim \frac{t^*(t^*/\tau_\mathrm{Q}+2)}{t^*/\tau_\mathrm{Q}+1}, \tag{5.13}$$

or equivalently,

$$\tau_\mathrm{Q}\left[\frac{t^*}{\tau_\mathrm{Q}}\left(\frac{t^*}{\tau_\mathrm{Q}}+2\right)\right]^{3/2} \sim \frac{\hbar}{c_1 n}\left(\frac{t^*}{\tau_\mathrm{Q}}+1\right). \tag{5.14}$$

Here, we consider only slow quenches such that $\tau_\mathrm{Q} \gg \hbar/(c_1 n)$ in order for the system to have enough time to experience the criticality at the transition point. We assume *a priori* that the solution of Eq. (5.14) satisfies $t^*/\tau_\mathrm{Q} \ll 1$. Then, Eq. (5.14) leads us to

$$t^* \sim \left(\frac{\hbar}{c_1 n}\right)^{2/3} \tau_\mathrm{Q}^{1/3}, \tag{5.15}$$

which justifies the assumption. From Eq. (5.9), since $|q(t^*)| \ll c_1 n$, we find $\xi(t^*)$ to be proportional to $|q(t^*)|^{-1/2}$. Consequently, the correlation length at time t^* can be evaluated as

$$\xi(t^*) \propto \frac{1}{\sqrt{|q(t^*)|}} = \frac{1}{\sqrt{c_1 n}}\sqrt{\frac{\tau_\mathrm{Q}}{t^*}} \propto \tau_\mathrm{Q}^{1/3}. \tag{5.16}$$

Since the system starts to adiabatically follow the variation of the quadratic Zeeman coefficient from t^*, the correlation length at this time would determine the size of the spin domains, in which the transverse magnetization evolve almost independently (see Sec. 5.1). According to the Kibble-Zurek mechanism, $\xi(t^*)$ also gives the mean distance between the topological defects that emerge in a slow quenching dynamics [97, 98, 99, 100]. The density of topological defects in a d-dimensional system then has the following scaling law with respect to the quench time:

$$n_\mathrm{def} \sim \xi^{-d}(t^*) \propto \tau_\mathrm{Q}^{-d/3}. \tag{5.17}$$

This scaling is identical to that associated with the dynamics of a second-order phase transition [91, 94, 101].

Chapter 6

Quasi-Nambu-Goldstone modes

The Nambu-Goldstone (NG) theorem, which states that spontaneous breaking of a continuous symmetry is accompanied by gapless excitations, should hold at any order of approximation [23, 24]. However, at the mean-field level we sometimes encounter extra gapless excitations that do not stem from spontaneous symmetry breaking. They are called quasi-NG modes and were first introduced in the context of gauge theories and high energy physics [30, 31]. Quasi-NG modes later became an essential ingredient in models of technicolor and supersymmetry, which are candidates of the beyond-standard model [33, 34, 35]. They are also believed to appear in the weak-coupling limit of the A phase of superfluid ^{3}He [36] and spin-1 color superconductors [37]. Despite their prevalence in various fields of physics, no experimental evidence of the quasi-NG modes has hitherto been observed. Ultracold atomic systems are expected to be ideal for the probe of this special kind of excitations since they are readily manipulated and measured in experiments. Especially, it has recently been proposed that the nematic phase of spin-2 BECs can be a host of quasi-NG modes [38].

Although the quasi-NG modes are gapless at the mean-field level, it is predicted that these excitations would acquire a finite energy gap with quantum corrections. In this chapter, we explicitly prove this conjecture by calculating the emergent energy gap of quasi-NG modes in a spin-2 BEC caused by quantum fluctuations. At the mean-field approximation, all the nematic phases are degenerate in the ground-state manifold and there are a total of five gapless excitation modes (see Sec. 2.4.2). On the other hand, the number of symmetries of the Hamiltonian that are broken is just three. This means that the remaining two gapless excitations are not generated by spontaneous symmetry breaking; i.e., they are quasi-NG modes. However, since the zero-point fluctuations lift the degeneracy in the manifold of nematic phases [73, 74], it is predicted that the quasi-NG modes would become gapful as quantum corrections are taken into account [38]. By using the spinor Beliaev theory developed in Sec. 4.2, we succeed in deriving the analytic expression for the energy gap of quasi-NG modes in terms of the atomic number density and the fundamental interatomic interactions. These parameters can be readily measured and varied under control in ultracold atoms using, for example, the Feshbach resonance [77, 8, 9]. From the obtained magnitude of the energy gap, we can evaluate the critical temperature $T_{\mathbf{c}}$ above which a topological defect such as a spin vortex would decay by emitting the thermally excited quasiparticles. Conversely, below this temperature the vortex would be stabilized by suppressing the emission of the quasi-NG modes.

In the previous study [38], the energy gap of quasi-NG modes is assumed to be of the same order of magnitude as the zero-point energy. This assumption is based on the fact that the zero-point energy lifts the degeneracy in the manifold of nematic phases at the mean-field level, making the ground state either the UN phase for $c_1 > 0$ or the BN phase for $c_1 < 0$. However, as shown at the beginning of Chap. 5, there is no level crossing in the UN-BN phase transition

at $c_1 = 0$. As c_1 traverses the phase boundary from the positive (negative) to the negative (positive) side, the UN (BN) state would become dynamically unstable with the excitation spectrum becoming a complex number with a nonzero imaginary part. These excitations would grow exponentially (see Sec. 5.1), rendering the UN (BN) state not an excited state. Therefore, the energy gap of quasi-NG modes is not necessarily of the same order of magnitude as the zero-point energy. We show in Sec. 6.1 that its magnitude depends on the relative strength of the two spin-dependent interactions c_1 and c_2. Similarly, the scaling law of the energy gap with respect to the characteristic dimensionless parameter na^3 also varies with the ratio c_2/c_1.

Since the quasi-NG modes arise from the nematic phase of spin-2 BECs, these excitations represent the spatially periodic modulations of the system's density of spin nematicity. In Sec. 6.2, we study how the particle-number density fluctuations affect the propagation of the quasi-NG modes. A comparison with those effects on phonons and magnons is made. We find that the propagation velocity of the quasi-NG modes is suppressed in a manner similar to magnons but as opposed to phonons whose sound velocity is enhanced. The difference in the effects on these types of quasiparticles will be discussed in terms of the particle-number density correlation.

6.1 Emergent energy gap

Since the magnitudes of the spin-dependent interactions measured in spin-dynamics experiments [77] imply that the ground state of the spin-2 ^{87}Rb BEC is likely to be the uniaxial-nematic phase, in the following we consider the quasi-NG modes arising from the UN phase. The magnitude of c_1 is fairly well determinate but that of c_2 suffers a large error bar:

$$\frac{c_1}{4\pi\hbar^2/M} = 0.99 \pm 0.06\, a_{\rm B}, \tag{6.1}$$

$$\frac{c_2}{4\pi\hbar^2/M} = -0.53 \pm 0.58\, a_{\rm B}, \tag{6.2}$$

where $a_{\rm B} \simeq 0.5$ Å is the Bohr radius.

The Bogoliubov spectra of the UN phase consist of five gapless excitation modes given by Eqs. (2.75a)–(2.75e). Among them, one phonon mode

$$\hbar\omega^{(1)}_{0,\mathbf{p}} = \sqrt{\epsilon^0_{\mathbf{p}}[\epsilon^0_{\mathbf{p}} + 2(c_0 + c_2/5)n]} \tag{6.3}$$

and two magnon modes

$$\hbar\omega^{(1)}_{\pm 1,\mathbf{p}} = \sqrt{\epsilon^0_{\mathbf{p}}[\epsilon^0_{\mathbf{p}} + 2(3c_1 - c_2/5)n]} \tag{6.4}$$

result from spontaneous symmetry breaking of the Hamiltonian. The Hamiltonian of spin-2 BECs for generic $c_1 \neq 0$ has a $\mathrm{U}(1)_\phi \times \mathrm{SO}(3)_{\mathbf{f}}$ symmetry corresponding to the gauge and SO(3) rotation invariances. On the other hand, the UN phase possesses an SO(2) rotation symmetry about the z axis in spin space. The two magnon excitation modes represent the spatially periodic modulations of the transverse magnetization whose direction is aligned in the xy plane. The remaining two gapless modes

$$\hbar\omega^{(1)}_{\pm 2,\mathbf{p}} = \sqrt{\epsilon^0_{\mathbf{p}}(\epsilon^0_{\mathbf{p}} - 2c_2 n/5)} \tag{6.5}$$

are therefore not generated by spontaneous symmetry breaking; they are quasi-NG modes.

Since the phonon and magnon excitations arise from spontaneous symmetry breaking of the

Hamiltonian, they should be gapless at any order of approximation according to the Nambu-Goldstone theorem [23, 24]. In contrast, the quasi-NG modes, which are gapless excitations at the mean-field level, can generally acquire a finite energy gap at higher-order approximations. In Sec. 4.3, we have calculated the zero-momentum energy of the quasi-NG modes of the UN phase [Eq. (4.20)] by using the spinor Beliaev theory. As the right-hand side of Eq. (4.20) is positive, the energy gap of the quasi-NG modes is given by

$$\Delta \simeq \frac{\sqrt{\left[A-\mu^{(2)}+C\right]\left[-\frac{2c_2n_0}{5}+A-\mu^{(2)}-C\right]}}{1-B}, \tag{6.6}$$

where A, B, and C are the coefficients in the frequency expansions of the second-order self-energies [Eqs. (4.17)–(4.19)]. By summing all the contributions to the self-energies and the chemical potential from second-order Feynman diagrams, we obtain

$$\frac{A-\mu^{(2)}+C}{(Mn_0)^{3/2}} = \frac{1}{\pi^2\hbar^3}\left(8\sqrt{3}\tilde{c}_1^{5/2} - \frac{32}{\sqrt{3}}\tilde{c}_1^{3/2}\tilde{c}_2 + \frac{16}{3}\tilde{c}_1\tilde{c}_2^{3/2} + \frac{8}{\sqrt{3}}\tilde{c}_1^{1/2}\tilde{c}_2^2 - \frac{16}{9}\tilde{c}_2^{5/2}\right), \tag{6.7}$$

$$\frac{A-\mu^{(2)}-C}{(Mn_0)^{3/2}} = -\frac{16\sqrt{3}c_1^{5/2}}{\pi^2\hbar^3} + \mathcal{O}\left(c_2n_0\sqrt{na^3}\right), \tag{6.8}$$

$$B = 0 + \mathcal{O}\left(\sqrt{na^3}\right), \tag{6.9}$$

where $\tilde{c}_1$, $\tilde{c}_2$, and a have been defined below Eqs. (4.33) and (4.1), respectively. Here we have ignored terms containing the factor $\sqrt{na^3} \ll 1$. Substituting Eqs. (6.7)–(6.9) in Eq. (6.6), we find the energy gap of the quasi-NG modes to be

$$\begin{aligned}\Delta \simeq c_1 n\Bigg\{&\left[8\sqrt{3}\left(\frac{\tilde{c}_1}{c_1}\right)^{\frac{5}{2}} - \frac{32}{\sqrt{3}}\left(\frac{\tilde{c}_1}{c_1}\right)^{\frac{3}{2}}\frac{\tilde{c}_2}{c_1} + \frac{16}{3}\frac{\tilde{c}_1}{c_1}\left(\frac{\tilde{c}_2}{c_1}\right)^{\frac{3}{2}} + \frac{8}{\sqrt{3}}\left(\frac{\tilde{c}_1}{c_1}\right)^{\frac{1}{2}}\left(\frac{\tilde{c}_2}{c_1}\right)^2 - \frac{16}{9}\left(\frac{\tilde{c}_2}{c_1}\right)^{\frac{5}{2}}\right] \\ &\times\left[\frac{2|c_2|}{5c_1} - \frac{128\sqrt{3}}{\sqrt{\pi}}\left(\frac{c_1}{c_0}\right)^{\frac{3}{2}}\sqrt{na^3}\right]\frac{8}{\sqrt{\pi}}\left(\frac{c_1}{c_0}\right)^{\frac{3}{2}}\sqrt{na^3}\Bigg\}^{\frac{1}{2}}.\end{aligned} \tag{6.10}$$

Using the parameters of ^{87}Rb with an atomic number density $n = 10^{15}\,\mathrm{cm}^{-3}$, in Fig. 6.1 we plot Δ as a function of $|c_2|/c_1$ over the uncertainty range of parameter c_2. The magnitude of the energy gap varies significantly with the relative strength of the spin-dependent interactions. In the limit of $|c_2| \sim c_1\sqrt{na^3}(c_1/c_0)^{3/2} \ll c_1$, the energy gap reduces to

$$\Delta \simeq \frac{32\sqrt[4]{3}\sqrt{\pi}}{\sqrt{5}}c_1n\sqrt{na^3}\left(\frac{c_1}{c_0}\right)^{3/2}\sqrt{\frac{1}{8\pi^{3/2}\sqrt{na^3}}\frac{|c_2|}{c_1}\left(\frac{c_0}{c_1}\right)^{3/2} - \frac{40\sqrt{3}}{\pi^2}}. \tag{6.11}$$

In this limit, we have

$$\Delta \sim c_1n\left(\frac{c_1}{c_0}\right)^{3/2}\sqrt{na^3}. \tag{6.12}$$

On the other hand, the zero-point energy that lifts the degeneracy in the manifold of nematic phases is obtained from the difference in the LHY correction given by Eq. (C.1). Its order of magnitude is $\delta E(\eta)/N \sim M^{3/2}c_1^{5/2}n^{3/2}/\hbar^3 \sim c_1n(c_1/c_0)^{3/2}\sqrt{na^3}$. Equation (6.12) then implies that Δ has the same order of magnitude as the zero-point energy in the limit of $|c_2| \ll c_1$. The

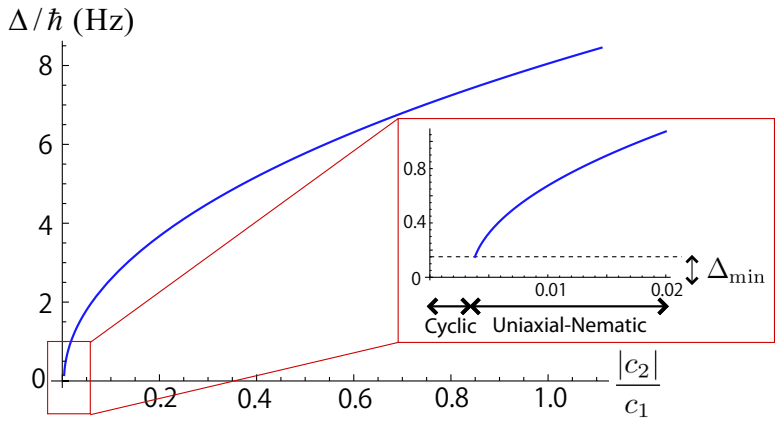

Figure 6.1: Energy gap of quasi-Nambu-Goldstone modes in the uniaxial-nematic (UN) phase of spin-2 BECs as a function of the relative strength of the spin-dependent interactions [Eq. (6.10)]. For the ground state to be the UN phase, c_2 must be negative [Eq. (4.2)]. We use the parameters of spin-2 ^{87}Rb obtained from experimental measurements [77] with an atomic number density $n = 10^{15}\,\mathrm{cm}^{-3}$ and plot the energy gap over a range of values of $|c_2|/c_1$ [Eqs. (6.1) and (6.2)] . The inset shows the energy gap in the limit of $|c_2| \ll c_1$ [Eq. (6.11)]. There obviously exists a lower bound $\Delta_{\min}$ for the energy gap of quasi-NG modes [Eq. (6.17)]. Note that the UN-cyclic phase boundary is shifted from its mean-field counterpart at $c_2 = 0$ due to the zero-point energy [Eq. (4.2)].

scaling laws of Δ with respect to c_1 and n are given by

$$\Delta \propto c_1^{5/2} n^{3/2}, \tag{6.13}$$

where c_1 is related to the difference between the s-wave scattering lengths [Eq. (2.15b)].

In contrast, in the limit of $|c_2| \sim c_1$ the energy gap reduces to

$$\Delta \simeq \frac{4}{\sqrt{5}\pi^{1/4}} c_1 n \sqrt[4]{na^3} \left(\frac{c_1}{c_0}\right)^{3/4} \left[8\sqrt{3} \left(\frac{\tilde{c}_1}{c_1}\right)^{\frac{5}{2}} - \frac{32}{\sqrt{3}} \left(\frac{\tilde{c}_1}{c_1}\right)^{\frac{3}{2}} \frac{\tilde{c}_2}{c_1} + \frac{16}{3} \frac{\tilde{c}_1}{c_1} \left(\frac{\tilde{c}_2}{c_1}\right)^{\frac{3}{2}} + \frac{8}{\sqrt{3}} \left(\frac{\tilde{c}_1}{c_1}\right)^{\frac{1}{2}} \left(\frac{\tilde{c}_2}{c_1}\right)^{2} - \frac{16}{9} \left(\frac{\tilde{c}_2}{c_1}\right)^{\frac{5}{2}} \right]^{1/2}. \tag{6.14}$$

Its magnitude is given by

$$\Delta \sim c_1 n \left(\frac{c_1}{c_0}\right)^{3/4} \sqrt[4]{na^3}; \tag{6.15}$$

i.e., the energy gap of quasi-NG modes in this limit is much larger than the zero-point energy since $na^3 \ll 1$. The scaling laws of Δ with respect to c_1 and n also differ from those of the zero-point energy:

$$\Delta \propto c_1^{7/4} n^{5/4}. \tag{6.16}$$

From these scaling laws, we know that the energy gap can be made much larger either by, for example, loading the atoms into an optical lattice to raise the atomic number density n or by adjusting the relative strengths of the s-wave scattering lengths to increase the ratio of c_1/c_0.

Especially, with the latter approach the energy gap can be made as much as about 3000 times larger if the difference $a_4 - a_2$ can be adjusted to be of the same order of magnitude as the scattering lengths themselves.

Noting that due to the zero-point energy the UN-cyclic phase boundary is shifted from its mean-field counterpart $c_2 = 0$ to $c_2^{\mathrm{UN-CL}}$ given by Eq. (4.2). It indicates the lowest value of $|c_2|$ for which the ground state is the UN phase. This is also obvious from Fig. 6.1. Since $|c_2^{\mathrm{UN-CL}}| \ll c_1$, by substituting Eq. (4.2) in Eq. (6.11) we find the lower bound for the energy gap of the quasi-NG modes to be

$$\begin{aligned}\Delta_{\mathrm{min}} &\simeq \frac{64\sqrt{2}\sqrt[4]{3}}{\sqrt{\pi}}\left(\frac{7\sqrt{3}-8\sqrt{2}}{5}\right)^{\frac{1}{2}} c_1 n \left(\frac{c_1}{c_0}\right)^{\frac{3}{2}}\sqrt{na^3} \\ &\simeq 27.06\, c_1 n \left(\frac{c_1}{c_0}\right)^{\frac{3}{2}}\sqrt{na^3}. \end{aligned} \tag{6.17}$$

Since the right-hand side of Eq. (6.17) is always positive, it is evident that the quasi-NG modes acquire a finite energy gap due to quantum fluctuations. Thus, the conjecture of quasi-NG modes becoming gapful with quantum corrections has been proved.

On the other hand, the precise magnitude of interaction c_2 for spin-2 ^{87}Rb is still indeterminate from experimental measurements [77] with a large error bar [Eq. (6.2)]. The derived analytic expression for Δ as a function of c_2 [Eq. (6.10)] also suggests an alternative way to measure the magnitude of the interatomic interactions via the quasi-NG modes. The average value of c_2 determined from the measurement outcomes is $c_2^{\mathrm{avr}} \simeq 0.53 \times (4\pi\hbar^2 a_{\mathrm{B}}/M)$. Substituting this value in Eq. (6.14), we find the energy gap of the quasi-NG modes to be $\Delta \simeq \hbar \times 6\,\mathrm{Hz}$. Although this energy scale is small compared with that of typical ultracold atomic experiments, it should be noted that this energy gap can be made much larger as discussed below Eq. (6.16).

In a previous study [38], it has been shown that at zero temperature a topological defect such as a vortex of spin nematicity would be stable as long as the energy gap of the quasi-NG modes is finite. However, as we artificially make the energy gap vanish, the vortex decays by emitting the quasi-NG modes. This is illustrated by a numerical simulation, which is performed by using the Gross-Pitaevskii equation, as shown in Fig. 1 of Ref. [38]. The vortex of spin nematicity is displayed in terms of the spin-singlet trio amplitude

$$\begin{aligned} A_{30} &\equiv \frac{3\sqrt{6}(\xi_2\xi_{-1}^2 + \xi_1^2\xi_{-2})}{2} + \xi_0(\xi_0^2 - 3\xi_1\xi_{-1} + 6\xi_2\xi_{-2}) \\ &= \cos(3\eta), \end{aligned} \tag{6.18}$$

which is a function of the parameter η characterizing a nematic phase [Eq. (2.41)]. Similar to the mean-field approximation, that the energy gap is set to be zero is equivalent to that the ground-state manifold is enlarged from the uniaxial-nematic phase to the whole manifold of degenerate nematic phases. The original vortex then becomes unstable against the homotopy group of the new ground-state manifold as it can continuously transform to a nonsingular configuration. Now at finite temperatures, there should be a critical temperature above which the vortex would decay by emitting the thermally excited quasi-NG modes as these excitations become effectively gapless. Conversely, below this temperature the quasi-NG modes would behave as gapful excitations, and thus the vortex is stabilized by suppressing the emission of quasi-NG modes. With the obtained numerical value of the energy gap $\Delta \simeq \hbar \times 6\,\mathrm{Hz}$ for ^{87}Rb, we find the critical temperature to be $T^{\mathrm{c}} \simeq 0.04\,\mathrm{nK}$. As mentioned above, the magnitude of the energy gap of quasi-NG modes and the critical temperature can be raised to the regime accessible with typical ultracold atomic experiments by, for example, adjusting the relative strengths of the

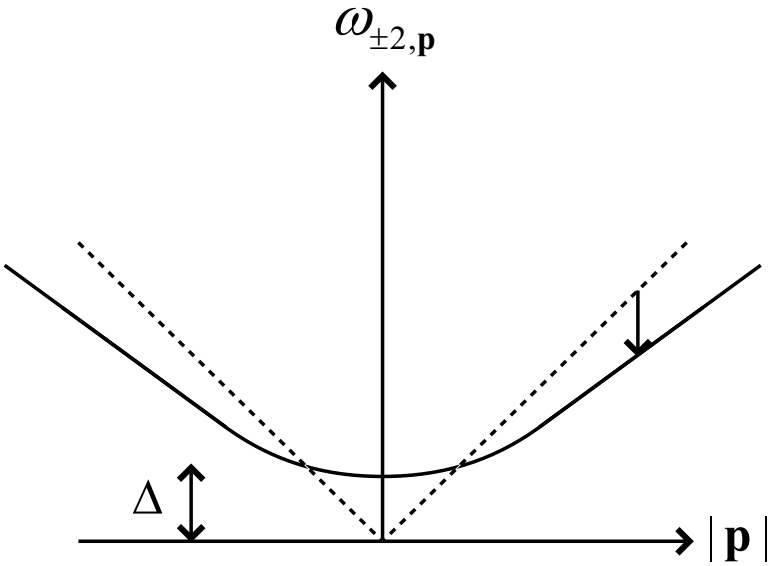

Figure 6.2: Modification of the dispersion relation of quasi-NG modes due to quantum fluctuations. Besides the emergence of a finite energy gap as shown in Sec. 6.1, there is a slight modification of the propagation velocity of quasi-NG modes as indicated by the arrow.

s-wave scattering lengths.

6.2 Suppression of the propagation velocity

In addition to the emergence of a finite energy gap, quantum fluctuations can bring about a slight modification of the propagation velocity of quasi-NG modes as illustrated in Fig. 6.2. In the low-momentum regime, the Bogoliubov spectrum of the quasi-NG modes [Eq. (6.5)] has a linear form of $\omega^{(1)}_{\pm 2,\mathbf{p}} = v^{(1)}_{\mathrm{q-NG}}|\mathbf{p}|$ with the propagation velocity given by

$$v^{(1)}_{\mathrm{q-NG}} = \sqrt{\frac{|c_2|n}{5M}}. \tag{6.19}$$

We now study how this propagation velocity is modified by quantum fluctuations. To this end, we apply the spinor Beliaev theory developed in Sec. 4.2 to finite momenta to obtain the dispersion relation of quasi-NG modes. For spin-2 ^{87}Rb, since $c_0 \gg c_1, |c_2|$, the effects of the spin-independent interaction, if it is nonvanishing, would dominate over the effects of spin-dependent ones. Therefore, regarding the modification of the propagation velocity, we can focus on the effects of c_0 corresponding to the effects of the particle-number density fluctuations and ignore those of the spin density fluctuations. In the regime $\Delta \ll \epsilon^0_{\mathbf{p}} \ll |c_2|n$ where the modified dispersion relation has a linear form, the spectrum of the quasi-NG modes can be expressed in terms of the second-order self-energies as

$$\omega_{\pm 2,\mathbf{p}} \simeq \omega^{(1)}_{\pm 2,\mathbf{p}} + \frac{\Sigma^{11(2)}_{22} - \Sigma^{22(2)}_{22}}{2}. \tag{6.20}$$

Here we ignored terms containing small factors of $\Delta/\epsilon^0_{\mathbf{p}}$ and $\epsilon^0_{\mathbf{p}}/|c_2|n$. By summing all the

contributions to the self-energies from the second-order Feynman diagrams, we obtain

$$\Sigma_{22}^{11(2)}(p) = A_1 + B_1(\omega_{\pm 2,\mathbf{p}} - \omega_{\pm 2,\mathbf{p}}^{(1)}) + \mathcal{O}\left[(\omega_{\pm 2,\mathbf{p}} - \omega_{\pm 2,\mathbf{p}}^{(1)})^2\right], \tag{6.21}$$

$$\Sigma_{22}^{22(2)}(p) = A_2 + B_2(\omega_{\pm 2,\mathbf{p}} - \omega_{\pm 2,\mathbf{p}}^{(1)}) + \mathcal{O}\left[(\omega_{\pm 2,\mathbf{p}} - \omega_{\pm 2,\mathbf{p}}^{(1)})^2\right] \tag{6.22}$$

with

$$A_1 = \frac{5M^{3/2}n_0^{3/2}c_0^{5/2}}{3\pi^2\hbar^3} - \frac{8\sqrt{2}|c_2|^{1/2}n_0^{1/2}}{3\sqrt{5\pi}}\sqrt{\epsilon_{\mathbf{p}}^0}, \tag{6.23}$$

$$A_2 = \frac{5M^{3/2}n_0^{3/2}c_0^{5/2}}{3\pi^2\hbar^3} + \frac{8\sqrt{2}|c_2|^{1/2}n_0^{1/2}}{3\sqrt{5\pi}}\sqrt{\epsilon_{\mathbf{p}}^0}, \tag{6.24}$$

$$B_1, B_2 = 0 + \mathcal{O}(\sqrt{na^3}). \tag{6.25}$$

Here, since it is expected that quantum fluctuations in a dilute weakly interacting Bose gas would bring about only a slight modification of the propagation velocity, i.e., $|\omega_{\pm 2,\mathbf{p}}/\omega_{\pm 2,\mathbf{p}}^{(1)} - 1| \ll 1$, we can make Taylor expansions in powers of $\omega_{\pm 2,\mathbf{p}} - \omega_{\pm 2,\mathbf{p}}^{(1)}$ and ignore the quadratic and higher-order terms. The validity of these expansions can be *a posteriori* justified from the final result. Substituting Eqs. (6.21)–(6.25) in Eq. (6.20), we obtain the second-order dispersion relation of the quasi-NG modes

$$\begin{aligned}\hbar\omega_{\pm 2,\mathbf{p}}^{(2)} &\simeq \left(1 - \frac{8}{3\sqrt{\pi}}\sqrt{n_0 a^3}\right)\sqrt{\frac{2|c_2|n_0\epsilon_{\mathbf{p}}^0}{5}} \\ &= \left(1 - \frac{4}{\sqrt{\pi}}\sqrt{na^3}\right)\sqrt{\frac{2|c_2|n\epsilon_{\mathbf{p}}^0}{5}},\end{aligned} \tag{6.26}$$

which also has a linear form with the modified propagation velocity

$$v_{\mathrm{q-NG}}^{(2)} = \left(1 - \frac{4}{\sqrt{\pi}}\sqrt{na^3}\right)\sqrt{\frac{|c_2|n}{5M}}. \tag{6.27}$$

Here in deriving the second equality in Eq. (6.26) we used the relation (3.2) between the total particle-number density n and that of the condensate n_0. From Eqs. (6.19) and (6.27), it is evident that the propagation velocity of the quasi-NG modes is suppressed by a factor of $1 - 4\sqrt{na^3}/\sqrt{\pi}$ due to the particle-number density fluctuations. The suppression factor is proportional to the fraction of noncondensed atoms [Eq. (3.1)], implying that the propagation of the quasi-NG modes is hindered by the interaction with these particles. It is analogous to the resistance to the motion of a particle or a quasiparticle in a random potential such as a medium filled with random impurities [102]. This can be understood by noting that the quasi-NG modes represent the spatially periodic modulations of the spin nematicity which have no correlation with the particle-number density fluctuations and thus leading to the random behavior.

In contrast, the propagation velocity of phonons, i.e., the sound velocity, is enhanced due to particle-number density fluctuations as

$$v_{\mathrm{ph}}^{(2)} \simeq \left(1 + \frac{8}{\sqrt{\pi}}\sqrt{na^3}\right)v_{\mathrm{ph}}^{(1)}, \tag{6.28}$$

where

$$v_{\rm ph}^{(1)} = \sqrt{\frac{(c_0 + c_2/5)n}{M}} \tag{6.29}$$

is the first-order (Bogoliubov) sound velocity. The modifications of the propagation velocities of the quasi-NG modes and phonons as functions of the characteristic dimensionless parameter $\sqrt{na^3}$ are shown in Fig. 6.3. The enhancement of the sound velocity due to the particle-number density fluctuations can be attributed to their correlations with phonons, which are spatially periodic modulations of the particle-number density. It is this correlation that leads to a nontrivial effect on the motion of phonons as opposed to the resistant effect on the quasi-NG modes. Indeed, at zero temperature the population of noncondensed atoms with momentum $\hbar\mathbf{p}$ is given by [19]

$$N_{\mathbf{p}} = \frac{1}{2}\left\{\frac{\epsilon_{\mathbf{p}}^0 + (c_0 + c_2/5)n_0}{\sqrt{\epsilon_{\mathbf{p}}^0[\epsilon_{\mathbf{p}}^0 + 2(c_0 + c_2/5)n_0]}} - 1\right\}. \tag{6.30}$$

Their contribution to the particle-number density correlation can be calculated straightforwardly, and we obtain

$$\langle \delta\hat{n}(\mathbf{r}, t)\delta\hat{n}(\mathbf{r}', t')\rangle = 2\frac{n_0 N_{\mathbf{p}}}{V}\cos[\mathbf{p}\cdot(\mathbf{r} - \mathbf{r}') - \omega_{0,\mathbf{p}}(t - t')], \tag{6.31}$$

where $\delta\hat{n} \equiv \hat{n} - n_0$ denotes the deviation of the particle-number density operator from the homogeneous distribution of the condensate. This contribution to the density correlation is related to the peak of the system's dynamic structure factor $S(\mathbf{p}, \omega)$ which can be directly measured by using either the inelastic neutron scattering in superfluid ^{4}He [103] or the Bragg scattering in ultracold atoms [104]. The restoring force resulting from the inhomogeneity brought about by the particle-number density correlation makes the system more rigid with a smaller compressibility $\kappa = -(1/V)\partial V/\partial p$ compared to a homogeneous state, and in turn leads to a larger sound velocity $c = \sqrt{\partial p/\partial\rho}$.

As similar to the quasi-NG modes, the propagation velocity of magnons is suppressed due to the particle-number density fluctuations as

$$v_{\rm mag}^{(2)} = \left(1 - \frac{4}{\sqrt{\pi}}\sqrt{na^3}\right) v_{\rm mag}^{(1)}, \tag{6.32}$$

where

$$v_{\rm mag}^{(1)} = \sqrt{\frac{(3c_1 - c_2/5)n}{M}}. \tag{6.33}$$

This suppression of the velocity of magnons is similar to the resistance to the motion of magnons in spin-1 BECs, which is exhibited by an enhancement of the effective mass of these quasiparticles [79]. From Eqs. (6.27) and (6.32), we know that the suppression factor of the magnons' propagation velocity is the same as that of the quasi-NG modes. This can be understood by noticing that the effects of the particle-number density fluctuations under consideration should be spin independent. On the other hand, it follows from Eq. (6.28) that the enhancement factor of the propagation velocity of phonons is twice the suppression factor of the magnons and quasi-NG modes' propagation velocities. Combined with the fact that there is a twofold degeneracy in the magnons and quasi-NG modes compared with a single mode of phonons (see Sec. 4.2), it

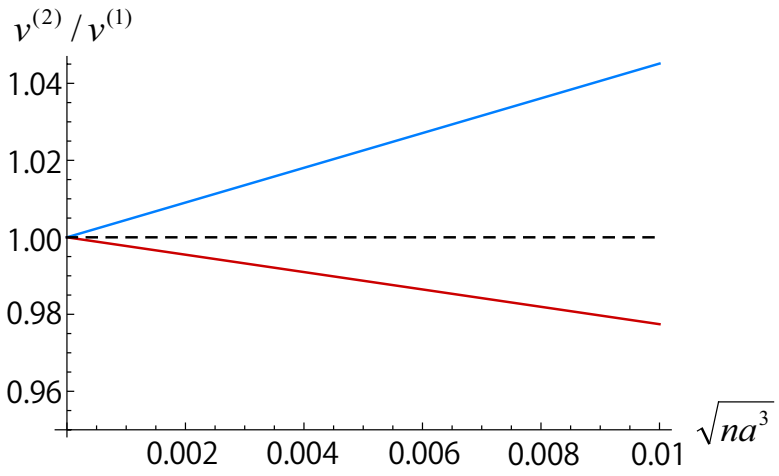

Figure 6.3: Modifications of the propagation velocities of the quasi-NG modes (red) and phonons (blue) as functions of the dimensionless parameter $\sqrt{na^3}$. Here n and a denote the atomic number density and the s-wave scattering length defined below Eq. (4.1), respectively. $v^{(1)}$ and $v^{(2)}$ represent the first- and second-order propagation velocities, respectively.

might suggest a total conservation of the effects of the particle-number density fluctuations on the propagations of different types of quasiparticles in a spinor BEC.

Chapter 7

Beliaev dampings of magnons and phonons

In the previous chapters, we have seen how quantum fluctuations affect the phase diagram and elementary excitations of a spinor BEC. In this chapter we study yet another important effect of quantum fluctuations on the lifetime of a quasiparticle. At the level of the Bogoliubov approximation, quasiparticles have infinite lifetimes. However, as we go to higher-order approximations, the lifetime of, for example, phonons becomes finite [26]. This physical phenomenon is called the Beliaev damping and can be interpreted as a consequence of the collisions of phonons with the condensate atoms [105]. Understanding the decay processes of quasiparticles gives us a deeper insight into the beyond-mean-field interaction in a many-body system. The Beliaev damping of phonons in liquid ^{4}He has been observed in which the momentum threshold of the damping determines the boundary between the phonon and roton regimes [106, 107, 108]. With the realization of atomic Bose-Einstein condensates at ultralow temperatures, the Beliaev dampings of collective modes in a trapped Bose gas [109] and of phonons in a locally homogeneous system [110] have been observed and measured. The effects of confinement [111], an optical lattice [112], and a presence of a single vortex [113, 114] on the damping rates of quasiparticles have also been studied extensively.

In this chapter, we investigate the Beliaev dampings of various types of quasiparticles in a homogeneous spin-2 ^{87}Rb BEC whose ground state is likely to be the uniaxial-nematic (UN) phase. Compared with scalar BECs, in spin-2 BECs there exist magnons and quasi-NG modes in addition to phonons as shown in Chap.6. Each type of these quasiparticles can, in principle, decay via one of numerous collision channels. We find that the energy conservation in collisions prohibits all decay channels of the quasi-NG modes, while there are one and four channels for magnons and phonons, respectively. We will derive analytic expressions for the damping rates of these quasiparticles as functions of the fundamental interatomic interactions. The obtained damping rates also suggest an efficient approach to measure the magnitudes of the interactions through the lifetimes of the quasiparticles. We propose a scheme to measure the Beliaev damping rates of magnons in the spin-2 ^{87}Rb BEC by temporarily switching on an external magnetic field.

The Hamiltonian of spin-2 BECs [Eq. (2.16)] is composed of three interactions

$$\hat{V} = \hat{V}_0 + \hat{V}_1 + \hat{V}_2, \tag{7.1}$$

where

$$\hat{V}_0 = \frac{c_0}{2}\int \mathrm{d}^3\mathbf{r}\ :\hat{n}^2(\mathbf{r}):, \tag{7.2}$$

$$\hat{V}_1 = \frac{c_1}{2}\int \mathrm{d}^3\mathbf{r}\ :\hat{\mathbf{F}}^2(\mathbf{r}):, \tag{7.3}$$

$$\hat{V}_2 = \frac{c_2}{2}\int \mathrm{d}^3\mathbf{r}\ :\hat{A}^\dagger_{00}(\mathbf{r})\hat{A}_{00}(\mathbf{r}):. \tag{7.4}$$

Each of these interactions can contribute to its own possible decay channels of the quasiparticles.

In the low-momentum regime $\epsilon^0_{\mathbf{p}} \ll c_0 n, c_1 n, |c_2| n$, the Bogoliubov spectra of phonons [Eq. (6.3)], magnons [Eq. (6.4)], and quasi-NG modes [Eq. (6.5)] all have linear dispersion relations characterized by their propagation velocities:

$$\omega_{0,\mathbf{p}} \simeq v_0|\mathbf{p}| \equiv \sqrt{\frac{\tilde{c}_0 n}{M}}|\mathbf{p}|, \tag{7.5}$$

$$\omega_{\pm1,\mathbf{p}} \simeq v_{\pm1}|\mathbf{p}| \equiv \sqrt{\frac{3\tilde{c}_1 n}{M}}|\mathbf{p}|, \tag{7.6}$$

$$\omega_{\pm2,\mathbf{p}} \simeq v_{\pm2}|\mathbf{p}| \equiv \sqrt{\frac{\tilde{c}_2 n}{M}}|\mathbf{p}|, \tag{7.7}$$

where $\tilde{c}_0 \equiv c_0 + c_2/5$, and $\tilde{c}_1$ and $\tilde{c}_2$ have been defined below Eq. (4.33). In the following, we restrict our study to the low-momentum regime so that their dispersion relations are given by the linear equations (7.5)-(7.7).

Let us consider a general decay channel of a quasiparticle with momentum $\mathbf{p}$ in spin state $m_F = j$ in which the quasiparticle interacts with a condensate atom to generate two quasiparticles with momenta $\mathbf{q}$ and $\mathbf{p}-\mathbf{q}$ and spin states $m_F = j'$ and $m_F = j''$, respectively. This process is illustrated in Fig. 7.1. The damping rate is obtained by summing the probability of the transition $(j,\mathbf{p})+(0,\mathbf{0}) \to (j',\mathbf{q})+(j",\mathbf{p}-\mathbf{q})$ over all possible values of $\mathbf{q}$, j', and $j"$. Since the momentum $\mathbf{q}$ forms a continuum of the final state, the Fermi's golden rule can be applied. At the lowest order, it is given by

$$P_{\mathrm{damp}} \simeq \frac{2\pi}{\hbar^2}\sum_{(\mathbf{q},j',j'')} |V_{\mathrm{if}}|^2\,\delta\left(\omega_{j,\mathbf{p}} - \omega_{j',\mathbf{q}} - \omega_{j",\mathbf{p}-\mathbf{q}}\right), \tag{7.8}$$

where the transition amplitude

$$V_{\mathrm{if}} \equiv \langle \mathrm{vac}|\hat{b}_{j',\mathbf{q}}\hat{b}_{j",\mathbf{p}-\mathbf{q}}\hat{V}\hat{b}^\dagger_{j,\mathbf{p}}|\mathrm{vac}\rangle \tag{7.9}$$

is given by the matrix element of the interaction Hamiltonian $\hat{V}$ with the initial state $|\mathrm{i}\rangle = \hat{b}^\dagger_{j,\mathbf{p}}|\mathrm{vac}\rangle$ and the final state $|\mathrm{f}\rangle = \hat{b}^\dagger_{j',\mathbf{q}}\hat{b}^\dagger_{j",\mathbf{p}-\mathbf{q}}|\mathrm{vac}\rangle$. Here $\hat{b}_{j,\mathbf{p}}$ ($\hat{b}^\dagger_{j,\mathbf{p}}$) is the annihilation (creation) operator of a quasiparticle with momentum $\mathbf{p}$ and spin state $m_F = j$, and $|\mathrm{vac}\rangle$ denotes the vacuum of the quasiparticles, i.e., the ground state of the system. The Fermi's golden rule relates the transition probability in quantum mechanics to the classical energy conservation

$$\omega_{j,\mathbf{p}} = \omega_{j',\mathbf{q}} + \omega_{j",\mathbf{p}-\mathbf{q}}, \tag{7.10}$$

which is expressed by the Dirac's delta function in Eq. (7.8). Note that the sum in Eq. (7.8) is taken over all possible final states of $(\mathbf{q}, j', j")$. In the case of $j' = j''$, we need to multiply the sum by a factor of $1/2$ to avoid double counting of the final states.

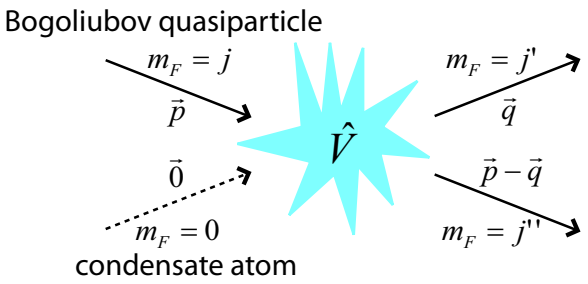

Figure 7.1: A general decay channel of a quasiparticle with momentum $\mathbf{p}$ and spin state $m_F = j$. Its interaction with a condensate atom (the dashed line) generates two quasiparticles with momenta $\mathbf{q}$ and $\mathbf{p} - \mathbf{q}$ and spin states $m_F = j'$ and $m_F = j''$, respectively. Here $\hat{V}$ denotes the interaction Hamiltonian given by Eq. (7.1).

The Dirac's delta function imposes a constraint on the possible decay channels for a given quasiparticle with initial state $(j, \mathbf{p})$. For the quasi-NG modes ($j = \pm 2$), by using the dispersion relations (7.5)-(7.7), it can be shown that there is no channel satisfying condition (7.10) (see Appendix E.1). Therefore, the quasi-NG modes in spin-2 BECs have long lifetimes compared with the other quasiparticles.

7.1 Magnons

For $j = \pm 1$, the spin conservation combined with condition (7.10) allows the only final spin state $j' = \pm 2$ and j" $= \mp 1$ (see Appendix E.2). This decay process proceeds through interaction $\hat{V}_1$ [Eq. (7.3)], which is written explicitly as

$$\hat{V}_1 = \frac{c_1}{2V} \sum_{\substack{\mathbf{p},\mathbf{q},\mathbf{k} \\ j,j',m,m'}} \mathbf{f}_{j,j'} \cdot \mathbf{f}_{m,m'} \hat{a}^\dagger_{m',\mathbf{p}-\mathbf{k}} \hat{a}^\dagger_{j',\mathbf{q}+\mathbf{k}} \hat{a}_{j,\mathbf{q}} \hat{a}_{m,\mathbf{p}}, \tag{7.11}$$

where $\hat{a}_{j,\mathbf{p}}$ ($\hat{a}^\dagger_{j,\mathbf{p}}$) is the annihilation (creation) operator of a bare particle, i.e., a single atom, and $\mathbf{f}_{j,j'}$ are the matrix elements of the spin-2 matrices [Eq. (2.18)]. The transition amplitude (7.9) can then be evaluated straightforwardly by using the relations between the operators $\hat{b}_{\pm j,\mathbf{p}}$ and $\hat{b}^\dagger_{\pm j,\mathbf{p}}$ of the Bogoliubov quasiparticles and those of single atoms $\hat{a}_{\pm j,\mathbf{p}}$ and $\hat{a}^\dagger_{\pm j,\mathbf{p}}$, which are given for the UN phase as [12]

$$\begin{aligned} \hat{a}_{\pm j,\mathbf{p}} &= u_{\pm j,\mathbf{p}} \hat{b}_{\pm j,\mathbf{p}} - v_{\pm j,\mathbf{p}} \hat{b}^\dagger_{\mp j,-\mathbf{p}}, \\ \hat{a}^\dagger_{\pm j,\mathbf{p}} &= u_{\pm j,\mathbf{p}} \hat{b}^\dagger_{\pm j,\mathbf{p}} - v_{\pm j,\mathbf{p}} \hat{b}_{\mp j,-\mathbf{p}}. \end{aligned} \tag{7.12}$$

Here $u_{j,\mathbf{p}}$ and $v_{j,\mathbf{p}}$ are the coefficients of the Bogoliubov transformations (see Sec. 2.4), which are given by

$$u_{0,\mathbf{p}} = \sqrt{\frac{\epsilon_{\mathbf{p}}^0 + \tilde{c}_0 n + \hbar\omega_{0,\mathbf{p}}}{2\hbar\omega_{0,\mathbf{p}}}},\ v_{0,\mathbf{p}} = \sqrt{\frac{\epsilon_{\mathbf{p}}^0 + \tilde{c}_0 n - \hbar\omega_{0,\mathbf{p}}}{2\hbar\omega_{0,\mathbf{p}}}}, \tag{7.13}$$

$$u_{\pm1,\mathbf{p}} = \sqrt{\frac{\epsilon_{\mathbf{p}}^0 + 3\tilde{c}_1 n + \hbar\omega_{\pm1,\mathbf{p}}}{2\hbar\omega_{\pm1,\mathbf{p}}}},\ v_{\pm1,\mathbf{p}} = \sqrt{\frac{\epsilon_{\mathbf{p}}^0 + 3\tilde{c}_1 n - \hbar\omega_{\pm1,\mathbf{p}}}{2\hbar\omega_{\pm1,\mathbf{p}}}}, \tag{7.14}$$

$$u_{\pm2,\mathbf{p}} = \sqrt{\frac{\epsilon_{\mathbf{p}}^0 + \tilde{c}_2 n + \hbar\omega_{\pm2,\mathbf{p}}}{2\hbar\omega_{\pm2,\mathbf{p}}}},\ v_{\pm2,\mathbf{p}} = -\sqrt{\frac{\epsilon_{\mathbf{p}}^0 + \tilde{c}_2 n - \hbar\omega_{\pm2,\mathbf{p}}}{2\hbar\omega_{\pm2,\mathbf{p}}}}. \tag{7.15}$$

Here the minus sign in front of the square root in the expression for $v_{\pm2,\mathbf{p}}$ in Eq. (7.15) results from the negative coupling constant c_2 of $\hat{V}_2$ [Eq. (7.4)], which is the only interaction that can generate a pair of noncondensed atoms in spin states $m_F = \pm2$ out of the condensate. A straightforward calculation of the matrix element $V_{\rm if}$ in Eq. (7.9) gives

$$V_{\rm if} = \frac{c_1\sqrt{6N_0}}{V} F(u,v), \tag{7.16}$$

where $N_0 = n_0 V$ is the total number of condensate particles, and

$$\begin{aligned} F(u,v) \equiv{}& (u_{-1,\mathbf{k}} - v_{1,-\mathbf{k}})\,(u_{1,\mathbf{p}} u_{2,\mathbf{q}} + v_{-1,-\mathbf{p}} v_{-2,-\mathbf{q}}) \\ & - (u_{1,\mathbf{p}} - v_{-1,-\mathbf{p}})\,(u_{2,\mathbf{q}} v_{1,-\mathbf{k}} + u_{-1,\mathbf{k}} v_{-2,-\mathbf{q}})\,. \end{aligned} \tag{7.17}$$

On the other hand, the zero of the argument of the Dirac's delta function in Eq. (7.8) is found to be

$$|\mathbf{q}| = q_0 \equiv 2\left(\frac{3\tilde{c}_1\cos\theta - \sqrt{3\tilde{c}_1\tilde{c}_2}}{3\tilde{c}_1 - \tilde{c}_2}\right)|\mathbf{p}|, \tag{7.18}$$

$$0 \leqslant \theta \leqslant \theta_0, \tag{7.19}$$

where θ denotes the angle between $\mathbf{q}$ and $\mathbf{p}$, and $\theta_0 \equiv \sqrt{\tilde{c}_2/3\tilde{c}_1} < 1$. By using the identity $\delta(f(x)) = \delta(x - x_0)/|f'(x_0)|$, where x_0 is the zero of $f(x)$, and replacing the sum in Eq. (7.8) by an integral, the damping rate can be rewritten as

$$P_{\rm damp} \simeq \frac{3\sqrt{2}c_1^2 n_0 M^{3/2}}{\pi\hbar^5} \int_0^\infty \mathrm{d}\epsilon_{\mathbf{q}}^0 \sqrt{\epsilon_{\mathbf{q}}^0} \int_{\cos\theta_0}^1 \mathrm{d}(\cos\theta) \frac{F(u,v)^2}{|\partial(\omega_{1,\mathbf{p}} - \omega_{2,\mathbf{q}} - \omega_{-1,\mathbf{k}})/\partial\epsilon_{\mathbf{q}}^0|} \delta\left(\epsilon_{\mathbf{q}}^0 - \frac{\hbar^2|\mathbf{q}_0|^2}{2M}\right). \tag{7.20}$$

The integral in Eq. (7.20) can be calculated straightforwardly, giving the damping rate as

$$P_{\rm damp} \simeq \frac{3\sqrt{2}c_1^2|\mathbf{p}|^3}{\pi\hbar(3c_1 - c_2/5)} \lambda\left(\frac{|c_2|}{c_1}\right), \tag{7.21}$$

where $\lambda(|c_2|/c_1) \equiv \tilde{\lambda}(\tilde{c}_2/3\tilde{c}_1)$ with

$$\tilde{\lambda}(x) \equiv \frac{\sqrt{x}\left(7 + 20\sqrt{x} + 30x + 10x^{3/2} + 5x^2\right)}{15\sqrt{2}(1+\sqrt{x})^5}. \tag{7.22}$$

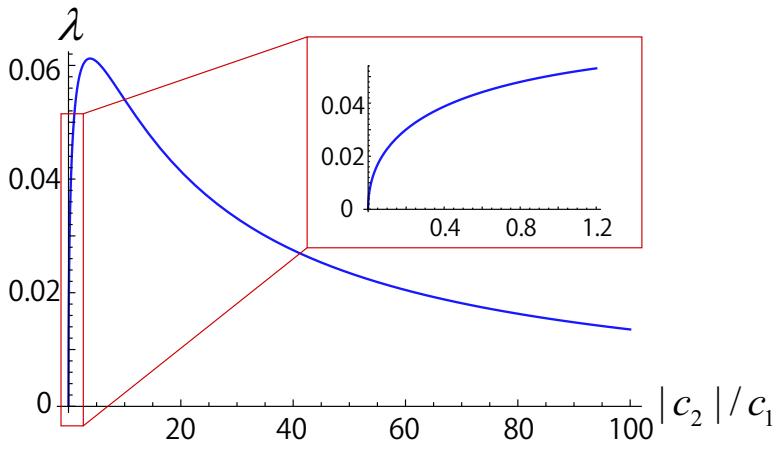

Figure 7.2: Function $\lambda(|c_2|/c_1)$ in Eq. (7.21). The inset shows λ over the uncertainty region of the ratio $|c_2|/c_1$ which is determined from the measurements [Eq. (6.2)] in Ref. [77]. Note that we need $c_2 < 0$ for the ground state to be the uniaxial-nematic phase.

It is evident from Eq. (7.21) that the damping rate of a magnon with momentum $\hbar\mathbf{p}$ is proportional to $|\mathbf{p}|^3$, and the damping strength depends on the interatomic interactions via function $\lambda(|c_2|/c_1)$. It is plotted in Fig. 7.2 in which the inset shows λ over the uncertainty region of parameter c_2 for ^{87}Rb [Eq. (6.2)].

Equation (7.21) suggests an alternative approach to measure the magnitudes of the interactions through the damping rates of magnons. We therefore propose a scheme to measure their damping rates. In ultracold atomic experiments, atoms can be prepared in arbitrary hyperfine spin states by using an adiabatic passage [115]. For a spin-2 ^{87}Rb BEC, the ground state is likely to be the uniaxial-nematic phase, i.e., almost all atoms occupy the $m_F = 0$ spin state. This is the initial state of the system. However, if an external magnetic field is applied, the system becomes dynamically unstable as the excitation spectrum of the magnon mode

$$\hbar\omega_{\pm1,\mathbf{p}} = \sqrt{(\epsilon^0_{\mathbf{p}} + q)(\epsilon^0_{\mathbf{p}} + q + 2\tilde{c}_1 n_0)} \tag{7.23}$$

acquires a nonzero imaginary part. Here q denotes the quadratic Zeeman coefficient. Note that q is negative for spin-2 ^{87}Rb, and its absolute value is proportional to the square of the field strength. This dynamical instability results in an exponential growth of the number of atoms in the $m_F = \pm1$ spin states, which has been observed in the Stern-Gerlach measurement [17]. If the external field is then suddenly switched off, the ground state returns to the uniaxial-nematic phase, leading to a stop of the generation of new magnons due to the dynamical instability. The lifetimes of the previously created magnons are then completely determined by the Beliaev damping. Their damping rates can be deduced from the measured time evolution of the atomic populations in the $m_F = \pm1$ spin states. It should, however, be noted that the obtained damping rate (7.21) is restricted to the low-momentum regime $\epsilon^0_{\mathbf{p}} \ll c_0 n, c_1 n, |c_2| n$.

The damping rates of magnons can also be derived from the beyond-Bogoliubov spectrum of these excitations. Indeed, using the spinor Beliaev theory developed in Sec. 4.2, we find the second-order energy spectrum of magnons with a nonzero imaginary part given by (see Appendix F)

$$\mathrm{Im}\left\{\omega^{(2)}_{\pm1,\mathbf{p}}\right\} = -\frac{3c_1^2|\mathbf{p}|^3}{\sqrt{2}\pi\hbar(3c_1 - c_2/5)}\lambda\left(\frac{|c_2|}{c_1}\right), \tag{7.24}$$

where function $\lambda(|c_2|/c_1)$ is the same as that in Eq. (7.21). On the other hand, the damping rate of a magnon is related to the imaginary part of its energy spectrum by

$$P_{\rm damp} = -2{\rm Im}\omega^{(2)}_{\pm 1,\mathbf{p}} \tag{7.25}$$

since the probability density of finding a quasiparticle is equal to the square of its wavefunction. It follows from Eqs. (7.24) and (7.25) that the damping rate (7.21) can be reproduced by using the spinor Beliaev theory.

It is worth noting that the scaling law of the damping rate of magnons with respect to the momentum $P_{\rm damp} \propto |\mathbf{p}|^3$ can be obtained indirectly without a need to carry out the tedious integral in Eq. (7.20). By a dimensional analysis, we find that the general expression for the damping rate must take the form of

$$P_{\rm damp} = \frac{c_0 n_0}{\hbar}\sqrt{n_0 a^3} f\left(\frac{c_1}{c_0}, \frac{c_2}{c_0}\right)\left(\frac{\epsilon^0_{\mathbf{p}}}{c_0 n_0}\right)^{\alpha}, \tag{7.26}$$

where f is a function of the only two dimensionless ratios of interactions c_1/c_0 and c_2/c_0. Here the dimensionless parameter $\sqrt{n_0 a^3}$ characteristic of a weakly interacting dilute Bose gas appears in Eq. (7.26) since the Beliaev damping only emerges at the second-order approximation [Eq. (7.25)] where the self-energies and the excitation spectra are evaluated up to the order of $\sqrt{n_0 a^3}$ (see, for example, Chap. 3). The power α in Eq. (7.26) would determine simultaneously the scaling laws of $P_{\rm damp}$ with respect to $|\mathbf{p}|$ and n_0. Therefore, the scaling law with respect to $|\mathbf{p}|$ can be obtained from that with respect to n_0, which is much easier to be found. Using Eqs. (7.13)–(7.15) for $u_{j,\mathbf{p}}$ and $v_{j,\mathbf{p}}$, we find the first term on the right-hand side of Eq. (7.17) to be

$$\begin{aligned}
&\left(u_{-1,\mathbf{k}} - v_{1,-\mathbf{k}}\right)\left(u_{1,\mathbf{p}}u_{2,\mathbf{q}} + v_{-1,-\mathbf{p}}v_{-2,-\mathbf{q}}\right)\\
=&\sqrt{\frac{\tilde{c}_1\tilde{c}_2 n_0^2 \epsilon^0_{\mathbf{k}}}{4\hbar^3\omega_{1,\mathbf{p}}\omega_{2,\mathbf{q}}\omega_{-1,\mathbf{k}}}}\left[\frac{\hbar\omega_{1,\mathbf{p}}}{\tilde{c}_1 n_0} + \frac{\hbar\omega_{2,\mathbf{q}}}{\tilde{c}_2 n_0} + \mathcal{O}\left(\frac{\epsilon^0_{\mathbf{p}}}{\tilde{c}_1 n_0}, \frac{\epsilon^0_{\mathbf{p}}}{\tilde{c}_2 n_0}\right)\right]\\
\propto& n_0^{-1/4},
\end{aligned} \tag{7.27}$$

where we used $\epsilon^0_{\mathbf{p},\mathbf{q},\mathbf{k}} \ll \tilde{c}_1 n_0, \tilde{c}_2 n_0$ in the low-momentum regime, and $\omega_{j,\mathbf{p}} \propto n_0^{1/2}$ as shown in Eqs. (7.5)-(7.7). Similarly, the second term on the right-hand side of Eq. (7.17) reduces to

$$\begin{aligned}
&-\left(u_{1,\mathbf{p}} - v_{-1,-\mathbf{p}}\right)\left(u_{2,\mathbf{q}}v_{1,-\mathbf{k}} + u_{-1,\mathbf{k}}v_{-2,-\mathbf{q}}\right)\\
=&\sqrt{\frac{\tilde{c}_1\tilde{c}_2 n_0^2 \epsilon^0_{\mathbf{p}}}{4\hbar^3\omega_{1,\mathbf{p}}\omega_{2,\mathbf{q}}\omega_{-1,\mathbf{k}}}}\left[\frac{\hbar\omega_{-1,\mathbf{k}}}{\tilde{c}_1 n_0} - \frac{\hbar\omega_{2,\mathbf{q}}}{\tilde{c}_2 n_0} + \mathcal{O}\left(\frac{\epsilon^0_{\mathbf{p}}}{\tilde{c}_1 n_0}, \frac{\epsilon^0_{\mathbf{p}}}{\tilde{c}_2 n_0}\right)\right]\\
\propto& n_0^{-1/4}.
\end{aligned} \tag{7.28}$$

The last contribution to the n_0-dependence of $P_{\rm damp}$ comes from the factor of $1/|\partial(\omega_{1,\mathbf{p}} - \omega_{2,\mathbf{q}} - \omega_{-1,\mathbf{k}})/\partial\epsilon^0_{\mathbf{q}}|$ in Eq. (7.20), which is proportional to $n_0^{-1/2}$ since $\omega_{j,\mathbf{p}} \propto n_0^{1/2}$. It follows from Eqs. (7.17), (7.20), (7.27), and (7.28) that $P_{\rm damp} \propto n_0^0$. We then find that $\alpha = 3/2$ in Eq. (7.26), leading to the scaling law $P_{\rm damp} \propto |\mathbf{p}|^3$.

7.2 Phonons

Unlike magnons, phonons can decay through various collision channels for which the energy conservation condition (7.10) is satisfied. The first one is that with the final state involving two phonons; i.e., $j' = j" = 0$. This is similar to the case of scalar BECs [26]. However, for spin-2 BECs the interaction in this channel can be either the spin-independent one $\hat{V}_0$ or the spin-dependent one $\hat{V}_2$. Therefore, the net coupling constant for this channel would be given by $\tilde{c}_0 = c_0 + c_2/5$, where the factor of 1/5 stems from the spin-singlet amplitude [Eq. (2.17)] in $\hat{V}_2$. The contribution of this decay channel to the damping rate of phonons is then found to be

$$\begin{aligned} P^{(1)}_{\rm damp} =& \frac{3\hbar}{320\pi M}\sqrt{n\tilde{c}_0{}^3}\frac{|\mathbf{p}|^5}{(\tilde{c}_0 n)^{3/2}} \\ =& \frac{3\hbar|\mathbf{p}|^5}{320\pi M n}. \end{aligned} \tag{7.29}$$

It is identical to the damping rate of phonons in scalar BECs since it turns out to be independent of the interaction in the low-momentum regime $\epsilon^0_{\mathbf{p}} \ll \tilde{c}_0 n$.

The second decay channel of phonons is that in which two magnons are generated in the final state; i.e., $j' = 1$ and $j" = -1$. The interaction in this channel can be either $\hat{V}_1$ or $\hat{V}_2$. For the former interaction, the transition amplitude is found to be

$$\begin{aligned} V_{\rm if} = \frac{3c_1\sqrt{N_0}}{V}\Big[&(u_{-1,\mathbf{k}} - v_{1,-\mathbf{k}})(u_{0,\mathbf{p}}u_{1,\mathbf{q}} + v_{0,-\mathbf{p}}v_{-1,-\mathbf{q}}) \\ &+ (u_{1,\mathbf{q}} - v_{-1,-\mathbf{q}})(u_{0,\mathbf{p}}u_{-1,\mathbf{k}} + v_{0,-\mathbf{p}}v_{1,-\mathbf{k}})\Big], \end{aligned} \tag{7.30}$$

where $u_{j,\mathbf{p}}$ and $v_{j,\mathbf{p}}$ are given by Eqs. (7.13)–(7.15). By replacing the sum over $\mathbf{q}$ in Eq. (7.8) by an integral, the contribution to the damping rate of phonons can be straightforwardly calculated to be

$$P^{(2)}_{\rm damp} = \frac{9c_1^2 nM|\mathbf{p}|}{\sqrt{2}\pi\hbar^3}\gamma_1\left(\frac{3\tilde{c}_1}{\tilde{c}_0}\right), \tag{7.31}$$

where $\gamma_1(x) \equiv 1/(2\sqrt{2}x^{3/2})$. It is plotted in Fig. 7.3.

Similarly, for the latter interaction, i.e., $\hat{V}_2$, the transition amplitude is given by

$$V_{\rm if} = -\frac{2c_2\sqrt{N_0}}{5V}\left(u_{0,\mathbf{p}}u_{1,\mathbf{q}}u_{-1,\mathbf{k}} - v_{0,-\mathbf{p}}v_{-1,-\mathbf{q}}v_{1,-\mathbf{k}}\right). \tag{7.32}$$

The contribution to the damping rate of phonons is then found to be

$$P^{(3)}_{\rm damp} = \frac{2\sqrt{2}c_2^2 nM|\mathbf{p}|}{25\pi\hbar^3}\gamma_2\left(\frac{3\tilde{c}_1}{\tilde{c}_0}\right), \tag{7.33}$$

where $\gamma_2(x) \equiv (1+x)^2/(8\sqrt{2}x^{3/2})$. It is plotted in Fig. 7.4.

In the last decay channel of phonons, two quasi-NG modes are generated, i.e., $j' = 2$ and $j'' = -2$, due to interaction $\hat{V}_2$. The transition amplitude is given by

$$V_{\rm if} = \frac{2c_2\sqrt{N_0}}{5V}\left(u_{0,\mathbf{p}}u_{2,\mathbf{q}}u_{-2,\mathbf{k}} - v_{0,-\mathbf{p}}v_{-2,-\mathbf{q}}v_{2,-\mathbf{k}}\right). \tag{7.34}$$

It has a form similar to Eq. (7.32) with the spin state $m_F = \pm 1$ being replace by $m_F = \pm 2$.

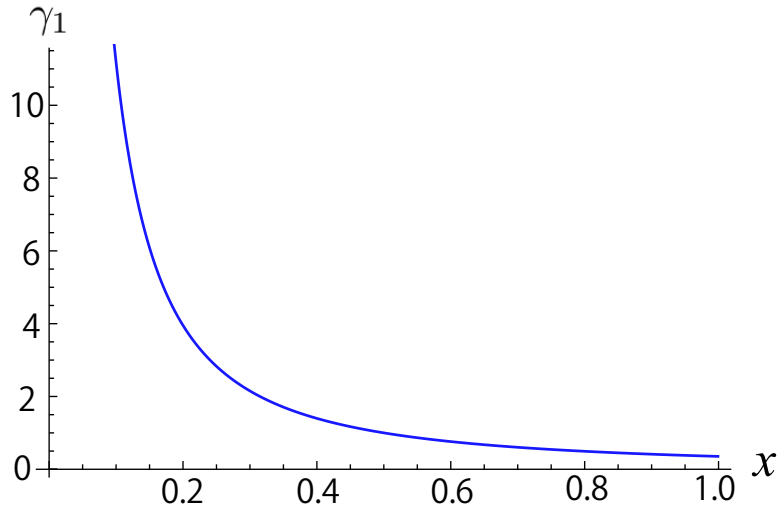

Figure 7.3: Function $\gamma_1(x)$ defined below Eq. (7.31).

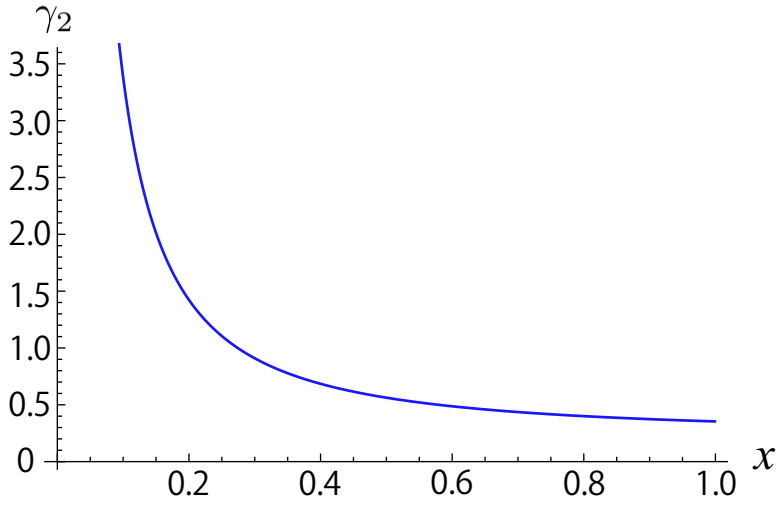

Figure 7.4: Function $\gamma_2(x)$ defined below Eq. (7.35).

The contribution of this channel to the damping rate of phonons is then obtained as

$$P_{\text{damp}}^{(4)} = \frac{2\sqrt{2}c_2^2 nM|\mathbf{p}|}{25\pi\hbar^3}\gamma_2\left(\frac{\tilde{c}_2}{\tilde{c}_0}\right). \tag{7.35}$$

In summary, the total damping rate of phonons in spin-2 BECs can be expressed as a sum of two contributions. Their scaling laws with respect to the momentum are $P_{\text{damp}} \propto |\mathbf{p}|^5$ and $P_{\text{damp}} \propto |\mathbf{p}|$, respectively. The former is the only contribution to the damping rate of phonons in scalar BECs, while the latter would be dominant in the regime of low momenta.

Chapter 8

Summary and Discussion

We have studied the effects of quantum fluctuations on the phase diagram, elementary excitations, and phase transitions of spinor Bose-Einstein condensates (BECs). This study is based on the development of the spinor version of the Beliaev theory. By taking into account the contributions from the second-order Feynman diagrams, we have derived analytically the excitation spectrum that contains a quantum correction to the Bogoliubov spectrum. From the obtained Beliaev spectrum, we have been able to address various problems in spinor BECs such as the stability of a quantum phase, the quantum symmetry breaking, and the lifetime of quasiparticles. In the following, we summarize the main results of our study and discuss some outstanding open issues.

In Chapter 4, we have discovered two special classes of first-order quantum phase transitions in spinor BECs which are characterized by their possibilities of metastability. The first one is accompanied with metastable states that are induced by quantum fluctuations. Conventional first-order phase transitions are often associated with the existence of metastable states around the phase boundaries [29, 116, 117, 118]; however, the Bogoliubov analysis implies no metastability at all. Only by going to the next-order approximation, i.e., the Beliaev theory, can we show that metastable states indeed appear around the phase boundaries. This result has shed light on the pivotal role of quantum fluctuations in the study of the phase diagram and the stability of a spinor condensate. The presence of a metastable condensate also suggests an interesting possibility of macroscopic quantum tunneling (MQT) in which all atoms tunnel simultaneously from a metastable state to the ground state. In Sec. 4.4, we have estimated the time scale of the MQT for a spin-2 ^{87}Rb BEC and found that in order to observe MQT within the lifetime of the BEC (i.e., a few seconds), the total number of atoms must be limited by that of a microcondensate (i.e., a few tens). Since a large fraction of particles can be excited out of a small condensate due to fluctuations, the effects of fluctuations in such a microcondensate might become significant and thus merit a thorough investigation in the future.

In contrast, in the second class of first-order phase transitions, the metastability is absent to all orders of approximation. This is because the metastable state is prohibited by the high symmetry of the Hamiltonian at the phase boundary, resulting in a flat energy landscape. It is this flat energy landscape that leads to the abrupt change of the system from the ground state to an unstable state without undergoing a metastable regime. On the other hand, the flat energy landscape brings about the criticality in the dynamics of the condensate through these phase transitions. In Chapter 5, we have studied the dynamics of a spinor condensate and found the critical features in both instantaneous and slow quenches of a system's parameter. Consequently, despite being first-order phase transitions, their dynamics is similar to that of second-order phase transitions. Some of the quantum phase transitions in both spin-1 and spin-2 BECs are within reach of current experiments, bringing hope that our theoretical predictions can

be verified experimentally. Furthermore, similar types of first-order quantum phase transitions might also appear in other physical systems with internal degrees of freedom including the superfluid ^{3}He, superconductors with high angular momenta, and color superconductors.

In Chapter 6, we have succeeded in deriving the analytic expression for the energy gap of the so-called quasi-Nambu-Goldstone (quasi-NG) mode in the nematic phase of spin-2 BECs. Quasi-NG modes are the gapless excitations at the mean-field level that do not stem from spontaneous symmetry breaking. However, it has been predicted that they would acquire a nonzero energy gap with quantum corrections [38]. By deriving the emergent energy gap of the quasi-NG modes due to quantum fluctuations, we have been able to prove the conjecture. To our knowledge, this is the first time for the energy gap of the quasi-NG modes to be evaluated quantitatively. Regarding the magnitude of the energy gap, it is predicted in a previous study [38] that it is of the same order as the zero-point energy, which lifts the degeneracy in the manifold of nematic phases. However, we show that the truth is beyond such a simple prognostication. Since there is no level crossing in the phase transition associated with the nematic phases, the energy gap of the quasi-NG modes and the zero-point energy do not necessarily have the same order of magnitude. The energy gap turns out to strongly depend on the relative strengths of the spin-dependent interactions. The scaling laws of the energy gap with respect to the system's parameters also vary with the ratio of interactions.

Furthermore, from the obtained magnitude of the energy gap, we have been able to evaluate the critical temperature above which a topological defect such as a vortex of spin nematicity would decay by emitting thermally excited quasi-NG modes. Conversely, below this temperature the quasi-NG modes behave as gapful excitations, and thus the vortex would be stabilized by suppressing their emission. The magnitude of the energy gap and the critical temperature can be increased to a regime accessible with typical ultracold atomic experiments by, for example, adjusting the relative strengths of the s-wave scattering lengths. In addition to the emergence of a finite energy gap, we find that the propagation velocity of the quasi-NG modes is suppressed due to the particle-number density fluctuations. This is opposed to the enhancement of the sound velocity, and a qualitative account of the difference is given in terms of the particle-number density correlation. Our study of quasi-NG modes is also related to the problems of Coleman-Weinberg mechanism of quantum symmetry breaking [32] and the quantum anomaly [119] where the effects of quantum fluctuations play an essential role.

In Chapter 7, we have calculated the damping rates of various types of quasiparticles in spin-2 BECs. They include phonons, magnons, and quasi-NG modes, which represent the spatially periodic modulations of the particle-number, spin-magnetic, and spin-nematic densities, respectively. At the level of the Bogoliubov theory, all of these quasiparticles have infinite lifetimes. However, with higher-order approximations, their lifetimes become finite since they can decay through numerous channels of collision with the condensate atoms. By using Fermi's golden rule to calculate the transition probabilities, we find that the damping of the quasi-NG modes is suppressed due to the energy conservation. In contrast, the damping rates of phonons and magnons are found to be finite with their own scaling laws with respect to the momentum. It is worth noting that the damping rates of these quasiparticles can be reproduced by using the developed spinor Beliaev theory. The obtained analytic expressions for the damping rates as functions of the fundamental interactions also suggest an alternative approach to measuring precisely the magnitudes of the spin-dependent interactions. We have proposed a scheme to measure the lifetime of magnons in the spin-2 ^{87}Rb condensate by temporarily switching on an external magnetic field.

As shown above, spinor BECs provide us with a table-top playground for the study of the effects of quantum fluctuations on various physical phenomena. They can be classified into two categories. In the first one, the effects of quantum fluctuations become significant, leading to re-

markable changes in the features of the system. Noticeable examples are the fluctuation-induced metastability and the emergent energy gap of the quasi-NG modes. In the second category, the system's properties remain unchanged to all orders of approximation. It is because they are protected by the symmetry of the Hamiltonian. Typical examples are the symmetry-prohibited metastability and the gapless excitations generated by spontaneous symmetry breaking. In contrast to the quasi-NG modes, these excitations, which include phonons and magnons, are gapless at any order of approximation. In the language of Green's functions, this is guaranteed by the Hugenholtz-Pines theorem [120] which relates the self-energies at zero wavelength and zero frequency to the chemical potential. In scalar BECs, it is written as

$$\Sigma^{11}(p=0) - \Sigma^{12}(p=0) = \mu. \tag{8.1}$$

For the uniaxial-nematic phase in spin-2 BECs, the Hugenholtz-Pines theorem is predicted to have the form of

$$\Sigma^{11}_{00}(p=0) - \Sigma^{12}_{00}(p=0) = \mu \tag{8.2}$$

for phonons, and

$$\Sigma^{11}_{11}(p=0) - \Sigma^{12}_{1,-1}(p=0) = \mu \tag{8.3}$$

for magnons. Equalities (8.2) and (8.3) are expected to hold at any order of approximation. Although Eq. (8.2) can be proved for a given order of approximation by using the relation between the Feynman diagrams for Σ^{11}_{00} and Σ^{12}_{00} in a manner similar to scalar BECs [120], the proof of Eq. (8.3) is nontrivial since we do not have a similar simple relation between the diagrams for Σ^{11}_{11} and $\Sigma^{12}_{1,-1}$. Even its proof at the second-order approximation requires a tedious calculation. Therefore, an attempt to prove this fundamental theorem for spinor BECs at a general order of approximation is left for a future study. On the other hand, a similar equality for the quasi-NG modes

$$\Sigma^{11}_{22}(p=0) - \Sigma^{12}_{2,-2}(p=0) = \mu \tag{8.4}$$

holds only at the first-order approximation. From the second-order approximation, it breaks down due to quantum fluctuations, leading to the emergence of a finite energy gap.

Appendix A

T-matrix and vacuum scattering amplitude

The T-matrix $\Gamma(p_1, p_2; p_3, p_4)$ defined by Eq. (3.25) satisfies the Bethe-Salpeter equation [121]:

$$\Gamma(p_1, p_2; p_3, p_4) = V(\mathbf{p}_1 - \mathbf{p}_3) + \frac{i}{\hbar}\int \frac{\mathrm{d}^4 q}{(2\pi)^4} V(\mathbf{q}) G^0(p_1 - q) G^0(p_2 + q) \Gamma(p_1 - q, p_2 + q; p_3, p_4). \tag{A.1}$$

This iterative equation is illustrated in Fig. A.1 by using Feynman diagrams.

Let us introduce the center-of-mass four-vector $\hbar P = \hbar p_1 + \hbar p_2 = \hbar p_3 + \hbar p_4$, where the second equality implies the conservations of momentum and energy, and the initial and final relative four-vectors $\hbar p = (1/2)(\hbar p_1 - \hbar p_2)$, $\hbar p' = (1/2)(\hbar p_3 - \hbar p_4)$ for a pair of scattering particles. Equation (A.1) can then be rewritten as

$$\Gamma(p, p', P) = V(\mathbf{p} - \mathbf{p}') + \frac{i}{\hbar}\int \frac{\mathrm{d}\omega_{\mathbf{q}}}{2\pi}\int \frac{\mathrm{d}^3\mathbf{q}}{(2\pi)^3} V(\mathbf{q}) G^0(P/2 + p - q) G^0(P/2 - p + q) \Gamma(p - q, p', P), \tag{A.2}$$

or in the form of an infinite series as

$$\begin{aligned}\Gamma(p, p', P) =& V(\mathbf{p} - \mathbf{p}') + \frac{i}{\hbar}\int \frac{\mathrm{d}^3\mathbf{q}}{(2\pi)^3} V(\mathbf{q}) V(\mathbf{p} - \mathbf{q} - \mathbf{p}') \\ & \times \int \frac{\mathrm{d}\omega_{\mathbf{q}}}{2\pi} G^0(\omega_{\mathbf{P}}/2 + \omega_{\mathbf{p}} - \omega_{\mathbf{q}}, \mathbf{P}/2 + \mathbf{p} - \mathbf{q}) G^0(\omega_{\mathbf{P}}/2 - \omega_{\mathbf{p}} + \omega_{\mathbf{q}}, \mathbf{P}/2 - \mathbf{p} + \mathbf{q}) \\ & + \cdots .\end{aligned} \tag{A.3}$$

Using the transformation of variables $\omega_{\mathbf{q}} = \tilde{\omega}_{\mathbf{q}} + \omega_{\mathbf{p}}$, the integral in the second line of Eq. (A.3) reduces to

$$\int \frac{\mathrm{d}\tilde{\omega}_{\mathbf{q}}}{2\pi} G^0(\omega_{\mathbf{P}}/2 - \tilde{\omega}_{\mathbf{q}}, \mathbf{P}/2 + \mathbf{p} - \mathbf{q}) G^0(\omega_{\mathbf{P}}/2 + \tilde{\omega}_{\mathbf{q}}, \mathbf{P}/2 - \mathbf{p} + \mathbf{q}), \tag{A.4}$$

which is independent of $\omega_{\mathbf{p}}$. Similarly, the higher-order terms represented by the dots in Eq. (A.3) can be shown to be independent of $\omega_{\mathbf{p}}$ and $\omega_{\mathbf{p}'}$ by iteration. Therefore, the T-matrix is independent of $\omega_{\mathbf{p}}$ and $\omega_{\mathbf{p}'}$ and can be written as $\Gamma(\mathbf{p}, \mathbf{p}', P)$.

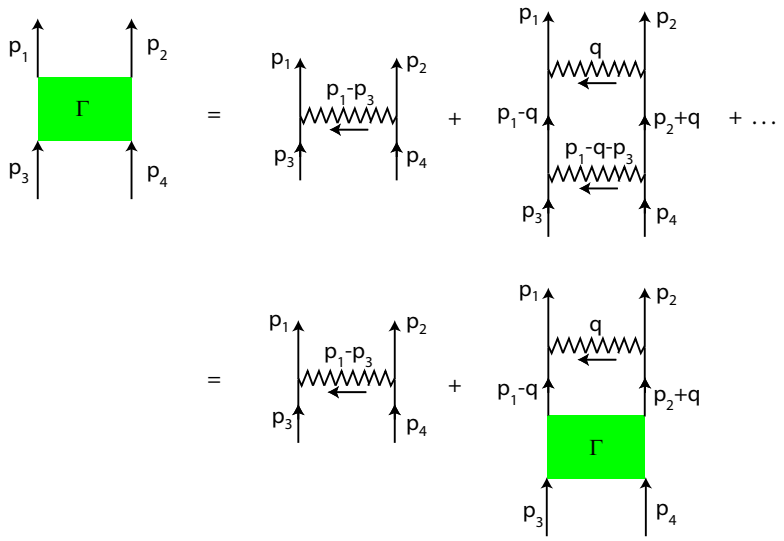

Figure A.1: Bethe-Salpeter equation (A.1) for the T-matrix $\Gamma(p_1, p_2; p_3, p_4)$. The squares represent the T-matrix, while the free propagators given by the noninteracting Green's function G^0 are represented by the solid lines with arrows. The wavy lines indicate the interatomic interaction V.

Next, we introduce $\chi(\mathbf{p}, \mathbf{p}', P)$ which is the integration kernel of $\Gamma(\mathbf{p}, \mathbf{p}', P)$ [26, 20]:

$$\Gamma(\mathbf{p}, \mathbf{p}', P) = \int \frac{\mathrm{d}^3\mathbf{q}}{(2\pi)^3} V(\mathbf{q}) \chi(\mathbf{p} - \mathbf{q}, \mathbf{p}', P). \tag{A.5}$$

Equation (A.5) has a form similar to the equation relating the vacuum scattering amplitude $-M\tilde{f}(\mathbf{k}, \mathbf{k}')/(4\pi\hbar^2)$ to the scattering wavefunction $\psi_{\mathbf{k}}(\mathbf{p})$ in momentum space:

$$\tilde{f}(\mathbf{k}, \mathbf{k}') = \int \frac{\mathrm{d}^3\mathbf{q}}{(2\pi)^3} V(\mathbf{q}) \psi_{\mathbf{k}}(\mathbf{k}' - \mathbf{q}). \tag{A.6}$$

From Eqs. (A.2) and (A.5), we obtain the equation for $\chi(\mathbf{p}, \mathbf{p}', P)$ as

$$\chi(\mathbf{p}, \mathbf{p}', P) = (2\pi)^3 \delta(\mathbf{p} - \mathbf{p}') + \frac{i}{\hbar} \int \frac{\mathrm{d}\omega_{\mathbf{p}}}{2\pi} G^0(P/2 + p) G^0(P/2 - p) \int \frac{\mathrm{d}^3\mathbf{q}}{(2\pi)^3} V(\mathbf{q}) \chi(\mathbf{p} - \mathbf{q}, \mathbf{p}', P). \tag{A.7}$$

This is confirmed by substituting Eq. (A.7) in Eq. (A.5) so that Eq. (A.2) is reproduced. With a straightforward calculation of the integral $\int \mathrm{d}\omega_{\mathbf{p}}$ in Eq. (A.7) using $G^0(p) = [\omega_{\mathbf{p}} - (\epsilon^0_{\mathbf{p}} - \mu)/\hbar + i\eta]^{-1}$, we obtain

$$\chi(\mathbf{p}, \mathbf{p}', P) = (2\pi)^3 \delta(\mathbf{p} - \mathbf{p}') + \frac{1}{\hbar\omega_{\mathbf{P}} - \frac{\hbar^2\mathbf{P}^2}{4M} + 2\mu - \frac{\hbar^2\mathbf{p}^2}{M} + i\eta} \int \frac{\mathrm{d}^3\mathbf{q}}{(2\pi)^3} V(\mathbf{q}) \chi(\mathbf{p} - \mathbf{q}, \mathbf{p}', P). \tag{A.8}$$

On the other hand, the Schrodinger equation for the scattering wave function $\psi_{\mathbf{k}}(\mathbf{p})$ in momen-

tum space is given by

$$\psi_{\mathbf{k}}(\mathbf{p}) = (2\pi)^3\delta(\mathbf{p}-\mathbf{k}) - \frac{1}{\frac{\hbar^2\mathbf{p}^2}{M} - \frac{\hbar^2\mathbf{k}^2}{M} - i\eta}\int \frac{\mathrm{d}^3\mathbf{q}}{(2\pi)^3}\, V(\mathbf{q})\psi_{\mathbf{k}}(\mathbf{p}-\mathbf{q}). \tag{A.9}$$

Using Eqs. (A.6), (A.8) and (A.9), $\chi(\mathbf{p},\mathbf{p}',P)$ can be expressed in terms of $\psi_{\mathbf{k}}(\mathbf{p})$ and $\tilde{f}(\mathbf{k}',\mathbf{k})$ as [20]

$$\chi(\mathbf{p},\mathbf{p}',P) = \psi_{\mathbf{p}'}(\mathbf{p}) + \int \frac{\mathrm{d}^3\mathbf{q}}{(2\pi)^3}\,\psi_{\mathbf{q}}(\mathbf{p})\Big(\frac{1}{\hbar\omega_{\mathbf{P}} - \frac{\hbar^2\mathbf{P}^2}{4M} + 2\mu - \frac{\hbar^2\mathbf{q}^2}{M} + i\eta} + \frac{1}{\frac{\hbar^2\mathbf{q}^2}{M} - \frac{\hbar^2\mathbf{p}'^2}{M} - i\eta}\Big) \times \tilde{f}(\mathbf{p}',\mathbf{q})^*. \tag{A.10}$$

Substituting Eq. (A.10) in Eq. (A.5), we obtain the T-matrix as

$$\Gamma(\mathbf{p},\mathbf{p}',P) = \tilde{f}(\mathbf{p},\mathbf{p}') + \int \frac{\mathrm{d}^3\mathbf{q}}{(2\pi)^3}\,\tilde{f}(\mathbf{p},\mathbf{q})\Big(\frac{1}{\hbar\omega_{\mathbf{P}} - \frac{\hbar^2\mathbf{P}^2}{4M} + 2\mu - \frac{\hbar^2\mathbf{q}^2}{M} + i\eta} + \frac{1}{\frac{\hbar^2\mathbf{q}^2}{M} - \frac{\hbar^2\mathbf{p}'^2}{M} - i\eta}\Big) \times \tilde{f}(\mathbf{p}',\mathbf{q})^*. \tag{A.11}$$

From Eq. (A.11), it is clear that the T-matrix $\Gamma(p_1,p_2;p_3,p_4) = \Gamma(\mathbf{p},\mathbf{p}',P)$ can be expressed in terms of the vacuum scattering amplitude $-M\tilde{f}(\mathbf{p},\mathbf{p}')/(4\pi\hbar^2)$. This scattering amplitude is well defined even for a singular interaction potential.

Appendix B

Ground-state energy with the LHY correction

For a dilute system of spinless bosons, the ground-state energy density with the LHY correction is given by [70, 71]

$$\frac{E}{V} = \frac{2\pi\hbar^2 a n^2}{M}\left(1 + \frac{128}{15\sqrt{\pi}}\sqrt{na^3}\right), \tag{B.1}$$

where n, a, and M are the particle-number density, the s-wave scattering length, and the atomic mass, respectively. The first term on the right-hand side of Eq. (B.1) is the Hartree mean-field energy, while the second term gives the leading-order correction first derived by Lee, Huang, and Yang [70, 71]. The LHY correction arises from quantum fluctuations of the condensate and is proportional to the fraction of quantum depletion $n^{\rm qd}/n = 8\sqrt{na^3}/(3\sqrt{\pi})$. In the following, we compare the energies of the different phases of spin-2 BECs, by which the phase boundaries in Fig. 4.1 are determined.

Ferromagnetic-BN phase boundary. The energy densities with the LHY corrections of the ferromagnetic and BN phases in the proximity of the mean-field phase boundary at $c_1 < 0$ and $c_2 = 20c_1$ are given by [68]

$$\frac{E^{\rm FM}}{V} = \left(\frac{c_0}{2} + 2c_1\right) n^2 \left[1 + \frac{16M^{3/2}}{15\pi^2\hbar^3}\sqrt{n(c_0 + 4c_1)^3}\right] \tag{B.2}$$

and

$$\begin{aligned}\frac{E^{\rm BN}}{V} = {} & \left(\frac{c_0}{2} + \frac{c_2}{10}\right) n^2 \left[1 + \frac{16M^{3/2}}{15\pi^2\hbar^3}\sqrt{n\,(c_0 + 4c_1)^3}\right] + \frac{8M^{3/2}}{15\pi^2\hbar^3}(32 + 18\sqrt{3})(|c_1|n)^{5/2} \\ & + \mathcal{O}\left[\frac{M^{3/2}n^{5/2}\max\left\{c_0^{3/2}, |c_1|^{3/2}\right\}|c_2 - 20c_1|}{\hbar^3}\right],\end{aligned} \tag{B.3}$$

respectively. By noting that $|c_2 - 20c_1| \sim M^{3/2}n^{1/2}|c_1|^{5/2}/\hbar^3$ at the phase boundary [see Eq. (4.1)], the last term on the right-hand side of Eq. (B.3) is smaller than the other terms by a factor of $\sqrt{na^3} \ll 1$ with $a \equiv (4a_2 + 3a_4)/7 = c_0 M/(4\pi\hbar^2)$ and thus is negligible. Consequently,

the ferromagnetic-BN phase boundary is shifted from the mean-field counterpart to

$$c_2^{\mathrm{FM-BN}} \simeq 20c_1 - \frac{32(16+9\sqrt{3})M^{3/2}n^{1/2}|c_1|^{5/2}}{3\pi^2\hbar^3} \simeq 20c_1 - 1521\left(\frac{|c_1|}{c_0}\right)^{3/2}\sqrt{na^3}\,|c_1|. \tag{B.4}$$

Thus, we have derived Eq. (4.1).

UN-cyclic phase boundary. Similarly, the energy densities with the LHY corrections of the cyclic and UN phases for $c_1 > 0$ and $c_2 \leq 0$ are given by [68]

$$\frac{E^{\mathrm{CL}}}{V} = \frac{c_0 n^2}{2} + \frac{8M^{3/2}}{15\pi^2\hbar^3}\left[(nc_0)^{5/2} + 12\sqrt{2}(nc_1)^{5/2}\right] \tag{B.5}$$

and

$$\frac{E^{\mathrm{UN}}}{V} = \left(c_0 + \frac{c_2}{5}\right)\frac{n^2}{2} + \frac{8M^{3/2}}{15\pi^2\hbar^3}\left[(nc_0)^{5/2} + 18\sqrt{3}(nc_1)^{5/2}\right] + \mathcal{O}\left[\frac{M^{3/2}n^{5/2}\max\left\{c_0^{3/2}, c_1^{3/2}\right\}|c_2|}{\hbar^3}\right], \tag{B.6}$$

respectively. Here E^{UN} was expanded in powers of c_2/c_0 and c_2/c_1, which are expected to be small near the cyclic-UN phase boundary. Indeed, since $|c_2| \sim M^{3/2}n^{1/2}c_1^{5/2}/\hbar^3$ at the phase boundary [see Eq. (4.2)], the last term on the right-hand side of Eq. (B.6) is smaller than the others by a factor of $\sqrt{na^3} \ll 1$ and thus can be ignored. By comparing the energies in Eqs. (B.5) and (B.6), we find that the UN-cyclic phase boundary is given by

$$c_2^{\mathrm{UN-CL}} \simeq -\frac{16(18\sqrt{3}-12\sqrt{2})M^{3/2}n^{1/2}c_1^{5/2}}{3\pi^2\hbar^3} \simeq -342\left(\frac{c_1}{c_0}\right)^{3/2}\sqrt{na^3}\,c_1. \tag{B.7}$$

Thus, we have derived Eq. (4.2).

Appendix C

First derivative of the ground-state energy

By definition, a thermal phase transition is first order if there is a discontinuity in the first derivative of the free energy with respect to temperature. Similarly, a quantum phase transition is first order if a finite jump appears in the first derivative of the ground-state energy with respect to the parameter that drives the transition. In the following, the first derivative of the energy is evaluated at the phase boundaries in Fig. 4.1. The energies of the ferromagnetic and cyclic phases are given by Eqs. (B.2) and (B.5), respectively, while those of the UN and BN phases are obtained from the expression for the energies of nematic phases [74, 68]:

$$\frac{E(\eta)}{V} = \left(c_0 + \frac{c_2}{5}\right)\frac{n^2}{2}\left[1 + \frac{16M^{\frac{3}{2}}n^{\frac{1}{2}}}{15\pi^2\hbar^3}\left(c_0 + \frac{c_2}{5}\right)^{\frac{3}{2}}\right] + \frac{8M^{\frac{3}{2}}n^{\frac{5}{2}}}{15\pi^2\hbar^3}\left\{\left(\frac{|c_2|}{5}\right)^{\frac{5}{2}} + \left(2c_1 - \frac{c_2}{5}\right)^{\frac{5}{2}}\sum_{j=0}^{2}\left[1 - \frac{2c_1}{2c_1 - c_2/5}\cos\left(2\eta + \frac{2\pi j}{3}\right)^{\frac{5}{2}}\right]\right\}, \quad \text{(C.1)}$$

where $\eta = n\pi/3$ ($\eta = \pi/6 + n\pi/3$) corresponds to the UN (BN) phase.

Ferromagnetic-BN phase transition. We have

$$\frac{\partial(E^{\mathrm{FM}}/V)}{\partial c_2} = 0, \quad \text{(C.2a)}$$

$$\frac{\partial(E^{\mathrm{BN}}/V)}{\partial c_2}\Big|_{c_2 = c_2^{\mathrm{FM-BN}}} = \frac{n^2}{10}\left[1 + \mathcal{O}(\sqrt{na^3})\right], \quad \text{(C.2b)}$$

where $c_2^{\mathrm{FM-BN}}$ [Eq. (4.1)] indicates the ferromagnetic-BN phase boundary. Equation (C.2) implies that there is a finite jump in $\partial E/\partial c_2$ for the ferromagnetic-BN transition, and thus it is first order.

UN-cyclic phase transition. Similarly, the first derivatives of the energies at the UN-cyclic phase boundary [Eq. (4.2)] are evaluated to be

$$\frac{\partial(E^{\mathrm{CL}}/V)}{\partial c_2} = 0, \quad \text{(C.3)}$$

$$\frac{\partial(E^{\mathrm{UN}}/V)}{\partial c_2}\Big|_{c_2 = c_2^{\mathrm{UN-CL}}} = \frac{n^2}{10}\left[1 + \mathcal{O}(\sqrt{na^3})\right]. \quad \text{(C.4)}$$

Therefore, the UN-cyclic phase transition is first order.

Ferromagnetic-cyclic phase transition. The first derivatives of the energies with respect to c_1, which is the parameter that drives the phase transition, are given at the phase boundary $c_1 = 0$ and $c_2 > 0$ by

$$\frac{\partial(E^{\mathrm{FM}}/V)}{\partial c_1}\Big|_{c_1=0} = n^2 \left[2 + \mathcal{O}(\sqrt{na^3})\right], \tag{C.5}$$

$$\frac{\partial(E^{\mathrm{CL}}/V)}{\partial c_1}\Big|_{c_1=0} = 0. \tag{C.6}$$

This implies that the ferromagnetic-cyclic phase transition is first order.

UN-BN phase transition. The first derivatives of the energies with respect to c_1 at the phase boundary $c_1 = 0, c_2 < 0$ are given up to the level of the LHY correction by

$$\frac{\partial(E^{\mathrm{UN}}/V)}{\partial c_1}\Big|_{c_1=0} = \frac{8M^{3/2}n^{5/2}|c_2|^{3/2}}{\pi^2\hbar^3}, \tag{C.7}$$

$$\frac{\partial(E^{\mathrm{BN}}/V)}{\partial c_1}\Big|_{c_1=0} = \frac{8M^{3/2}n^{5/2}|c_2|^{3/2}}{\pi^2\hbar^3}. \tag{C.8}$$

Up to this order, the first derivative changes continuously. However, since there is a discontinuity in the transformation of the order parameter and the associated symmetry at the UN-BN phase boundary, this phase transition must be first order. Therefore, it is expected that with higher-order corrections to the ground-state energy, a finite jump in $\partial E/\partial c_1$ should appear at $c_1 = 0$. The difference in the order of approximation at which the discontinuity in the first derivative of the ground-state energy appears between the UN-BN and the other phase transitions in spin-2 BECs is related to the fact that the UN-BN phase transition does not appear in the mean-field phase diagram as opposed to the other phase transitions. The UN-BN phase transition is exhibited only if the zero-point fluctuations are taken into account.

Similarly, the fact that the ferromagnetic-BA and antiferromagnetic-polar phase transitions in spin-1 BECs are first order can be confirmed by a finite jump in the first derivative of the ground-state energy with respect to the quadratic Zeeman coefficient q. These phase transitions occur at $q = 0$.

Ferromagnetic-BA phase transition. The first derivatives of the energies with respect to q at the phase boundary are given by [68, 12].

$$\frac{\partial(E^{\mathrm{FM}}/V)}{\partial q}\Big|_{q=0} = n, \tag{C.9}$$

$$\frac{\partial(E^{\mathrm{BA}}/V)}{\partial q}\Big|_{q=0} = \frac{n}{2}\left[1 + \mathcal{O}(\sqrt{na^3})\right]. \tag{C.10}$$

Antiferromagnetic-polar phase transition. Similarly, we obtain

$$\frac{\partial(E^{\mathrm{AFM}}/V)}{\partial q}\Big|_{q=0} = n\left[1 + \mathcal{O}(\sqrt{na^3})\right], \tag{C.11}$$

$$\frac{\partial(E^{\mathrm{PL}}/V)}{\partial q}\Big|_{q=0} = 0 + \mathcal{O}(\sqrt{na^3}). \tag{C.12}$$

Appendix D

Second-order self-energies

In this Appendix, we show the derivations of the second-order self-energies that are used in Secs. 4.3 and 4.5.

Ferromagnetic-BN phase transition. The instability in the $m_F = -2$ excitation mode of the ferromagnetic state gives rise to the phase transition as discussed in Sec. 4.3. The energy spectrum of this mode is given by Eq. (4.6) in terms of the self-energy $\Sigma^{11}_{-2,-2}$ and the chemical potential μ. In the following, we therefore evaluate their second-order contributions. The contribution to $\Sigma^{11}_{-2,-2}$ from each of the second-order Feynman diagrams can be calculated straightforwardly (see, for example, Ref. [79]). By summing all of these contributions, we obtain

$$\begin{aligned}\hbar\Sigma^{11(2)}_{-2,-2}(p) = &\left[(c_0-4c_1)^2+\frac{4c_2^2}{25}+\frac{4c_0c_2}{5}-\frac{16c_1c_2}{5}\right]n_0\int\frac{\mathrm{d}^3\mathbf{q}}{(2\pi)^3}\left[\frac{A_{2,\mathbf{k}}+B_{2,\mathbf{k}}-2C_{2,\mathbf{k}}}{\hbar\left(\omega_{\mathbf{p}}-\omega^{(1)}_{-2,\mathbf{q}}-\omega^{(1)}_{2,\mathbf{k}}\right)+i\eta}\right.\\ &\left.-\mathrm{P}\frac{1}{\epsilon^0_{\mathbf{p}}-\epsilon^0_{\mathbf{q}}-\epsilon^0_{\mathbf{k}}+i\eta}\right]+4\left(c_1-\frac{c_2}{5}\right)^2n_0\int\frac{\mathrm{d}^3\mathbf{q}}{(2\pi)^3}\left[\frac{1}{\hbar\left(\omega_{\mathbf{p}}-\omega^{(1)}_{-1,\mathbf{q}}-\omega^{(1)}_{1,\mathbf{k}}\right)+i\eta}\right.\\ &\left.-\mathrm{P}\frac{1}{\epsilon^0_{\mathbf{p}}-\epsilon^0_{\mathbf{q}}-\epsilon^0_{\mathbf{k}}+i\eta}\right]+\frac{2c_2^2n_0}{25}\int\frac{\mathrm{d}^3\mathbf{q}}{(2\pi)^3}\left[\frac{1}{\hbar\left(\omega_{\mathbf{p}}-\omega^{(1)}_{0,\mathbf{q}}-\omega^{(1)}_{0,\mathbf{k}}\right)+i\eta}\right.\\ &\left.-\mathrm{P}\frac{1}{\epsilon^0_{\mathbf{p}}-\epsilon^0_{\mathbf{q}}-\epsilon^0_{\mathbf{k}}+i\eta}\right]+\left(c_0-4c_1+\frac{2c_2}{5}\right)\int\frac{\mathrm{d}^3\mathbf{q}}{(2\pi)^3}\,B_{2,\mathbf{q}},\end{aligned}\tag{D.1}$$

where $\mathbf{k}\equiv\mathbf{q}-\mathbf{p}$ and P denotes the principal value of the integral. Here the first-order (Bogoliubov) excitation spectra of the ferromagnetic phase are given by

$$\hbar\omega^{(1)}_{2,\mathbf{p}} = \sqrt{\epsilon^0_{\mathbf{p}}[\epsilon^0_{\mathbf{p}}+2(c_0+4c_1)n_0]},\tag{D.2}$$

$$\hbar\omega^{(1)}_{1,\mathbf{p}} = \epsilon^0_{\mathbf{p}},\tag{D.3}$$

$$\hbar\omega^{(1)}_{0,\mathbf{p}} = \epsilon^0_{\mathbf{p}}-4c_1n_0,\tag{D.4}$$

$$\hbar\omega^{(1)}_{-1,\mathbf{p}} = \epsilon^0_{\mathbf{p}}-6c_1n_0,\tag{D.5}$$

$$\hbar\omega^{(1)}_{-2,\mathbf{p}} = \epsilon^0_{\mathbf{p}}-8c_1n_0+\frac{2c_2n_0}{5},\tag{D.6}$$

and

$$A_{2,\mathbf{k}} \equiv \frac{\hbar\omega^{(1)}_{2,\mathbf{k}} + \epsilon^0_{\mathbf{k}} + (c_0+4c_1)n_0}{2\hbar\omega^{(1)}_{2,\mathbf{k}}}, \tag{D.7}$$

$$B_{2,\mathbf{k}} \equiv \frac{-\hbar\omega^{(1)}_{2,\mathbf{k}} + \epsilon^0_{\mathbf{k}} + (c_0+4c_1)n_0}{2\hbar\omega^{(1)}_{2,\mathbf{k}}}, \tag{D.8}$$

$$C_{2,\mathbf{k}} \equiv \frac{(c_0+4c_1)n_0}{2\hbar\omega^{(1)}_{2,\mathbf{k}}}. \tag{D.9}$$

To find the zero-momentum excitation energy, we take $\mathbf{p}=\mathbf{0}$. Moreover, since it is expected that $|\omega_{-2,\mathbf{p}=\mathbf{0}} - \omega^{(1)}_{-2,\mathbf{p}=\mathbf{0}}| \ll |c_1|n, |c_2|n$, which is justified by Eq. (4.13), we can replace the argument $\omega_{\mathbf{p}}$ in $\Sigma^{11(2)}_{-2,-2}$ by $\omega^{(1)}_{-2,\mathbf{p}=\mathbf{0}}$. Equation (D.1) can then be evaluated straightforwardly, and we obtain

$$\begin{aligned}\hbar\Sigma^{11(2)}_{-2,-2} =& \frac{(Mn_0)^{3/2}}{\hbar^3}\left\{ \frac{4(c_0+4c_1)^{1/2}}{3\pi^2}\left[(c_0-4c_1)^2 + \frac{4c_2^2}{25} + \frac{4c_0c_2}{5} - \frac{16c_1c_2}{5}\right] + \frac{\sqrt{2}}{\pi}\left(c_1 - \frac{c_2}{5}\right)^{5/2} \right.\\ &\left. + \frac{1}{\sqrt{2}\pi}\left(\frac{-c_2}{5}\right)^{5/2} + \frac{1}{3\pi^2}(c_0+4c_1)^{3/2}\left(c_0 - 4c_1 + \frac{2c_2}{5}\right)\right\}. \end{aligned} \tag{D.10}$$

Similarly, the total contribution to the chemical potential μ from the second-order Feynman diagrams is calculated to be

$$\begin{aligned}\mu^{(2)} =& 2(c_0+4c_1)\int \frac{\mathrm{d}^3\mathbf{q}}{(2\pi)^3}\, B_{2,\mathbf{q}} + (c_0+4c_1)\int \frac{\mathrm{d}^3\mathbf{q}}{(2\pi)^3}\left(-C_{2,\mathbf{q}} + \frac{(c_0+4c_1)n_0}{2\epsilon^0_{\mathbf{q}}}\right)\\ =& \frac{5(Mn_0)^{3/2}(c_0+4c_1)^{5/2}}{3\pi^2\hbar^3}. \end{aligned} \tag{D.11}$$

Near the ferromagnetic-BN phase boundary where $c_1, c_2 < 0$ and $c_2 \simeq 20c_1$, from Eqs. (D.10) and (D.11) we have

$$\hbar\Sigma^{11(2)}_{-2,-2} - \mu^{(2)} = \frac{(36\sqrt{3}+64)|c_1|^{5/2}(Mn_0)^{3/2}}{2\sqrt{2}\pi\hbar^3} + \mathcal{O}\left(|c_1|^{5/2}(Mn_0)^{3/2}\sqrt{na^3}/\hbar^3\right). \tag{D.12}$$

Here, we used $na^3 \ll 1$ with $a \equiv c_0M/(4\pi\hbar^2)$ so that the second term on the right-hand side of Eq. (D.12) can be ignored. Thus, we have derived Eq. (4.12).

Ferromagnetic-cyclic phase transition. The instability in the $m_F = -1$ excitation mode of the ferromagnetic phase brings about the phase transition. Therefore, we now evaluate the second-order contribution to $\Sigma^{11(2)}_{-1,-1}$ for the ferromagnetic phase. By summing all of the

contributions to $\Sigma^{11}_{-1,-1}$ from the second-order Feynman diagrams, we obtain

$$\begin{aligned}\hbar\Sigma^{11(2)}_{-1,-1}(\omega_{\mathbf{p}},\mathbf{p}) =& n_0(c_0-2c_1)^2\int\frac{\mathrm{d}^3\mathbf{q}}{(2\pi)^3}\left[\frac{A_{2,\mathbf{k}}+B_{2,\mathbf{k}}-2C_{2,\mathbf{k}}}{\hbar\left(\omega_{\mathbf{p}}-\omega^{(1)}_{-1,\mathbf{q}}-\omega^{(1)}_{2,\mathbf{k}}\right)+i\eta}-\mathrm{P}\frac{1}{\epsilon^0_{\mathbf{p}}-\epsilon^0_{\mathbf{q}}-\epsilon^0_{\mathbf{k}}}\right]\\ &+(c_0-2c_1)\int\frac{\mathrm{d}^3\mathbf{q}}{(2\pi)^3}B_{2,\mathbf{q}}+12n_0c_1^2\int\frac{\mathrm{d}^3\mathbf{q}}{(2\pi)^3}\left[\frac{1}{\hbar\left(\omega_{\mathbf{p}}-\epsilon^0_{\mathbf{q}}-\epsilon^0_{\mathbf{k}}\right)+i\eta}\right.\\ &\left.-\mathrm{P}\frac{1}{\epsilon^0_{\mathbf{p}}-\epsilon^0_{\mathbf{q}}-\epsilon^0_{\mathbf{k}}}\right],\end{aligned}\tag{D.13}$$

where $\omega^{(1)}_{-1,\mathbf{q}},\omega^{(1)}_{2,\mathbf{k}},A_{2,\mathbf{k}},B_{2,\mathbf{k}},C_{2,\mathbf{k}}$ are given by Eqs. (D.2)-(D.9). For a reason similar to that below Eq. (D.9), the arguments $\omega_{\mathbf{p}}$ and $\mathbf{p}$ of $\Sigma^{11(2)}_{-1,-1}$ can be replaced by $\omega^{(1)}_{-1,\mathbf{p}=\mathbf{0}}$ and $\mathbf{0}$, respectively. Each term in Eq. (D.13) can then be calculated straightforwardly, and we obtain

$$\begin{aligned}\hbar\Sigma^{11(2)}_{-1,-1} =& \frac{c_0^{5/2}(Mn_0)^{3/2}}{\hbar^3}\left[\frac{4}{3\pi^2}\left(\frac{c_0+4c_1}{c_0}\right)^{1/2}\left(\frac{c_0-2c_1}{c_0}\right)^2+\frac{1}{3\pi^2}\left(\frac{c_0+4c_1}{c_0}\right)^{3/2}\left(\frac{c_0-2c_1}{c_0}\right)\right.\\ &\left.+\frac{6}{\pi}\left(\frac{|c_1|}{c_0}\right)^{5/2}\right].\end{aligned}\tag{D.14}$$

Combined with $\mu^{(2)}$ given by Eq. (D.11), we have

$$\hbar\Sigma^{11(2)}_{-1,-1}-\mu^{(2)}=\frac{c_0^{5/2}(Mn_0)^{3/2}}{\pi^2\hbar^3}\left(-18x+6\pi|x|^{5/2}\right),\tag{D.15}$$

where $x\equiv c_1/c_0$. Since $|c_1|\ll c_0$ for typical alkali-metal atoms, the second term inside the brackets in Eq. (D.15) is negligible compared to the first term. We thus have derived Eq. (4.30).

UN-cyclic phase transition. The excitation mode that drives the UN-cyclic phase transition is a superposition of the magnetic sublevels $m_F=\pm2$ (see Sec. 4.3). Its zero-momentum energy is given by Eq. (4.16). Now we evaluate the second-order self-energies in Eq. (4.16). By summing

all of the contributions to Σ_{22}^{11} from the second-order Feynman diagrams, we obtain

$$\begin{aligned}\hbar\Sigma_{22}^{11(2)} =& n_0 c_0^2 \int \frac{\mathrm{d}^3\mathbf{q}}{(2\pi)^3} \left\{ (A_{0,\mathbf{k}} + B_{0,\mathbf{k}} - 2C_{0,\mathbf{k}}) \left[\frac{A_{2,\mathbf{q}}}{\hbar\left(\omega_{\mathbf{p}} - \omega_{2,\mathbf{q}}^{(1)} - \omega_{0,\mathbf{k}}^{(1)}\right) + i\eta} \right.\right. \\ & \left.\left. - \frac{B_{2,\mathbf{q}}}{\hbar\left(\omega_{\mathbf{p}} + \omega_{2,\mathbf{q}}^{(1)} + \omega_{0,\mathbf{k}}^{(1)}\right) - i\eta} \right] - \mathrm{P}\frac{1}{\epsilon_{\mathbf{p}}^0 - \epsilon_{\mathbf{q}}^0 - \epsilon_{\mathbf{k}}^0} \right\} + 6n_0 c_1^2 \int \frac{\mathrm{d}^3\mathbf{q}}{(2\pi)^3} \left[\right. \\ & \frac{A_{1,\mathbf{q}}(2A_{1,\mathbf{k}} + B_{1,\mathbf{k}} - 4C_{1,\mathbf{k}}) + C_{1,\mathbf{q}}C_{1,\mathbf{k}}}{\hbar\left(\omega_{\mathbf{p}} - \omega_{1,\mathbf{q}}^{(1)} - \omega_{1,\mathbf{k}}^{(1)}\right) + i\eta} - \frac{B_{1,\mathbf{q}}(2B_{1,\mathbf{k}} + A_{1,\mathbf{k}} - 4C_{1,\mathbf{k}}) + C_{1,\mathbf{q}}C_{1,\mathbf{k}}}{\hbar\left(\omega_{\mathbf{p}} + \omega_{1,\mathbf{q}}^{(1)} + \omega_{1,\mathbf{k}}^{(1)}\right) - i\eta} \\ & \left. - 2\mathrm{P}\frac{1}{\epsilon_{\mathbf{p}}^0 - \epsilon_{\mathbf{q}}^0 - \epsilon_{\mathbf{k}}^0} \right] + \frac{4n_0 c_0 c_2}{5} \int \frac{\mathrm{d}^3\mathbf{q}}{(2\pi)^3} \left[\frac{(C_{0,\mathbf{q}} - A_{0,\mathbf{q}})C_{2,\mathbf{k}}}{\hbar\left(\omega_{\mathbf{p}} - \omega_{0,\mathbf{q}}^{(1)} - \omega_{2,\mathbf{k}}^{(1)}\right) + i\eta} \right. \\ & \left. - \frac{(C_{0,\mathbf{q}} - B_{0,\mathbf{q}})C_{2,\mathbf{k}}}{\hbar\left(\omega_{\mathbf{p}} + \omega_{0,\mathbf{q}}^{(1)} + \omega_{2,\mathbf{k}}^{(1)}\right) - i\eta} \right] + \frac{4n_0 c_2^2}{25} \int \frac{\mathrm{d}^3\mathbf{q}}{(2\pi)^3} \left[\frac{A_{0,\mathbf{q}}B_{2,\mathbf{k}}}{\hbar\left(\omega_{\mathbf{p}} - \omega_{0,\mathbf{q}}^{(1)} - \omega_{2,\mathbf{k}}^{(1)}\right) + i\eta} \right. \\ & \left. - \frac{B_{0,\mathbf{q}}A_{2,\mathbf{k}}}{\hbar\left(\omega_{\mathbf{p}} + \omega_{0,\mathbf{q}}^{(1)} + \omega_{2,\mathbf{k}}^{(1)}\right) - i\eta} \right] + c_0 \int \frac{\mathrm{d}^3\mathbf{q}}{(2\pi)^3} (3B_{2,\mathbf{q}} + 2B_{1,\mathbf{q}} + B_{0,\mathbf{q}}) \\ & + c_1 \int \frac{\mathrm{d}^3\mathbf{q}}{(2\pi)^3} (2B_{1,\mathbf{q}} + 4B_{2,\mathbf{q}}) + \frac{2c_2}{5} \int \frac{\mathrm{d}^3\mathbf{q}}{(2\pi)^3} B_{2,\mathbf{q}}. \end{aligned} \tag{D.16}$$

Here the first-order (Bogoliubov) excitation spectra of the UN phase are given by

$$\hbar\omega_{\pm 2,\mathbf{p}}^{(1)} = \sqrt{\epsilon_{\mathbf{p}}^0[\epsilon_{\mathbf{p}}^0 - 2c_2 n_0/5]}, \tag{D.17}$$

$$\hbar\omega_{\pm 1,\mathbf{p}}^{(1)} = \sqrt{\epsilon_{\mathbf{p}}^0[\epsilon_{\mathbf{p}}^0 + 2(3c_1 - c_2/5)n_0]}, \tag{D.18}$$

$$\hbar\omega_{0,\mathbf{p}}^{(1)} = \sqrt{\epsilon_{\mathbf{p}}^0[\epsilon_{\mathbf{p}}^0 + 2(c_0 + c_2/5)n_0]}, \tag{D.19}$$

and

$$A_{2,\mathbf{p}} \equiv \frac{\hbar\omega_{2,\mathbf{p}}^{(1)} + \epsilon_{\mathbf{p}}^0 - c_2 n_0/5}{2\hbar\omega_{2,\mathbf{p}}^{(1)}},\ B_{2,\mathbf{p}} \equiv \frac{-\hbar\omega_{2,\mathbf{p}}^{(1)} + \epsilon_{\mathbf{p}}^0 - c_2 n_0/5}{2\hbar\omega_{2,\mathbf{p}}^{(1)}},\ C_{2,\mathbf{p}} \equiv \frac{c_2 n_0/5}{2\hbar\omega_{2,\mathbf{p}}^{(1)}}, \tag{D.20}$$

$$\begin{aligned} A_{1,\mathbf{p}} \equiv & \frac{\hbar\omega_{1,\mathbf{p}}^{(1)} + \epsilon_{\mathbf{p}}^0 + (3c_1 - c_2/5)n_0}{2\hbar\omega_{1,\mathbf{p}}^{(1)}},\ B_{1,\mathbf{p}} \equiv \frac{-\hbar\omega_{1,\mathbf{p}}^{(1)} + \epsilon_{\mathbf{p}}^0 + (3c_1 - c_2/5)n_0}{2\hbar\omega_{1,\mathbf{p}}^{(1)}}, \\ C_{1,\mathbf{p}} \equiv & \frac{(3c_1 - c_2/5)n_0}{2\hbar\omega_{1,\mathbf{k}}^{(1)}}, \end{aligned} \tag{D.21}$$

$$\begin{aligned} A_{0,\mathbf{p}} \equiv & \frac{\hbar\omega_{0,\mathbf{p}}^{(1)} + \epsilon_{\mathbf{p}}^0 + (c_0 + c_2/5)n_0}{2\hbar\omega_{0,\mathbf{p}}^{(1)}},\ B_{0,\mathbf{p}} \equiv \frac{-\hbar\omega_{0,\mathbf{p}}^{(1)} + \epsilon_{\mathbf{p}}^0 + (c_0 + c_2/5)n_0}{2\hbar\omega_{0,\mathbf{p}}^{(1)}}, \\ C_{0,\mathbf{p}} \equiv & \frac{(c_0 + c_2/5)n_0}{2\hbar\omega_{0,\mathbf{p}}^{(1)}}. \end{aligned} \tag{D.22}$$

The self-energy $\Sigma_{22}^{22(2)}$ is obtained from $\Sigma_{22}^{11(2)}$ by $\Sigma_{22}^{22(2)}(\omega_{\mathbf{p}},\mathbf{p}) = \Sigma_{22}^{11(2)}(-\omega_p,-\mathbf{p})$. Similarly, we obtain

$$\begin{aligned}
\hbar\Sigma_{2,-2}^{12(2)} =& n_0 c_0^2 \int \frac{\mathrm{d}^3\mathbf{q}}{(2\pi)^3}\, C_{2,\mathbf{q}}(2C_{0,\mathbf{k}} - A_{0,\mathbf{k}} - B_{0,\mathbf{k}}) \Bigg[\frac{1}{\hbar\left(\omega_{\mathbf{p}} - \omega_{2,\mathbf{q}}^{(1)} - \omega_{0,\mathbf{k}}^{(1)}\right) + i\eta} \\
&- \frac{1}{\hbar\left(\omega_{\mathbf{p}} + \omega_{2,\mathbf{q}}^{(1)} + \omega_{0,\mathbf{k}}^{(1)}\right) - i\eta}\Bigg] + 6n_0 c_1^2 \int \frac{\mathrm{d}^3\mathbf{q}}{(2\pi)^3}\Big[- C_{1,\mathbf{k}}(2A_{1,\mathbf{q}} + 2B_{1,\mathbf{q}} - 3C_{1,\mathbf{q}}) \\
&+ A_{1,\mathbf{q}}B_{1,\mathbf{k}}\Big]\left[\frac{1}{\hbar\left(\omega_{\mathbf{p}} - \omega_{1,\mathbf{q}}^{(1)} - \omega_{1,\mathbf{k}}^{(1)}\right) + i\eta} - \frac{1}{\hbar\left(\omega_{\mathbf{p}} + \omega_{1,\mathbf{q}}^{(1)} + \omega_{1,\mathbf{k}}^{(1)}\right) - i\eta}\right] \\
&+ \frac{2n_0 c_0 c_2}{5}\int \frac{\mathrm{d}^3\mathbf{q}}{(2\pi)^3}\Big[A_{2,\mathbf{q}}B_{0,\mathbf{k}} + A_{0,\mathbf{k}}B_{2,\mathbf{q}} - (A_{2,\mathbf{q}} + B_{2,\mathbf{q}})C_{0,\mathbf{k}}\Big] \\
&\times\left[\frac{1}{\hbar\left(\omega_{\mathbf{p}} - \omega_{2,\mathbf{q}}^{(1)} - \omega_{0,\mathbf{k}}^{(1)}\right) + i\eta} - \frac{1}{\hbar\left(\omega_{\mathbf{p}} + \omega_{2,\mathbf{q}}^{(1)} + \omega_{0,\mathbf{k}}^{(1)}\right) - i\eta}\right] \\
&+ \frac{4n_0 c_2^2}{25}\int \frac{\mathrm{d}^3\mathbf{q}}{(2\pi)^3}\, C_{2,\mathbf{q}}C_{0,\mathbf{k}}\left[\frac{1}{\hbar\left(\omega_{\mathbf{p}} - \omega_{2,\mathbf{q}}^{(1)} - \omega_{0,\mathbf{k}}^{(1)}\right) + i\eta} - \frac{1}{\hbar\left(\omega_{\mathbf{p}} + \omega_{2,\mathbf{q}}^{(1)} + \omega_{0,\mathbf{k}}^{(1)}\right) - i\eta}\right] \\
&+ c_0\int \frac{\mathrm{d}^3\mathbf{q}}{(2\pi)^3}\left(-C_{2,\mathbf{q}} + \frac{c_2 n_0}{10\epsilon_{\mathbf{q}}^0}\right) + 2c_1\int \frac{\mathrm{d}^3\mathbf{q}}{(2\pi)^3}\left[-C_{1,\mathbf{q}} + \frac{(3c_1 - c_2/5)n_0}{2\epsilon_{\mathbf{q}}^0}\right] \\
&- 4c_1\int \frac{\mathrm{d}^3\mathbf{q}}{(2\pi)^3}\left(-C_{2,\mathbf{q}} + \frac{c_2 n_0}{10\epsilon_{\mathbf{q}}^0}\right) + \frac{c_2}{5}\int \frac{\mathrm{d}^3\mathbf{q}}{(2\pi)^3}\Bigg\{2\left(-C_{2,\mathbf{q}} + \frac{c_2 n_0}{10\epsilon_{\mathbf{q}}^0}\right) \\
&- 2\left[-C_{1,\mathbf{q}} + \frac{(3c_1 - c_2/5)n_0}{2\epsilon_{\mathbf{q}}^0}\right] + \left[-C_{0,\mathbf{q}} + \frac{(c_0 + c_2/5)n_0}{2\epsilon_{\mathbf{q}}^0}\right]\Bigg\}, \qquad \text{(D.23)}
\end{aligned}$$

and

$$\begin{aligned}
\mu^{(2)} =& 2c_0\int \frac{\mathrm{d}^3\mathbf{q}}{(2\pi)^3}\,(B_{2,\mathbf{q}} + B_{1,\mathbf{q}} + B_{0,\mathbf{q}}) + 6c_1\int \frac{\mathrm{d}^3\mathbf{q}}{(2\pi)^3}\, B_{1,\mathbf{q}} + \frac{2c_2}{5}\int \frac{\mathrm{d}^3\mathbf{q}}{(2\pi)^3}\, B_{0,\mathbf{q}} \\
&+ c_0\int \frac{\mathrm{d}^3\mathbf{q}}{(2\pi)^3}\left[-C_{0,\mathbf{q}} + \frac{(c_0 + c_2/5)n_0}{2\epsilon_{\mathbf{q}}^0}\right] + 6c_1\int \frac{\mathrm{d}^3\mathbf{q}}{(2\pi)^3}\left[-C_{1,\mathbf{q}} + \frac{(3c_1 - c_2/5)n_0}{2\epsilon_{\mathbf{q}}^0}\right] \\
&+ \frac{c_2}{5}\int \frac{\mathrm{d}^3\mathbf{q}}{(2\pi)^3}\Bigg\{2\left[-C_{2,\mathbf{q}} + \frac{c_2 n_0}{10\epsilon_{\mathbf{q}}^0}\right] - 2\left[-C_{1,\mathbf{q}} + \frac{(3c_1 - c_2/5)n_0}{2\epsilon_{\mathbf{q}}^0}\right] \\
&+ \left[-C_{0,\mathbf{q}} + \frac{(c_0 + c_2/5)n_0}{2\epsilon_{\mathbf{q}}^0}\right]\Bigg\}. \qquad \text{(D.24)}
\end{aligned}$$

To find the zero-momentum excitation energy, we evaluate the above self-energies at $\mathbf{p} = \mathbf{0}$. Furthermore, since $\omega_{\pm 2,\mathbf{p}=\mathbf{0}} \ll |c_1|n_0$ near the phase boundary, which can be justified *a posteriori* from the final result, we make Taylor series expansions of $\Sigma_{22}^{11(2)}$, $\Sigma_{22}^{22(2)}$, and $\Sigma_{2,-2}^{12(2)}$ in powers of $\omega_{\pm 2,\mathbf{p}=\mathbf{0}}/(|c_1|n_0)$ and ignore the quadratic and higher-order terms as shown in Eqs. (4.17)-(4.19). The second-order self-energies and chemical potential can then be evaluated straightforwardly,

and we obtain

$$
\begin{aligned}
&\frac{\hbar^4\Sigma_{22}^{11(2)}(\omega_{\pm2,\mathbf{p}=\mathbf{0}},\mathbf{p}=\mathbf{0})}{M^{3/2}}\\
&=\frac{n_0c_0^2}{\pi^2}\sqrt{n_0\tilde{c}_0}+\frac{12n_0c_1^2}{\pi^2}\sqrt{3n_0\tilde{c}_1}+\frac{n_0c_0}{\pi^2}\sqrt{n_0\tilde{c}_2^3}+\frac{2n_0c_0}{3\pi^2}\sqrt{n_0(3\tilde{c}_1)^3}\\
&\quad+\frac{n_0c_0}{3\pi^2}\sqrt{n_0\tilde{c}_0^3}+\frac{2n_0c_1}{3\pi^2}\sqrt{n_0(3\tilde{c}_1)^3}+\frac{4n_0c_1}{3\pi^2}\sqrt{n_0\tilde{c}_2^3}+\frac{2n_0c_2}{15\pi^2}\sqrt{n_0\tilde{c}_2^3}\\
&\quad+\frac{3\sqrt{2}n_0c_1^2}{\pi^2}\left[\sqrt{6n_0\tilde{c}_1}-\frac{1}{\sqrt{6n_0\tilde{c}_1}}\hbar\omega_{\pm2,\mathbf{p}=\mathbf{0}}\right]+\frac{n_0c_0^2}{\sqrt{2}\pi^2}\\
&\quad\times\left\{\frac{\sqrt{10}n_0^{1/2}\left[5c_0\sqrt{5\tilde{c}_0}+c_2\left(\sqrt{5\tilde{c}_0}+\sqrt{5\tilde{c}_2}\right)\right]}{75c_0+30c_2}\right.\\
&\quad\left.-\frac{\sqrt{10}\left[5c_0\sqrt{5\tilde{c}_0}+4c_2\sqrt{5\tilde{c}_0}+2(5\tilde{c}_2)^{3/2}\right]}{3(5c_0+2c_2)^2n_0^{1/2}}\hbar\omega_{\pm2,\mathbf{p}=\mathbf{0}}\right\}+\frac{2\sqrt{2}n_0c_0c_2}{5\pi^2}\\
&\quad\times\left\{\frac{c_2n_0^{1/2}}{\sqrt{10}(\sqrt{5\tilde{c}_2}+\sqrt{5\tilde{c}_0})}+\left[\frac{\tilde{c}_2\left[(\sqrt{\tilde{c}_0}+\sqrt{\tilde{c}_2})^2\ln\left(\frac{\tilde{c}_0}{\tilde{c}_2}\right)-4(\tilde{c}_0-\tilde{c}_2)\right]}{4\sqrt{2}(\sqrt{\tilde{c}_0}+\sqrt{\tilde{c}_2})(\tilde{c}_0-\tilde{c}_2)^2n_0}\right.\right.\\
&\quad\left.\left.-\frac{n_0\tilde{c}_2\sqrt{\tilde{c}_0}}{\sqrt{\tilde{c}_0}+\sqrt{\tilde{c}_2}}\alpha\right]\hbar\omega_{\pm2,\mathbf{p}=\mathbf{0}}\right\}+\frac{2\sqrt{2}n_0c_2^2}{25\pi^2}\left\{-\frac{\sqrt{n_0}(\sqrt{\tilde{c}_0}-\sqrt{\tilde{c}_2})^2}{3\sqrt{2}(\sqrt{\tilde{c}_0}+\sqrt{\tilde{c}_2})}-\tilde{c}_0\tilde{c}_2n_0^2\alpha\right.\\
&\quad+\left[\frac{3(\sqrt{\tilde{c}_0}+\sqrt{\tilde{c}_2})(\tilde{c}_0+\tilde{c}_2)\ln\left(\frac{\tilde{c}_0}{\tilde{c}_2}\right)-8\left(2\tilde{c}_0^{3/2}-3\tilde{c}_0\tilde{c}^{1/2}+3\tilde{c}_0^{1/2}\tilde{c}_2-2\tilde{c}_2^{3/2}\right)}{12\sqrt{2}(\tilde{c}_0-\tilde{c}_2)^2n_0^{1/2}}\right.\\
&\quad\left.\left.+\frac{n_0\sqrt{\tilde{c}_0\tilde{c}_2}(\sqrt{\tilde{c}_0}-\sqrt{\tilde{c}_2})}{\sqrt{\tilde{c}_0}+\sqrt{\tilde{c}_2}}\alpha\right]\hbar\omega_{\pm2,\mathbf{p}=\mathbf{0}}\right\},
\end{aligned}
\tag{D.25}
$$

where $\tilde{c}_0\equiv c_0+c_2/5,\tilde{c}_1\equiv c_1-c_2/15,\tilde{c}_2\equiv -c_2/5$, and

$$
\alpha\equiv\frac{1}{n_0^{3/2}}\int_0^\infty \mathrm{d}x\frac{1}{2x\sqrt{(x+2\tilde{c}_0)(x+2\tilde{c}_2)}(\sqrt{x+2\tilde{c}_0}+\sqrt{x+2\tilde{c}_2})}. \tag{D.26}
$$

Note that α is infrared divergent, but it does not affect the final results as in the case of scalar BECs (see Sec. 3.2). Similarly, we have

$$
\begin{aligned}
&\frac{\hbar^4\Sigma_{2,-2}^{12(2)}(\omega_{\pm2,\mathbf{p}=\mathbf{0}},\mathbf{p}=\mathbf{0})}{M^{3/2}}\\
&=\frac{3\sqrt{2}n_0c_1^2}{\pi^2}\sqrt{6\tilde{c}_1n_0}+\frac{n_0^{3/2}c_0^2c_2}{5\pi^2(\sqrt{\tilde{c}_2}+\sqrt{\tilde{c}_0})}-\frac{c_0(\tilde{c}_2n_0)^{3/2}}{\pi^2}+\frac{2c_1(3\tilde{c}_1n_0)^{3/2}}{\pi^2}\\
&\quad+\frac{4c_1(\tilde{c}_2n_0)^{3/2}}{\pi^2}+\frac{c_2}{5\pi^2}\left[-2(\tilde{c}_2n_0)^{3/2}-2(3\tilde{c}_1n_0)^{3/2}+(\tilde{c}_0n_0)^{3/2}\right]\\
&\quad+\frac{2\sqrt{2}n_0^3c_2^2\tilde{c}_2\tilde{c}_0}{25\pi^2}\alpha+\frac{2c_0c_2}{5\pi^2}\frac{\left[10c_0n_0\sqrt{\tilde{c}_0n_0}+5c_2n_0\sqrt{\tilde{c}_0n_0}+(5\tilde{c}_2n_0)^{3/2}\right]}{15c_0+6c_2},
\end{aligned}
\tag{D.27}
$$

and

$$\frac{\hbar^3\mu^{(2)}}{M^{3/2}} =\frac{2c_0n_0}{3\pi^2}\left(\sqrt{n_0\tilde{c}_2^3}+\sqrt{n_0(3\tilde{c}_1)^3}+\sqrt{n_0\tilde{c}_0^3}\right)+\frac{2c_1n_0}{\pi^2}\sqrt{n_0(3\tilde{c}_1)^3}+\frac{2c_2n_0}{15\pi^2}\sqrt{n_0\tilde{c}_0^3}$$
$$+\frac{c_0(\tilde{c}_0n_0)^{3/2}}{\pi^2}+\frac{6c_1(3\tilde{c}_1n_0)^{3/2}}{\pi^2}+\frac{c_2}{5\pi^2}\left[-2(\tilde{c}_2n_0)^{3/2}-2(3\tilde{c}_1n_0)^{3/2}+(\tilde{c}_0n_0)^{3/2}\right]. \tag{D.28}$$

Around the UN-cyclic phase boundary [Eq. (4.2)] where $c_2<0, c_1>0$, and $|c_2|\ll c_1$, we can make expansions of the self-energies in powers of $|c_2|/c_1$ and ignore the quadratic and higher-order terms. Then, $\Sigma_{2,2}^{11(2)}$, $\Sigma_{2,2}^{22(2)}$, and $\Sigma_{2,-2}^{12(2)}$ reduce to

$$\hbar\Sigma_{2,2}^{11(2)}(\omega_{\pm2,\mathbf{p}=\mathbf{0}},\mathbf{p}=\mathbf{0}) =A+B\hbar\omega_{\pm2,\mathbf{p}=\mathbf{0}}, \tag{D.29}$$
$$\hbar\Sigma_{2,2}^{22(2)}(\omega_{\pm2,\mathbf{p}=\mathbf{0}},\mathbf{p}=\mathbf{0}) =A-B\hbar\omega_{\pm2,\mathbf{p}=\mathbf{0}}, \tag{D.30}$$
$$\hbar\Sigma_{2,-2}^{12(2)}(\omega_{\pm2,\mathbf{p}=\mathbf{0}},\mathbf{p}=\mathbf{0}) =C, \tag{D.31}$$

with

$$\frac{A-\mu^{(2)}}{(Mn_0)^{3/2}}\simeq-\frac{4\sqrt{3}c_1^{5/2}}{\pi^2\hbar^3}+\frac{\left(42\sqrt{3}c_1^{3/2}-10c_0^{3/2}\right)c_2}{15\pi^2\hbar^3}+\mathcal{O}\left[\left(\frac{|c_2|}{c_1}\right)^2\right], \tag{D.32}$$

$$\frac{B}{M^{3/2}n_0^{1/2}}\simeq-\frac{\left(c_0^{3/2}+3\sqrt{3}c_1^{3/2}\right)}{3\pi^2\hbar^3}-\frac{\left(c_0^{1/2}+\sqrt{3}c_1^{1/2}\right)c_2}{30\pi^2\hbar^3}+\mathcal{O}\left[\left(\frac{|c_2|}{c_1}\right)^2\right], \tag{D.33}$$

$$\frac{C}{(Mn_0)^{3/2}}\simeq\frac{12\sqrt{3}c_1^{5/2}}{\pi^2\hbar^3}+\frac{\left(10c_0^{3/2}-30\sqrt{3}c_1^{3/2}\right)c_2}{15\pi^2\hbar^3}+\mathcal{O}\left[\left(\frac{|c_2|}{c_1}\right)^2\right]. \tag{D.34}$$

Thus, we have derived Eqs. (4.22)-(4.24).

UN-BN phase transition. The degenerate $m_F=\pm2$ excitation modes of the UN phase also brings about the UN-BN phase transition at $c_1=0$ and $c_2<0$ (see Sec. 4.5). By using Eqs. (D.16), (D.23), and (D.24), we obtain the coefficients A, B, C defined by Eqs. (4.17)-(4.19). However, around the UN-BN phase boundary where $c_2<0$ and $|c_2|\gtrsim|c_1|$, we cannot make Taylor series expansions in powers of $c_2/|c_1|$ and ignore higher-order terms as for the UN-cyclic phase transition. Instead, we have

$$\frac{A-\mu^{(2)}+C}{(Mn_0)^{3/2}}=\frac{1}{\pi^2\hbar^3}\left(8\sqrt{3}\tilde{c}_1^{5/2}-\frac{32}{\sqrt{3}}\tilde{c}_1^{3/2}\tilde{c}_2+\frac{16}{3}\tilde{c}_1\tilde{c}_2^{3/2}+\frac{8}{\sqrt{3}}\tilde{c}_1^{1/2}\tilde{c}_2^2-\frac{16}{9}\tilde{c}_2^{5/2}\right), \tag{D.35}$$

where $\tilde{c}_1,\tilde{c}_2>0$ have been defined below Eq. (D.25). On the other hand, the other term on the right-hand side of Eq. (4.21) is calculated to be

$$-\frac{2c_2n_0}{5}+A-\mu^{(2)}-C=-\frac{2c_2n_0}{5}+\mathcal{O}\left(\tilde{c}_1\tilde{c}_1^{3/2}(Mn_0)^{3/2}/\hbar^3\right)+\mathcal{O}\left(\tilde{c}_2c_0^{3/2}(Mn_0)^{3/2}/\hbar^3\right). \tag{D.36}$$

Here, the last two terms on the right-hand side of Eq. (D.36) are smaller than the first term by

a factor $\sqrt{na^3} \ll 1$ and thus are negligible. Thus, we have derived Eqs. (4.32) and (4.33).

Appendix E

Decay channels for quasiparticles

E.1 Quasi-Nambu-Goldstone modes

The interaction Hamiltonian (7.1) is a sum of three interactions with coupling constants c_0, c_1, and c_2. The transition amplitude (7.9) for the quasi-NG modes ($j = \pm 2$) then vanishes except for the two following combinations of the final state: $j' = \pm 2$ and $j" = 0$ with interaction $\hat{V}_0$ [Eq. (7.2)], and $j' = \pm 1$ and $j" = \pm 1$ with interaction $\hat{V}_1$ [Eq. (7.3)]. In the former case, condition (7.10) becomes

$$\omega_{\pm 2,\mathbf{p}} = \omega_{\pm 2,\mathbf{q}} + \omega_{0,\mathbf{p}-\mathbf{q}}. \tag{E.1}$$

Using the dispersion relations (7.5) and (7.7), Eq. (E.1) reduces to

$$\frac{|\mathbf{p}| - |\mathbf{q}|}{|\mathbf{p} - \mathbf{q}|} = \sqrt{\frac{5c_0 + c_2}{|c_2|}}. \tag{E.2}$$

Since $c_0 \gg |c_2|$ for spin-2 ^{87}Rb, the the right-hand side of Eq. (E.2) is much larger than unity, where as the left-hand side is smaller than unity. As a result, there is no final state that satisfies condition (7.10).

Similarly, in the latter case, the condition (7.10) is written as

$$\omega_{\pm 2,\mathbf{p}} = \omega_{\pm 1,\mathbf{q}} + \omega_{\pm 1,\mathbf{p}-\mathbf{q}}. \tag{E.3}$$

Substituting Eqs. (7.6) and (7.7) in Eq. (E.3), we obtain

$$\frac{|\mathbf{p}|}{|\mathbf{q}| + |\mathbf{p} - \mathbf{q}|} = \sqrt{\frac{15c_1 - c_2}{|c_2|}}. \tag{E.4}$$

Since $c_1 > 0$ and $c_2 < 0$, the right-hand side of Eq. (E.4) is invariably larger than unity, while the left-hand side is smaller than unity. Therefore, there is no decay channel for the quasi-NG modes that satisfies condition (7.10).

E.2 Magnon

We now consider the decay channels for a magnon with momentum $\hbar\mathbf{p}$ in spin state $m_F = j = \pm 1$. If the interaction is $\hat{V}_0$ [Eq. (7.2)], the final spin state must be $j' = \pm 1$ and $j" = 0$.

Condition (7.10) is then written as

$$\omega_{\pm 1,\mathbf{p}} = \omega_{\pm 1,\mathbf{q}} + \omega_{0,\mathbf{p}-\mathbf{q}}, \tag{E.5}$$

which by using Eqs. (7.5) and (7.6) reduces to

$$\frac{|\mathbf{p}| - |\mathbf{q}|}{|\mathbf{p}-\mathbf{q}|} = \sqrt{\frac{5c_0 + c_2}{15c_1 - c_2}}. \tag{E.6}$$

Since $c_0 \gg c_1, |c_2|$, the right-hand side of Eq. (E.6) is much larger than unity, while the left-hand side is invariably smaller than unity. Therefore, there is no final momentum $\mathbf{q}$ for this decay channel to satisfy condition (7.10).

If the interaction is $\hat{V}_1$ [Eq. (7.3)], the final spin state can be either $j' = 0$ and $j" = \pm 1$ or $j' = \pm 2$ and $j" = \mp 1$. In the former case, condition (7.10) reduces to

$$\omega_{\pm 1,\mathbf{p}} = \omega_{0,\mathbf{q}} + \omega_{\pm 1,\mathbf{p}-\mathbf{q}}, \tag{E.7}$$

which cannot be satisfied for any final momentum $\mathbf{q}$ in a manner similar to Eq. (E.5). In the latter case, condition (7.10) is written as

$$\omega_{\pm 1,\mathbf{p}} = \omega_{\pm 2,\mathbf{q}} + \omega_{\mp 1,\mathbf{p}-\mathbf{q}}. \tag{E.8}$$

Using the dispersion relations (7.6) and (7.7), we obtain

$$\frac{|\mathbf{p}| - |\mathbf{p}-\mathbf{q}|}{|\mathbf{q}|} = \sqrt{\frac{|c_2|}{15c_1 - c_2}}. \tag{E.9}$$

Since both sides of Eq. (E.9) are smaller than unity ($c_2 < 0, c_1 > 0$), there exist values of the final momentum $\mathbf{q}$ that satisfy condition (7.10). This leads to a finite damping rate of magnons.

Finally, if the interaction is $\hat{V}_2$ [Eq. (7.4)], which is expressed in terms of only the spin-singlet pair amplitude, the transition amplitude (7.9) is nonvanishing only if the two particles in the initial state, i.e., a magnon and a condensate atom, form a spin-singlet pair amplitude. However, since the magnon and condensate atom, whose spin states are $m_F = j = \pm 1$ and $m_F = 0$, respectively, cannot form a spin-singlet pair, there is no contribution from interaction $\hat{V}_2$ to the damping rate of magnons.

E.3 Phonon

For the decay of a phonon in spin state $m_F = j = 0$, all of the three interactions contribute to the damping rate. If the interaction is $\hat{V}_0$, which is spin independent, two phonons with momenta $\mathbf{q}$ and $\mathbf{p}-\mathbf{q}$ would be generated. Similar to the case of scalar BECs, the contribution to the damping rate of the phonon is then given by

$$P^{(1)}_{\text{damp}} = \frac{3\hbar|\mathbf{p}|^5}{320\pi Mn}. \tag{E.10}$$

If the interaction is $\hat{V}_1$, the final spin states must be $j' = \pm 1$ and $j" = \mp 1$. Condition (7.10) is then written as

$$\omega_{0,\mathbf{p}} = \omega_{\pm 1,\mathbf{q}} + \omega_{\mp 1,\mathbf{p}-\mathbf{q}}, \tag{E.11}$$

which, by using Eqs. (7.5) and (7.6), reduces to

$$\frac{|\mathbf{p}|}{|\mathbf{q}|+|\mathbf{p}-\mathbf{q}|}=\sqrt{\frac{15c_1-c_2}{5c_0+c_2}}. \tag{E.12}$$

Since $c_0 \gg c_1, |c_2|$, there exist values of $\mathbf{q}$ that satisfy Eq. (E.12), leading to a nonvanishing contribution of this channel to the damping rate of phonons.

If the interaction is $\hat{V}_2$, the possible final spin states are given by $j' = m$ and $j" = -m$ with $m = -2, \ldots, 2$. Condition (7.10) then becomes

$$\omega_{0,\mathbf{p}} = \omega_{m,\mathbf{q}} + \omega_{-m,\mathbf{p}-\mathbf{q}}. \tag{E.13}$$

Substituting Eqs. (7.5)-(7.7) in Eq. (E.13), we obtain

$$\frac{|\mathbf{p}|}{|\mathbf{q}|+|\mathbf{p}-\mathbf{q}|}=\begin{cases} \sqrt{\frac{|c_2|}{5c_0+c_2}} & \text{for } m=\pm 2; \\ \sqrt{\frac{15c_1-c_2}{5c_0+c_2}} & \text{for } m=\pm 1; \\ 1 & \text{for } m=0. \end{cases} \tag{E.14}$$

Since $c_0 \gg c_1, |c_2|$, for any of the above final spin states, there exist values of $\mathbf{q}$ that satisfy Eq. (E.14), leading to a finite contribution to the damping rate of phonons.

Appendix F

Imaginary part of the excitation spectrum of magnons

The damping rate of a magnon is related to the imaginary part of its energy spectrum by Eq. (7.25). At the level of the Bogoliubov theory, the energy spectra of all quasiparticles are real numbers [Eqs. (2.75a)–(2.75e)], implying that the quasiparticles have infinitely long lifetime. However, as we go to the next order of approximation, i.e., the Beliaev theory, nonzero imaginary parts emerge in their energy spectra; thus, their lifetimes become finite. The decay of these quasiparticles can be interpreted as due to their collisions with the condensate particles as discussed in the main text. In this Appendix, we will show that the damping rate of magnons for the uniaxial-nematic (UN) phase [Eq. (7.21)] can be reproduced from the imaginary part of the second-order energy spectrum of these quasiparticles. The calculation is based on the spinor Beliaev theory that has been developed in Sec. 4.2. According to the Lehmann representation, the energy spectrum of magnons can be obtained from the poles of the Green's function $G^{11}_{\pm1,\pm1}(p)$ given by Eqs. (4.7) and (4.8) with $j=\pm1$. There is a twofold degeneracy due to the equivalence of the magnetic sublevels $m_F=\pm1$ in the UN phase [Eqs. (4.10a)–(4.10c)]. The poles of $G^{11}_{\pm1,\pm1}(p)$ at finite momenta are given by

$$\omega_{\pm1,\mathbf{p}} = \frac{\Sigma^{11}_{1,1}-\Sigma^{22}_{1,1}}{2} + \left\{ -\left(\Sigma^{12}_{1,-1}\right)^2 + \left[\frac{\epsilon^0_{\mathbf{p}}-\mu}{\hbar} + \frac{\left(\Sigma^{11}_{1,1}+\Sigma^{22}_{1,1}\right)}{2}\right]^2 \right\}^{1/2}. \tag{F.1}$$

Note that the self-energies on the right-hand side of Eq. (F.1) are functions of $\mathbf{p}$ and $\omega_{\pm1,\mathbf{p}}$, and we take only the plus sign in front of the square root for a reason similar to the argument above Eq. (3.59).

By separating the contributions to Σ and μ in Eq. (F.1) from the first- and second-order Feynman diagrams, the excitation spectrum of magnons is given up to the second order by

$$\begin{aligned}
\omega^{(2)}_{\pm1,\mathbf{p}} &= \frac{\Sigma^{11(2)}_{1,1}-\Sigma^{22(2)}_{1,1}}{2} + \left\{ -\left[\frac{\tilde{c}_1 n_0}{\hbar}+\Sigma^{12(2)}_{1,-1}\right]^2 + \left[\frac{\epsilon^0_{\mathbf{p}}+\tilde{c}_1 n_0}{\hbar} - \frac{\mu^{(2)}}{\hbar} + \frac{\Sigma^{11(2)}_{1,1}+\Sigma^{22(2)}_{1,1}}{2}\right]^2 \right\}^{1/2} \\
&\simeq \frac{\Sigma^{11(2)}_{1,1}-\Sigma^{22(2)}_{1,1}}{2} + \left\{ \left[\omega^{(1)}_{\pm1,\mathbf{p}}\right]^2 + \frac{\epsilon^0_{\mathbf{p}}+\tilde{c}_1 n_0}{\hbar}\left[\Sigma^{11(2)}_{1,1}+\Sigma^{22(2)}_{1,1} - \frac{2\mu^{(2)}}{\hbar}\right] - \frac{2\tilde{c}_1 n_0 \Sigma^{12(2)}_{1,-1}}{\hbar} \right\}^{\frac{1}{2}} \\
&\simeq \omega^{(1)}_{\pm1,\mathbf{p}} + \Lambda,
\end{aligned} \tag{F.2}$$

where $\omega^{(1)}_{\pm1,\mathbf{p}}$ is the first-order (Bogoliubov) spectrum of magnons given by Eq. (6.4), and

$$\Lambda \equiv \frac{\Sigma^{11(2)}_{1,1} - \Sigma^{22(2)}_{1,1}}{2} + \frac{\tilde{c}_1 n_0}{2\hbar\omega^{(1)}_{\pm1,\mathbf{p}}}\left[\Sigma^{11(2)}_{1,1} + \Sigma^{22(2)}_{1,1} - 2\Sigma^{12(2)}_{1,-1} - \frac{2\mu^{(2)}}{\hbar}\right] + \frac{\epsilon^0_{\mathbf{p}}}{2\hbar\omega^{(1)}_{\pm1,\mathbf{p}}}\left[\Sigma^{11(2)}_{1,1} + \Sigma^{22(2)}_{1,1} - \frac{2\mu^{(2)}}{\hbar}\right]. \tag{F.3}$$

Here, in deriving the second and third (approximate) equalities of Eq. (F.2), we used the fact that the second-order self-energies and chemical potential are smaller than $\tilde{c}_1 n_0$ by a factor of $\sqrt{na^3} \ll 1$ so that their higher-order terms can be ignored. Since both $\omega^{(1)}_{\pm1,\mathbf{p}}$ and $\mu^{(2)}$ are real numbers, the imaginary part of $\omega^{(2)}_{\pm1,\mathbf{p}}$ reduces to

$$\mathrm{Im}\left\{\omega^{(2)}_{\pm1,\mathbf{p}}\right\} = \mathrm{Im}\left\{\frac{\Sigma^{11(2)}_{1,1} - \Sigma^{22(2)}_{1,1}}{2} + \frac{\tilde{c}_1 n_0}{2\hbar\omega^{(1)}_{\pm1,\mathbf{p}}}\left[\Sigma^{11(2)}_{1,1} + \Sigma^{22(2)}_{1,1} - 2\Sigma^{12(2)}_{1,-1}\right] + \frac{\epsilon^0_{\mathbf{p}}}{2\hbar\omega^{(1)}_{\pm1,\mathbf{p}}}\left[\Sigma^{11(2)}_{1,1} + \Sigma^{22(2)}_{1,1}\right]\right\}. \tag{F.4}$$

By summing all the nonvanishing contributions to the imaginary parts of $\Sigma^{11}_{1,1}$ and $\Sigma^{12}_{1,-1}$ from the second-order Feynman diagrams, we obtain

$$\mathrm{Im}\left\{\Sigma^{11(2)}_{1,1}\right\} = \frac{6n_0c_1^2}{\hbar^2}\int\frac{\mathrm{d}^3\mathbf{q}}{(2\pi)^3}\Big[4A_{2,\mathbf{q}}B_{-1,\mathbf{k}} + A_{-1,\mathbf{k}}B_{2,\mathbf{q}} + 4C_{2,\mathbf{q}}C_{-1,\mathbf{k}} - 2A_{-1,\mathbf{k}}C_{2,\mathbf{q}} - 4A_{2,\mathbf{q}}C_{-1,\mathbf{k}} + A_{2,\mathbf{q}}A_{-1,\mathbf{k}}\Big](-i\pi)\delta\left(\omega^{(2)}_{\pm1,\mathbf{p}} - \omega^{(1)}_{\pm2,\mathbf{q}} - \omega^{(1)}_{\mp1,\mathbf{k}}\right), \tag{F.5}$$

$$\mathrm{Im}\left\{\Sigma^{22(2)}_{1,1}\right\} = \frac{6n_0c_1^2}{\hbar^2}\int\frac{\mathrm{d}^3\mathbf{q}}{(2\pi)^3}\Big[4A_{-1,\mathbf{k}}B_{2,\mathbf{q}} + A_{2,\mathbf{q}}B_{-1,\mathbf{k}} + 4C_{2,\mathbf{q}}C_{-1,\mathbf{k}} - 2B_{-1,\mathbf{k}}C_{2,\mathbf{q}} - 4B_{2,\mathbf{q}}C_{-1,\mathbf{k}} + B_{2,\mathbf{q}}B_{-1,\mathbf{k}}\Big](-i\pi)\delta\left(\omega^{(2)}_{\pm1,\mathbf{p}} - \omega^{(1)}_{\pm2,\mathbf{q}} - \omega^{(1)}_{\mp1,\mathbf{k}}\right), \tag{F.6}$$

$$\mathrm{Im}\left\{\Sigma^{12(2)}_{1,1}\right\} = \frac{6n_0c_1^2}{\hbar^2}\int\frac{\mathrm{d}^3\mathbf{q}}{(2\pi)^3}\Big[2A_{2,\mathbf{q}}B_{-1,\mathbf{k}} + 2A_{-1,\mathbf{k}}B_{2,\mathbf{q}} + 6C_{2,\mathbf{q}}C_{-1,\mathbf{k}} - 2A_{-1,\mathbf{k}}C_{2,\mathbf{q}} - 2B_{-1,\mathbf{k}}C_{2,\mathbf{q}} - A_{2,\mathbf{q}}C_{-1,\mathbf{k}} - B_{2,\mathbf{q}}C_{-1,\mathbf{k}}\Big](-i\pi)\delta\left(\omega^{(2)}_{\pm1,\mathbf{p}} - \omega^{(1)}_{\pm2,\mathbf{q}} - \omega^{(1)}_{\mp1,\mathbf{k}}\right), \tag{F.7}$$

where $A_{\pm j,\mathbf{p}}$, $B_{\pm j,\mathbf{p}}$, and $C_{\pm j,\mathbf{p}}$ are defined by

$$A_{\pm j,\mathbf{p}} \equiv \frac{\epsilon^0_{\mathbf{p}} + \tilde{c}_j n_0 + \hbar\omega^{(1)}_{\pm j,\mathbf{p}}}{2\hbar\omega^{(1)}_{\pm j,\mathbf{p}}},\ B_{\pm j,\mathbf{p}} \equiv \frac{\epsilon^0_{\mathbf{p}} + \tilde{c}_j n_0 - \hbar\omega^{(1)}_{\pm j,\mathbf{p}}}{2\hbar\omega^{(1)}_{\pm j,\mathbf{p}}} \tag{F.8}$$

for $j = 0, 1, 2$, and

$$C_{0,\mathbf{p}} \equiv \frac{\tilde{c}_0 n_0}{2\hbar\omega^{(1)}_{0,\mathbf{p}}},\ C_{\pm1,\mathbf{p}} \equiv \frac{\tilde{c}_1 n_0}{2\hbar\omega^{(1)}_{\pm1,\mathbf{p}}},\ C_{\pm2,\mathbf{p}} \equiv -\frac{\tilde{c}_2 n_0}{2\hbar\omega^{(1)}_{\pm2,\mathbf{p}}}. \tag{F.9}$$

Here $\tilde{c}_0$, $\tilde{c}_1$, and $\tilde{c}_2$ are defined below Eqs. (4.33) and (7.7), and the minus sign in the expression for $C_{\pm2,\mathbf{p}}$ results from the negative coupling constant c_2 as discussed below Eq. (7.15).

Since the effects of quantum fluctuations are expected to be small in a weakly interacting

dilute Bose gas, we have $|\omega^{(2)}_{\pm1,\mathbf{p}}/\omega^{(1)}_{\pm1,\mathbf{p}} - 1| \sim \sqrt{na^3} \ll 1$, which can be justified *a posteriori* from the final result. Therefore, $\omega^{(2)}_{\pm1,\mathbf{p}}$ in Eqs. (F.5)-(F.7) can be replaced by $\omega^{(1)}_{\pm1,\mathbf{p}}$ up to the second-order approximation under consideration. The integrals $\int \mathrm{d}^3\mathbf{q}$ in these equations can then be calculated straightforwardly, and by substituting the obtained imaginary parts of the self-energies in Eq. (F.4), we find

$$\mathrm{Im}\left\{\omega^{(2)}_{\pm1,\mathbf{p}}\right\} = -\frac{3c_1^2|\mathbf{p}|^3}{\sqrt{2}\pi\hbar(3c_1 - c_2/5)}\lambda\left(\frac{c_2}{c_1}\right), \tag{F.10}$$

where $\lambda(c_2/c_1)$ is defined by Eq. (7.22). Thus, we have derived Eq. (7.24). It follows from Eqs. (7.25) and (F.10) that the damping rate of magnons [Eq. (7.21)] can be reproduced by using the spinor Beliaev theory.

Acknowledgement

I would like to express my sincere gratitude to Prof. Masahito Ueda, my supervisor, for his guidance, helpful comments, and continuous encouragements during my time of master and Ph. D. I would also like to thank Prof. Yuki Kawaguchi for guiding me to the study of spinor BECs and for her fruitful discussions and comments. I really appreciate the productive discussions and comments from the members of the Ueda group as well as collaborators overseas. I would like to thank Prof. Masaki Oshikawa, Prof. Yasutami Takada, Prof. Shin Inouye, Prof. Makoto Gonokami, and Prof. Yoshio Torii for refereeing my thesis and for valuable discussions.

Last but not least, I would like to express my great gratitude to my parents who have always supported me both physically and mentally.

Bibliography

[1] A. J. Leggett, *Quantum Liquids: Bose Condensation and Cooper Pairing in Condensed-Matter Systems* (Oxford University Press, New York, 2006).

[2] P. Kapitza, *Viscosity of Liquid Helium below the λ-Point*, Nature **141**, 74 (1938).

[3] J. F. Allen and A. D. Misener, *Flow Phenomena in Liquid Helium II*, Nature **142**, 643 (1938).

[4] A. J. Leggett, *A theoretical description of the new phases of liquid ^3He*, Rev. Mod. Phys. **47**, 331 (1975).

[5] M. H. Anderson, J. R. Ensher, J. R. Matthews, C. Wieman, E. A. Cornell, *Observation of Bose-Einstein Condensation in a Dilute Atomic Vapor*, Science **269**, 198 (1995).

[6] K. B. Davis, M. O. Mewes, M. R. Andrews, N. J. van Druten, D. S. Durfee, D. M. Kurn, W. Ketterle, *Bose-Einstein Condensation in a Gas of Sodium Atoms*, Phys. Rev. Lett. **75**, 3969 (1995).

[7] C. C. Bradley, C. A. Sackett, J. J. Tollett, R. G. Hulet, *Evidence of Bose-Einstein Condensation in an Atomic Gas with Attractive Interactions*, Phys. Rev. Lett. **75**, 1687 (1995); C. C. Bradley, C. A. Sackett, R. G. Hulet, *Bose-Einstein Condensation of Lithium: Observation of Limited Condensate Number*, Phys. Rev. Lett. **78**, 985 (1997).

[8] S. Inouye, M. R. Andrews, J. Stenger, H.-J. Miesner, D. M. Stamper-Kurn, and W. Ketterle, *Observation of Feshbach resonances in a Bose-Einstein condensate*, Nature **392**, 151 (1998).

[9] C. Chin, R. Grimm, P. Julienne, and E. Tiesinga, *Feshbach resonances in ultracold gases*, Rev. Mod. Phys. **82**, 1225 (2010).

[10] D. M. Stamper-Kurn, M. R. Andrews, A. P. Chikkatur, S. Inouye, H.-J. Miesner, J. Stenger, and W. Ketterle, *Optical Confinement of a Bose-Einstein Condensate*, Phys. Rev. Lett. **80**, 2027 (1998).

[11] D. M. Stamper-Kurn and M. Ueda, *Spinor Bose gases: Symmetries, magnetism, and quantum dynamics*, Rev. Mod. Phys. **85**, 1191 (2013).

[12] Y. Kawaguchi and M. Ueda, *Spinor Bose-Einstein condensates*, Phys. Rep. **520**, 253 (2012).

[13] M.-S. Chang, Q. Qin, W. Zhang, L. You and M. S. Chapman, *Coherent spinor dynamics in a spin-1 Bose condensate*, Nat. Phys. 1, 111 (2005).

[14] L. E. Sadler, J. M. Higbie, S. R. Leslie, M. Vengalattore and D. M. Stamper-Kurn, *Spontaneous symmetry breaking in a quenched ferromagnetic spinor Bose-Einstein condensate*, Nature **443**, 312 (2006).

[15] J. Kronjager, C. Becker, P. Soltan-Panahi, K. Bongs, and K. Sengstock , *Spontaneous Pattern Formation in an Antiferromagnetic Quantum Gas*, Phys. Rev. Lett. **105**, 090402 (2010).

[16] T. Lahaye, J. Metz, B. Frohlich, T. Koch, M. Meister, A. Griesmaier, T. Pfau, H. Saito, Y. Kawaguchi, and M. Ueda, *d-Wave Collapse and Explosion of a Dipolar Bose-Einstein Condensate*, Phys. Rev. Lett. **101**, 080401 (2008).

[17] H. Schmaljohann, M. Erhard, J. Kronjager, M. Kottke, S. van Staa, L. Cacciapuoti, J. J. Arlt, K. Bongs, and K. Sengstock, *Dynamics of F=2 Spinor Bose-Einstein Condensates*, Phys. Rev. Lett. **92**, 040402 (2004).

[18] N. Bogoliubov, *On the theory of superfluidity*, J. Phys. USSR **11**, 23 (1947).

[19] C. Pethick and H. Smith, *Bose-Einstein Condensation in Dilute Bose Gases* (Cambridge University Press, New York, 2008), 2nd edition.

[20] A. L. Fetter and J. D. Walecka, *Quantum Theory of Many-Particle Systems* (Dover Publication, New York,2003).

[21] P.C. Hohenberg and P.C. Martin, *Microscopic theory of superfluid helium*, Ann. Phys. **34**, 291 (1965).

[22] A. Griffin, *Conserving and gapless approximations for an inhomogeneous Bose gas at finite temperatures*, Phys. Rev. B **53**, 9341 (1996).

[23] Y. Nambu, *Quasi-Particles and Gauge Invariance in the Theory of Superconductivity*, Phys. Rev. **117**, 648 (1960).

[24] J. Goldstone, *Field Theories with Superconductor Solutions*, Nuovo Cimento **19** 154 (1961).

[25] H. Shi and A. Griffin, *Finite-temperature excitations in a dilute Bose-condensed gas*, Phys. Rep. **304**, 1-87 (1998).

[26] S. T. Beliaev, *Energy-spectrum of a non-ideal Bose gas*, Soviet Physics JETP **7**, 299 (1958).

[27] S. T. Beliaev, *Application of the methods of quantum field theory to a system of bosons*, Soviet Physics JETP **7**, 289 (1958).

[28] M. Takahashi, *Thermodynamics of One-Dimensional Solvable Models* (Cambridge University Press, Cambridge, 1999).

[29] K. Huang, *Statistical Mechanics* (John Wiley and Sons, Inc., New York, 1987), 2nd edition.

[30] S. Weinberg, *Approximate Symmetries and Pseudo-Goldstone Bosons*, Phys. Rev. Lett. **29**, 1698 (1972).

[31] H. Georgi and A. Pais, *Vacuum symmetry and the pseudo-Goldstone phenomenon*, Phys. Rev. D **12**, 508 (1975).

[32] S. Coleman and E. Weinberg, *Radiative Corrections as the Origin of Spontaneous Symmetry Breaking*, Phys. Rev. D **7**, 1888 (1973).

[33] S. Weinberg, *The Quantum Theory of Fields* (Cambridge University Press, Cambridge, England, 1995).

[34] T. Kugo, I. Ojima, and T. Yanagida, *Superpotential symmetries and pseudo Nambu-Goldstone supermultiplets*, Phys. Lett. B **135**, 402 (1984)

[35] M. Bando, T. Kugo, K. Yamawaki, *Nonlinear realization and hidden local symmetries*, Phys. Rep. 164, 217 (1988).

[36] G. E. Volovik, *The Universe in a Helium Droplet* (Oxford University, New York, 2003).

[37] Jin-yi Pang, T. Brauner, and Q. Wang, *Spin-one color superconductors: Collective modes and effective Lagrangian*, Nucl. Phys. A **852**, 175 (2011).

[38] S. Uchino, M. Kobayashi, M. Nitta, and M. Ueda, *Quasi-Nambu-Goldstone Modes in Bose-Einstein Condensates*, Phys. Rev. Lett. **105**, 230406 (2010).

[39] L. Pitaevskii and S. Stringari, *Bose-Einstein Condensation* (Oxford University Press Inc., New York, 2003).

[40] N. T. Phuc, Y. Kawaguchi, and M. Ueda, *Fluctuation-induced and symmetry-prohibited metastabilities in spinor Bose-Einstein condensates*, Phys. Rev. A **88**, 043629 (2013).

[41] N. T. Phuc, Y. Kawaguchi, and M. Ueda, *Critical dynamics of a first-order quantum phase transition without metastability*, in preparation.

[42] N. T. Phuc, Y. Kawaguchi, and M. Ueda, *Emergent energy gap of quasi-Nambu-Goldstone modes and their propagations in spinor Bose-Einstein condensates*, in preparation.

[43] N. T. Phuc, Y. Kawaguchi, and M. Ueda, *Beliaev dampings of magnons and phonons in spinor Bose-Einstein condensates*, in preparation.

[44] S. N. Bose, *Planks Gesetz und Lichtquantenhypothese*, Z. Phys. **26**, 178 (1924).

[45] A. Einstein, *Quantentheorie des einatomigen idealen Gases*, Sitzungsber. Kgl. Preuss. Akad. Wiss. **1924**, 261 (1924); ibid. **1925**, 3 (1925).

[46] O. Penrose and L. Onsager, *Bose-Einstein Condensation and Liquid Helium*, Phys. Rev. **104**, 579 (1956).

[47] S. L. Cornish, N. R. Claussen, J. L. Roberts, E. A. Cornell, and C. E. Wieman, *Stable ^{85}Rb Bose-Einstein Condensates with Widely Tunable Interactions*, Phys. Rev. Lett. **85**, 1795 (2000).

[48] G. Modugno, G. Ferrari, G. Roati, R. J. Brecha, A. Simoni, and M. Inguscio, *Bose-Einstein Condensation of Potassium Atoms by Sympathetic Cooling*, Science **294**, 1320 (2001).

[49] T. Weber, J. Herbig, M. Mark, H. C. Nagerl, and R. Grimm, *Bose-Einstein Condensation of Cesium*, Science **299**, 232 (2003).

[50] D. G. Fried, T. C. Killian, L. Willmann, D. Landhuis, S. C. Moss, D. Kleppner, and T. J. Greytak, *Bose-Einstein Condensation of Atomic Hydrogen*, Phys. Rev. Lett. **81**, 3811 (1998).

[51] F. Pereira D. Santos, J. Leonard, Junmin W, C. J. Barrelet, F. Perales, and E. Rasel, *Bose-Einstein Condensation of Metastable Helium*, Phys. Rev. Lett. **86**, 3459 (2001).

[52] J. Stenger, S. Inouye, D. M. Stamper-Kurn, H.-J. Miesner, A. P. Chikkatur and W. Ketterle, *Spin domains in ground-state Bose-Einstein condensates*, Nature **396**, 345 (1998).

[53] D. M. Stamper-Kurn, H.-J. Miesner, A. P. Chikkatur, S. Inouye, J. Stenger, and W. Ketterle, *Quantum Tunneling across Spin Domains in a Bose-Einstein Condensate*, Phys. Rev. Lett. **83**, 661 (1999).

[54] A. T. Black, E. Gomez, L. D. Turner, S. Jung, and P. D. Lett, *Spinor Dynamics in an Antiferromagnetic Spin-1 Condensate*, Phys. Rev. Lett. **99**, 070403 (2007).

[55] A. Gorlitz, T. L. Gustavson, A. E. Leanhardt, R. Low, A. P. Chikkatur, S. Gupta, S. Inouye, D. E. Pritchard, and W. Ketterle, *Sodium Bose-Einstein Condensates in the F=2 State in a Large-Volume Optical Trap*, Phys. Rev. Lett. **90**, 090401 (2003).

[56] M. D. Barrett, J. A. Sauer, and M. S. Chapman, *All-Optical Formation of an Atomic Bose-Einstein Condensate*, Phys. Rev. Lett. **87**, 010404 (2001).

[57] M.-S. Chang, C. D. Hamley, M. D. Barrett, J. A. Sauer, K. M. Fortier, W. Zhang, L. You, M. S. Chapman, *Observation of Spinor Dynamics in Optically Trapped* ^{87}*Rb Bose-Einstein Condensates*, Phys. Rev. Lett. **92**, 140403 (2004).

[58] T. Kuwamoto, K. Araki, T. Eno, and T. Hirano, *Magnetic field dependence of the dynamics of* ^{87}*Rb spin-2 Bose-Einstein condensates*, Phys. Rev. A **69**, 063604 (2004).

[59] J. P. Burke, J. L. Bohn, B. D. Esry, and C. H. Greene, *Impact of the* ^{87}*Rb singlet scattering length on suppressing inelastic collisions*, Phys. Rev. A **55**, R2511-R2514 (1997).

[60] K. Huang and C. N. Yang, *Quantum-Mechanical Many-Body Problem with Hard-Sphere Interaction*, Phys. Rev. **105**, 767 (1957).

[61] T.L. Ho, *Spinor Bose Condensates in Optical Traps*, Phys. Rev. Lett. **81**, 742 (1998).

[62] T. Ohmi and K. Machida, *Bose-Einstein Condensation with Internal Degrees of Freedom in Alkali Atom Gases*, J. Phys. Soc. Japan **67**, 1822 (1998).

[63] C. V. Ciobanu, S. K. Yip, and T. L. Ho, *Phase diagrams of F=2 spinor Bose-Einstein condensates*, Phys. Rev. A **61**, 033607 (2000).

[64] M. Koashi and M. Ueda, *Exact Eigenstates and Magnetic Response of Spin-1 and Spin-2 Bose-Einstein Condensates*, Phys. Rev. Lett **84**, 1066 (2000).

[65] K. Murata, H. Saito, and M. Ueda, *Broken-axisymmetry phase of a spin-1 ferromagnetic Bose-Einstein condensate*, Phys. Rev. A **75**, 013607 (2007).

[66] F. Gerbier, A. Widera, S. Folling, O. Mandel, and I. Bloch, *Resonant control of spin dynamics in ultracold quantum gases by microwave dressing*, Phys. Rev. A **73**, 041602 (2006).

[67] M. Ueda and M. Koashi, *Theory of spin-2 Bose-Einstein condensates: Spin correlations, magnetic response, and excitation spectra*, Phys. Rev. A **65**, 063602 (2002).

[68] S. Uchino, M. Kobayashi, and M. Ueda, *Bogoliubov theory and Lee-Huang-Yang corrections in spin-1 and spin-2 Bose-Einstein condensates in the presence of the quadratic Zeeman effect*, Phys. Rev. A 81, 063632 (2010).

[69] M. Ueda, *Many-body theory of dilute Bose-Einstein condensates with internal degrees of freedom*, Phys. Rev. A **63**, 013601 (2000).

[70] T. D. Lee and C. N. Yang, *Many-Body Problem in Quantum Mechanics and Quantum Statistical Mechanics*, Phys. Rev. **105**, 1119 (1957).

[71] T. D. Lee, K. Huang, C. N. Yang, *Eigenvalues and Eigenfunctions of a Bose System of Hard Spheres and Its Low-Temperature Properties*, Phys. Rev. **106**, 1135 (1957).

[72] N. Navon, S. Piatecki, K. Gunter, B. Rem, T.C. Nguyen, F. Chevy, W. Krauth, C. Salomon, *Dynamics and Thermodynamics of the Low-Temperature Strongly Interacting Bose Gas*, Phys. Rev. Lett. **107**, 135301 (2011).

[73] J. L. Song, G. W. Semenoff, and F. Zhou, *Uniaxial and Biaxial Spin Nematic Phases Induced by Quantum Fluctuations*, Phys. Rev. Lett. **98**, 160408 (2007).

[74] A. M. Turner, R. Barnett, E. Demler, and A. Vishwanath, *Nematic Order by Disorder in Spin-2 Bose-Einstein Condensates*, Phys. Rev. Lett. **98**, 190404 (2007).

[75] H. Saito and M. Ueda, *Diagnostics for the ground-state phase of a spin-2 Bose-Einstein condensate*, Phys. Rev. A **72** 053628 (2005).

[76] E. G. M. van Kempen, S. J. J. M. F. Kokkelmans, D. J. Heinzen, and B. J. Verhaar, *Interisotope Determination of Ultracold Rubidium Interactions from Three High-Precision Experiments*, Phys. Rev. Lett. **88**, 093201 (2002).

[77] A. Widera, F. Gerbier, S. Folling, T. Gericke, O. Mandel, and I. Bloch, *Precision measurement of spin-dependent interaction strengths for spin-1 and spin-2 ^{87}Rb atoms*, New J. Phys. **8**, 152 (2006).

[78] B. Pasquiou, E. Marechal, L. Vernac, O. Gorceix, and B. Laburthe-Tolra, *Thermodynamics of a Bose-Einstein Condensate with Free Magnetization*, Phys. Rev. Lett. **108**, 045307 (2012).

[79] N. T. Phuc, Y. Kawaguchi and M. Ueda, *Beliaev theory of spinor BoseEinstein condensates*, Ann. Phys. **328**, 158 (2013).

[80] H. Lehmann, *Über Eigenschaften von Ausbreitungsfunktionen und Renormierungskonstanten quantisierter Felder*, Nuovo Cimento **11**, 342 (1954).

[81] N. N. Klausen, J. L. Bohn, and C. H. Greene, *Nature of spinor Bose-Einstein condensates in rubidium*, Phys. Rev. A **64**, 053602 (2001).

[82] C. K. Law, H. Pu, and N. P. Bigelow, *Quantum Spins Mixing in Spinor Bose-Einstein Condensates*, Phys. Rev. Lett. **81**, 5257 (1998).

[83] H. Pu, C. K. Law, S. Raghavan, J. H. Eberly, and N. P. Bigelow, *Spin-mixing dynamics of a spinor Bose-Einstein condensate*, Phys. Rev. A **60**, 1463 (1999).

[84] X. Cui, Y. Wang, and F. Zhou, *Quantum-fluctuation-driven coherent spin dynamics in small condensates*, Phys. Rev. A **78** 050701 (2008).

[85] R. Barnett, H. -Y. Hui, C. -H. Lin, J. D. Sau, and S. DasSarma, *Quantum rotor theory of spinor condensates in tight traps*, Phys. Rev. A **83**, 023613 (2011).

[86] F. Serwane, G. Zrn, T. Lompe, T. B. Ottenstein, A. N. Wenz, S. Jochim, *Deterministic Preparation of a Tunable Few-Fermion System*, Science **332**, 336 (2011).

[87] A. N. Wenz, G. Zrn, S. Murmann, I. Brouzos, T. Lompe, S. Jochim, *From Few to Many: Observing the Formation of a Fermi Sea One Atom at a Time*, Science **342**, 457 (2013).

[88] D. Jacob, E. Mimoun, L. De Sarlo, M. Weitz, J. Dalibard and F. Gerbier, *Production of sodium BoseEinstein condensates in an optical dimple trap*, New J. Phys. **13**, 065022 (2011).

[89] E. M. Bookjans, A. Vinit, and C. Raman, *Quantum Phase Transition in an Antiferromagnetic Spinor Bose-Einstein Condensate*, Phys. Rev. Lett. **107**, 195306 (2011).

[90] A. Vinit, E. M. Bookjans, C. A. R. Sa de Melo, and C. Raman, *Antiferromagnetic Spatial Ordering in a Quenched One-Dimensional Spinor Gas*, Phys. Rev. Lett. **110**, 165301 (2013).

[91] H. Saito, Y. Kawaguchi, and M. Ueda, *Kibble-Zurek mechanism in a quenched ferromagnetic Bose-Einstein condensate*, Phys. Rev. A **76**, 043613 (2007).

[92] S. R. Leslie, J. Guzman, M. Vengalattore, J.D. Sau, M.L. Cohen, and D.M. Stamper-Kurn, *Amplification of fluctuations in a spinor Bose-Einstein condensate*, Phys. Rev. A **79**, 043631 (2009).

[93] J. D. Sau, S.R. Leslie, D.M. Stamper-Kurn, and M.L. Cohen, *Theory of domain formation in inhomogeneous ferromagnetic dipolar condensates within the truncated Wigner approximation*, Phys. Rev. A **80**, 023622 (2009).

[94] B. Damski and W. H. Zurek, *Dynamics of a Quantum Phase Transition in a Ferromagnetic Bose-Einstein Condensate*, Phys. Rev. Lett. **99**, 130402 (2007).

[95] W. H. Zurek, U. Dorner, and P. Zoller, *Dynamics of a Quantum Phase Transition*, Phys. Rev. Lett. **95**, 105701 (2005).

[96] B. Damski, *The Simplest Quantum Model Supporting the Kibble-Zurek Mechanism of Topological Defect Production: Landau-Zener Transitions from a New Perspective*, Phys. Rev. Lett. **95**, 035701 (2005).

[97] T.W. B. Kibble, *Topology of cosmic domains and strings*, J. Phys. A **9**, 1387 (1976)

[98] T.W. B. Kibble, *Some implications of a cosmological phase transition*, Phys. Rep. **67**, 183 (1980).

[99] W. H. Zurek, *Cosmological experiments in superfluid helium?*, Nature **317**, 505 (1985).

[100] W. H. Zurek, *Cosmological experiments in condensed matter systems*, Phys. Rep. **276**, 177 (1996).

[101] A. Lamacraft, *Quantum Quenches in a Spinor Condensate*, Phys. Rev. Lett. **98**, 160404 (2007).

[102] C. Gaul and C. Muller, *Bogoliubov excitations of disordered Bose-Einstein condensates*, Phys. Rev. A **83**, 063629 (2011).

[103] P. Sokol, in *Bose-Einstein Condensation*, edited by A. Griffin, D. W. Snoke, and S. Stringari (Cambridge University Press, Cambridge, 1995); P. Nozieres and D. Pines, *The Theory of Quantum Liquids* (Addison-Wesley, Reading, 1994).

[104] J. Stenger, S. Inouye, A. P. Chikkatur, D. M. Stamper-Kurn, D. E. Pritchard, and W. Ketterle, *Bragg Spectroscopy of a Bose-Einstein Condensate*, Phys. Rev. Lett. **82**, 4569 (1999).

[105] L. Pitaevskii and S. Stringari, *Bose-Einstein Condensation* (Oxford University Press Inc., New York, 2003).

[106] R. C. Dynes and V. Narayanamurti, *Evidence for Upward or "Anomalous" Dispersion in the Excitation Spectrum of He II*, Phys. Rev. Lett. **33**, 1195 (1974).

[107] A. F. G. Wyatt, N. A. Lockerbie, and R. A. Sherlock, *Liquid ^{4}He: A Tunable High-Pass Phonon Filter*, Phys. Rev. Lett. **33**, 1425 (1974).

[108] H. J. Maris, *Phonon-phonon interactions in liquid helium*, Rev. Mod. Phys. **49**, 341 (1977).

[109] E. Hodby, O.M. Marago, G. Hechenblaikner, and C. J. Foot, *Experimental Observation of Beliaev Coupling in a Bose-Einstein Condensate*, Phys. Rev. Lett. **86**, 2196 (2001).

[110] N. Katz, J. Steinhauer, R. Ozeri, and N. Davidson, *Beliaev Damping of Quasiparticles in a Bose-Einstein Condensate*, Phys. Rev. Lett. **89**, 220401 (2002).

[111] E. E. Rowen, N. Bar-Gill, R. Pugatch, and N. Davidson, *Energy-dependent damping of excitations over an elongated Bose-Einstein condensate*, Phys. Rev. A **77**, 033602 (2008).

[112] N. Bar-Gill, E. E. Rowen, G. Kurizki, and N. Davidson, *Short-time Enhancement of the Decay of Coherent Excitations in Bose-Einstein Condensates*, Phys. Rev. Lett. **102**, 110401 (2009).

[113] V. Bretin, P. Rosenbusch, F. Chevy, G.V. Shlyapnikov, and J. Dalibard, *Quadrupole Oscillation of a Single-Vortex Bose-Einstein Condensate: Evidence for Kelvin Modes*, Phys. Rev. Lett. **90**, 100403 (2003).

[114] T. Mizushima, M. Ichioka, and K. Machida, *Beliaev Damping and Kelvin Mode Spectroscopy of a Bose-Einstein Condensate in the Presence of a Vortex Line*, Phys. Rev. Lett. **90**, 180401 (2003).

[115] M.-O. Mewes, M. R. Andrews, D. M. Kurn, D. S. Durfee, C. G. Townsend, and W. Ketterle, *Output Coupler for Bose-Einstein Condensed Atoms*, Phys. Rev. Lett. **78**, 582 (1997).

[116] M. Kunimi and Y. Kato, *Mean-field and stability analyses of two-dimensional flowing soft-core bosons modeling a supersolid*, Phys. Rev. B **86**, 060510 (2012).

[117] I. Danshita and C. A. R. Sa de Melo, *Stability of Superfluid and Supersolid Phases of Dipolar Bosons in Optical Lattices*, Phys. Rev. Lett. **103**, 225301 (2009).

[118] E. J. Mueller, *Superfluidity and mean-field energy loops: Hysteretic behavior in Bose-Einstein condensates*, Phys. Rev. A **66**, 063603 (2002).

[119] M. Olshanii, H. Perrin, and V. Lorent, *Example of a Quantum Anomaly in the Physics of Ultracold Gases*, Phys. Rev. Lett. **105**, 095302 (2010).

[120] N. M. Hugenholtz and D. Pines, *Ground-State Energy and Excitation Spectrum of a System of Interacting Bosons*, Phys. Rev. **116**, 489 (1959).

[121] E. E. Salpeter and H. A. Bethe, *A Relativistic Equation for Bound-State Problems*, Phys. Rev. **84**, 1232 (1951).